Evaluation of the Antiviral Effect of Polyglycerols Functionalized with Sialic Acid on Influenza Virus

DISSERTATION

zur Erlangung des akademischen Grades

doctor rerum naturalium

(Dr. rer. Nat.)

im Fach Biologie

eingereicht an der

Lebenswissenschaftlichen Fakultät

der Humboldt-Universität zu Berlin

von

Marlena Nastassja Stadtmüller

Präsidentin der Humboldt-Universität zu Berlin

Prof. Dr.-Ing. Dr. Sabine Kunst

Dekan der Lebenswissenschaftlichen Fakultät

Prof. Dr. Dr. Christian Ulrichs

Gutachter: 1. Prof. Dr. Andreas Herrmann

2. PD Dr. Thorsten Wolff

3. Prof. Dr. Christian Hackenberger

Tag der mündlichen Prüfung: 29.09.2021

Abstract

Influenza viruses pose a serious threat to public health and the economy by causing seasonal epidemics and sporadic pandemics. The efficacy of influenza vaccinations varies despite yearly updates, often resulting in dissatisfactory protection. Several classes of antiviral drugs are available, but resistance develops readily due to the rapid evolution of influenza virus. Therefore, additional antiviral agents to combat influenza virus are needed urgently.

A promising approach to block influenza virus infections is competitive inhibition of virus attachment to host cells by interfering with binding of the viral surface protein hemagglutinin (HA) to sialylated glycan receptors. In this manner, multivalent, sialylated compounds can inhibit influenza virus propagation competitively. However, the high structural and genetic variability of the viral HA especially at the receptor binding site (RBS) has hampered the development of universal sialic acid (SA)-based antivirals.

Polyglycerols (PGs) are highly biocompatible, have a low molecular weight and are easy to modify. Therefore, PGs are an advantageous scaffold for multivalent, sialylated anti-influenza virus inhibitors. Here, the antiviral effect of PGs functionalized with SA on influenza A virus (IAV) was evaluated. To this end, firstly the inhibition of a panel of different IAV strains by prototypic sialylated PGs was assessed. As observed for other multivalent compounds, SA-functionalized PGs were only effective at inhibiting a narrow spectrum of IAV strains. Going forward, this study aimed at elucidating the molecular basis for this restriction in order to create a basis for improved, broadly active compounds. To this end, IAV mutants resistant to a prototypic sialylated PG were selected using serial passaging for the first time. Three independent resistant variants developed with single or double amino acid changes mapping to the HA RBS. By employing hemagglutination elution, single-virus force measurements and glycan array analyses, a reduced receptor binding stability as well as an altered receptor binding profile of mutant viruses compared to WT virus was shown. Mutant viruses lost high affinity binding to the typical human type glycan receptors with terminal SA and instead acquired or maintained binding to different glycan receptors. Reverse genetic experiments with an IAV strain not susceptible to prototypic sialylated PGs revealed that the positions in HA identified to confer resistance in the mutant viruses were not the sole determinants for resistance or susceptibility universal to all IAV.

Intriguingly, three different cases of virus binding and inhibition were observed using fluorescently labeled compound: 1) viral HA was bound by the compound and resulted in inhibition of replication, 2) viral HA was bound by the compound but replication was not inhibited and 3) viral HA was not bound by the compound and no inhibition occurred. Binding of compounds to the virus did not prove sufficient for effective inhibition of virus propagation. In combination with receptor binding stability data showing a decrease, not abolishment, of sialylated receptor binding, these results suggest that there is an affinity or avidity requirement for effective competitive inhibition of HA attachment.

The suitability of PGs as IAV inhibitors with potential for broad activity was demonstrated by modified PGs incorporating sialyllactose (SL) instead of SA and either amide or azide linkage. The SL-PG with amide linkage exclusively covered an extended spectrum of inhibited IAV strains, thus also highlighting the importance of the exact compound configuration.

Taken together, results described in this thesis provide valuable insights into the development of resistance against inhibitors of HA attachment in IAV and into the strategic design of sialylated, multivalent inhibitors aiming at broad activity against a large spectrum of influenza viruses.

Zusammenfassung

Influenzaviren verursachen saisonale Grippe-Epidemien sowie sporadische Pandemien und stellen somit eine ernste Bedrohung für Public Health und die Wirtschaft dar. Die Effektivität von Grippeimpfungen liegt trotz der jährlichen Aktualisierung oft unbefriedigend niedrig. Es gibt einige Gruppen von antiviralen Therapien, aber die rapide Evolution von Influenzaviren führt rasch zu Resistenzen. Deshalb werden weitere antivirale Mittel zur Bekämpfung von Influenzaviren dringend benötigt.

Ein vielversprechender Ansatz zur Verhinderung von Infektionen mit Influenzavirus ist die kompetitive Inhibition der Virusanhaftung an die Wirtszellen durch Behinderung der Bindung des viralen Oberflächenproteins Hemagglutinin (HA) an sialylierte Glykanrezeptoren. Allerdings erschwert die hohe strukturelle und genetische Variabilität des viralen HA, besonders an der Rezeptorbindestelle (RBS), die Entwicklung von universellen Sialinsäure (SA)-basierten Virostatika.
Polyglycerole (PGs) sind in hohem Maße biokompatibel, haben ein geringes Molekulargewicht und sind einfach zu modifizieren. Daher stellen sie ein vorteilhaftes Grundgerüst für multivalente, sialylierte Inhibitoren gegen Influenzaviren dar. In dieser Arbeit wurde der antivirale Effekt von mit SA funktionalisierten PGs auf Influenza A Viren (IAV) evaluiert. Dazu wurde zunächst die Inhibition einer Auswahl verschiedener IAV Stämme durch prototypische sialylierte PGs untersucht. Wie auch für andere multivalente Wirkstoffe beobachtet, waren SA-basierte PGs nur bei der Inhibition einer geringen Anzahl an IAV Stämmen effektiv. Im Folgenden strebte die vorliegende Arbeit an, die molekulare Grundlage für diese Beschränkung zu ergründen um somit eine Basis für das Design verbesserter, breit reaktiver Wirkstoffe zu schaffen. Zu diesem Zweck wurden zum ersten Mal mittels Serienpassagen IAV Mutanten selektiert, die gegen prototypisches sialyliertes PG resistent waren. Es entwickelten sich drei unabhängige resistente Virusvarianten, die einen einfachen bzw. doppelten Aminosäuren-Austausch in der HA RBS aufwiesen. Durch Hemagglutinations-Elution, Einzel-Virus Kraft-Untersuchungen und Glykanarray Analysen konnte eine verringerte Rezeptorbindungsstabilität sowie ein verändertes Rezeptorbindeprofil für diese Virusvarianten im Vergleich zum ursprünglichen Virus gezeigt werden. Im Austausch gegen die hochaffinen Bindungen an die typischen humanen Glykanrezeptoren mit terminaler SA erhielten oder behielten die Virusvarianten die Bindekapazität an andere Glykanrezeptoren. Experimente mit reverser Genetik an einem IAV Stamm, der nicht empfänglich für Inhibition mit prototypischen sialylierten PGs war, lieferten die Erkenntnis, dass die Stellen in HA, die den Virusvarianten ihre Resistenz verliehen, nicht generell ausschlaggebend für die Resistenz oder Empfänglichkeit von IAV waren.

Interessanterweise wurden drei unterschiedliche Fälle von Virusbindung und Inhibition mittels fluoeszenzmarkiertem Wirkstoff beobachtet: 1) Virales HA wurde vom PG gebunden und folglich wurde die Virusreplikation inhibiert, 2) virales HA wurde vom PG gebunden ohne Inhibition der Virusreplikation und 3) Virales HA wurde nicht vom PG gebunden und folglich gab es keine Inhibition. Für eine effektive Inhibition der Virusvermehrung war eine Bindung des Wirkstoffes an das Virus nicht hinreichend. Zusammen mit den Daten zur verringerten – nicht aufgehobenen – Rezeptorbindestabilität suggerieren diese Ergebnisse, dass es eine Mindestanforderung an die Affinität oder Avidität für eine effektive kompetitive Inhibition von HA gibt.

Durch modifizierte PGs, die Sialyllaktose (SL) statt SA und entweder einen Azid- oder einen Amidlinker enthielten, konnte die Eignung von PGs als IAV Inhibitoren mit Potenzial für breite Aktivität demonstriert werden. Allein ein SL-PG mit Amidlinker war in der Lage, ein erweitertes

Spektrum von IAV Stämmen zu inhibieren. Dies betont, wie wichtig die genaue Konfiguration eines Wirkstoffes ist.

Zusammenfassend bieten die Ergebnisse dieser Arbeit wertvolle Einblicke in die Entwicklung von Resistenzen in IAV gegen Inhibitoren des HA-Attachment und in das strategische Design von sialylierten mutlivalenten Inhibitoren gegen ein breites Spektrum an Influenzaviren.

Table of content

Table of content

1. Introduction

1.1. Influenza Virus

1.1.1. General introduction

Influenza virus is a respiratory virus and the agent responsible for influenza disease in humans, commonly called 'the flu'. Even though influenza infections can be found all year, influenza activity increases periodically, causing seasonal outbreaks during winter in temperate climates. Seasonal influenza viruses are predominantly transmitted via droplets and aerosols containing virus produced by infected people through coughing or sneezing or through respiratory secretions on surfaces including hands[6, 7]. The attack rate of seasonal influenza was estimated to be approximately 8 % between 2010 and 2016 in the US and varied between 3 % and 11% among seasons[8]. Symptoms are marked by a sudden onset of fever, cough, sore throat, headache, muscle aches, fatigue and a runny nose. Usually, people recover without medical assistance within one to two weeks. However, complications that can be life threatening such as pneumonia, multi-organ failure, myocarditis or encephalitis can arise. Annually, influenza virus infection leads to 3 to 5 million cases of severe illness and about 290.000 to 650.000 deaths worldwide. Small children, the elderly, pregnant women and people with medical conditions are especially at risk to develop severe complications[6, 9]. In addition to the disease burden of influenza, the economic burden to the healthcare system and society due to direct medical costs as well as indirect costs caused by absenteeism and lost productivity is substantial[7, 10].

On top of seasonal epidemics, sporadic pandemics that are characterized by devastatingly increased mortality and morbidity have occurred in 1918, 1957, 1968 and 2009 and may occur in the future[11, 12]. Pandemics occur when new influenza viruses that are antigenically different from existing strains are introduced into the human population. These new influenza viruses are usually a result from reassortment events with animal strains of influenza virus, but can also be a product of extreme antigenic drift[13, 14].

Influenza viruses are single stranded, negative sensed RNA viruses belonging to the family of *Orthomyxoviridae*[15]. Four genera of influenza viruses are known. Seasonal epidemics of Influenza A and B viruses (IAV and IBV) cause the major burden of disease in humans. Influenza C viruses are also able to infect humans but are associated with asymptomatic or very mild infections[6]. Influenza D viruses have been found in cattle and pigs[16]. Importantly, IAV is able to infect a broad host range covering several mammalian species, wild and domestic birds and bats[17]. Influenza A viruses are further subtyped according to their surface proteins hemagglutinin (HA) and neuraminidase (NA). 18 different HA and 11 different NA subtypes (H1-H18 and N1-N11, respectively) have been identified so far[18-20]. Only H3N2, H2N2 and H1N1 have caused seasonal epidemics in humans, but zoonotic influenza viruses such as avian H5N1, H7N9 and H9N2 and swine H1N1, H1N2 and H3N2 are also able to infect humans. Animal influenza viruses do not spread easily from human to human and the severity of the infection varies between viruses[21]. However, mortality for H5N1 and H7N9

virus infections is much higher than of seasonal influenza and the pandemic potential of especially H7N9 viruses is substantial[22, 23]. There are still some barriers, but constant exchange of viruses among aquatic birds and to mammals enable adaption and reassortment events that further the risk for pandemic potential[13, 15].

1.1.2. Structure and morphology

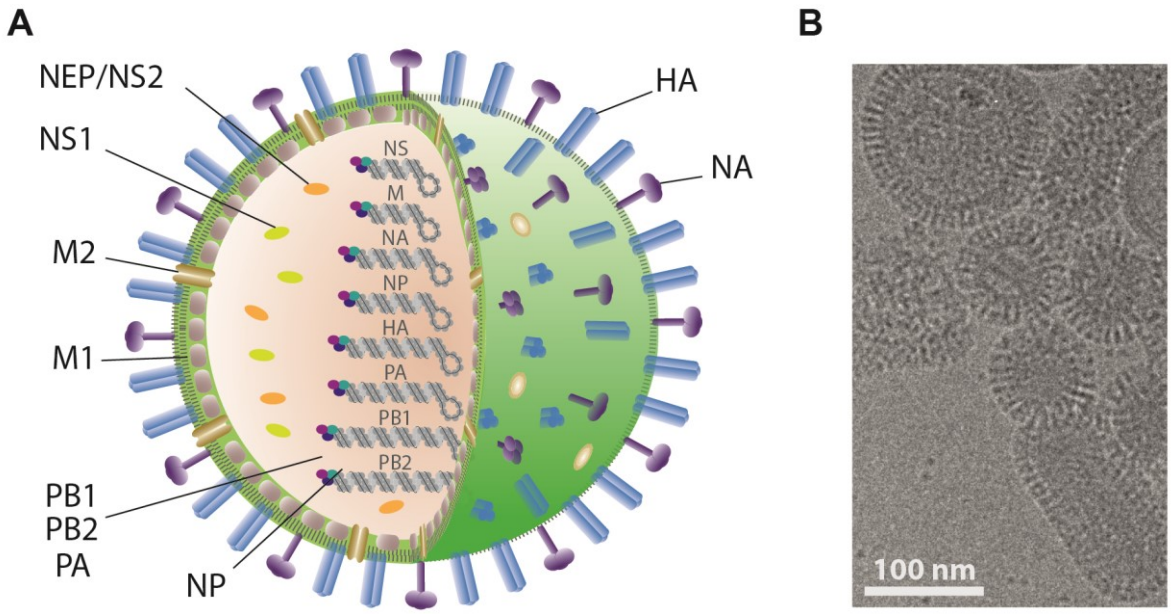

Figure 1: Structure and morphology of IAV particles.
(A) Schematic representation of an IAV virion.IAV virions are enveloped by a host cell derived lipid membrane that is lined by matrix protein 1 (M1) on the inside. The membrane contains matrix protein 2 (M2) and surface proteins hemagglutinin (HA) and neuraminidase (NA). Inside the particle, the 8 viral RNA segments form complexes with the nucleoprotein (NP) and the three polymerase proteins polymerase acid (PA), polymerase basic 1 (PB1) and polymerase basic 2 (PB2). Accessory proteins nonstructural protein 1 (NS1) and nuclear export protein/nonstructural protein 2 (NEP/NS2) are also located inside the virion. (B) Cryo-TEM electron microscopy picture of influenza A/X31 virus (Courtesy of Kai Ludwig, BioSupraMol, FU Berlin).

IAV viruses are enveloped in a lipid bilayer membrane derived from host cells during budding[24]. Virus particles are pleomorphic and heterogeneous and each virus produces pleomorphic and heterogeneous progeny in turn[25]. Spherical and filamentous particles with a diameter of 80-120nm are formed (Figure 1B) and the length of filamentous particles can exceed 300 nm[26]. Hemagglutinin (HA) and neuraminidase (NA) proteins protrude 10-14 nm from the membrane and thus are visible as spikes in electron microscopy (Figure 1). Matrix protein 2 (M2) is embedded in the envelope as well. HA is distributed rather uniformly on the virion surface whereas NA is distributed unevenly and in patches[27-29]. Spatial distribution of the membrane proteins is not random but organized asymmetrically to facilitate movement across mucus[30]. Matrix protein 1 (M1) lines the viral envelope on the inside (Figure 1A). The IAV genome is segmented into 8 segments and packaged into ribonucleoprotein (RNP) complexes. These viral RNP (vRNP) complexes consist of the viral RNA coated with several copies of the nucleoprotein (NP) and the polymerase complex composed of polymerase acid (PA), polymerase basic 1 (PB1) and polymerase basic 2 (PB2). One set of vRNPs containing one copy of the viral genome is packaged inside the virion[31, 32]. However, less than 50% of infected cells actually express all viral mRNAs, a fact that has been partially attributed to

incomplete packaging of segments into progeny virions[33, 34]. The segments are numbered from longest (2341 nucleotides (nt)) to shortest (890 nt). The coding regions of the viral segments are flanked by conserved non-coding regions containing the promotor region recognized by the polymerase complex[35, 36]. The far ends of all segments are conserved among all segments. A characteristic panhandle structure is formed due to base-pairing between complementary regions in the 5' and the 3' noncoding region[26, 37]. Nonstrucutral protein 1 (NS1) and nuclear export protein (NEP) were also shown to be packaged in the virion[38] (Figure 1A).

Table 1: The proteome of influenza A viruses. Modified from Vasin, Temkina, Egorov, Klotchenko, Plotnikova and Kiselev [39].

Segment	Protein	Protein length (aa)	Function
1	PB2	759	Subunit of the viral polymerase involved in recognition of 5'-capped host pre-mRNAs
2	PB1	757	Catalytical subunit of the viral polymerase
	PB1-N40	718	Maintains balance between PB1 and PB1-F2
	PB1-F2	87	Virulence factor and modulator of polymerase activity
3	PA	716	Subunit of the viral polymerase with RNA endonuclease activtiy
	PA-X	252	Modulates the host response and viral virulence
	PA-N155	568	Unknown function
	PAN182	535	Unknown function
4	HA	560	Receptor binding and membrane fusion
5	NP	498	Major component of the viral RNP complex, controls nuclear cytoplasmic transport of RNA
6	NA	465	Cleaves off SA to enable escape of progeny
7	M1	252	Main component of viral membrane with role in virion assembly
	M2	97	Proton channel important for unpacking during virus entry
	M42	99	Functional replacement of M2
8	NS1	217	Involved in numerous virus-host interactions including antagonism of antiviral mechanisms and regulation of host and viral gene expression
	NS2/NEP	121	Mediates vRNP export from the nucleus to the cytoplasm
	NS3	174	Host adaption
	NEG8/NSP	216	Unknown function

In addition to the proteins contained in the virus particle, IAV can produce further proteins upon infection of a cell (Table 1). Each of the eight segments encodes at least one major viral protein.

However, splicing, alternative translation initiation, leaky ribosomal scanning or ribosomal frameshift expand the number of expressed proteins to a minimum of 10 depending on the virus strain[39, 40]. Not only the total number of proteins expressed but also the amount of a protein are strain-specific[41].

1.1.3. Replication

The mains steps of the IAV replication cycle are visualized in Figure 2. Infection begins with attachment of IAV to terminal sialic acid (SA) on N-linked glycans on the surface of host cells via its surface protein HA[42, 43]. Multiple HA dissociation and association events move the virus across the cell surface before internalization[44]. One major entry route is clathrin-mediated endocytosis[42]. Clathrin-coated pits form *de novo* at virus attachment sites[45] and endocytosis commences in an epsin 1-dependent manner[46]. IAV can also enter clathrin-independently by micropinocytosis with comparable efficiency[47, 48]. Attachment to N-linked glycans is indispensable for subsequent internalization into the host cell via macropinocytosis[49]. After internalization, IAV is trafficked along microtubules in endosomal vesicles[50]. IAV escapes lysosomal degradation by membrane fusion and uncoating. The low pH in the endosome triggers opening of the M2 ion channel, which results in acidification of the virion interior[51]. IAV fusion occurs in early to late endosomes[52, 53] and contains two important components. Firstly, the low pH in the endosome triggers conformational change in HA that exposes the fusion peptide and thus facilitates merger of the viral and the endosomal membrane[43, 54]. Upon conformational change of the HA the fusion peptide is brought in proximity of the endosomal membrane into which it inserts. Further conformational changes result in a rupture in the endosomal membrane, ultimately opening a fusion pore[54, 55] through which the vRNPs escape into the cytoplasm and diffuse to the nucleus[56]. Secondly, acidification of the virion causes M1 to detach from the membrane and release the vRNPs, thus collapsing the structure of the virion, enabling vRNP escape and promoting membrane fusion[52, 57, 58].

vRNPs are imported into the nucleus via cellular importins depending on the nuclear localization signal present on all vRNP protein components, specifically the one on the NP vRNA[59, 60]. Inside the nucleus, the viral RNA dependent RNA polymerase, which is part of the vRNPs, uses the vRNA as template for viral genome replication and transcription of viral mRNA[15, 61]. Transcription is initiated from 5' cap-structures derived from host cell pre-mRNA by PB2 binding and then PA cleaving the 5'cap in a process termed cap-snatching[62, 63]. A 3' poly A tail is encoded by a polyuracil stretch within the vRNA and added to the mRNA by reiterative copying in the template[64]. Translation of viral mRNA takes place in the cytoplasm and depends on the cellular translation machinery[65]. Viral proteins with a nuclear localization signal, such as PB1, PB2, PA and NP, enter the nucleus where they aid viral transcription and replication[66]. NS1 enters the nucleus as well and modulates host cell functions in multiple ways including countering the cellular innate immune response by interfering with interferon signaling[67]. Viral membrane proteins are synthesized by ER-associated ribosomes due to their signal peptides and subjected to posttranslational modifications in the ER. HA is assembled to its trimeric form in the ER[68] and receives several N-glycosylations depending on

subtype. The viral membrane proteins are further trafficked through the trans-golgi network and transported to the plasma membrane, where they accumulate in lipid rafts[69].

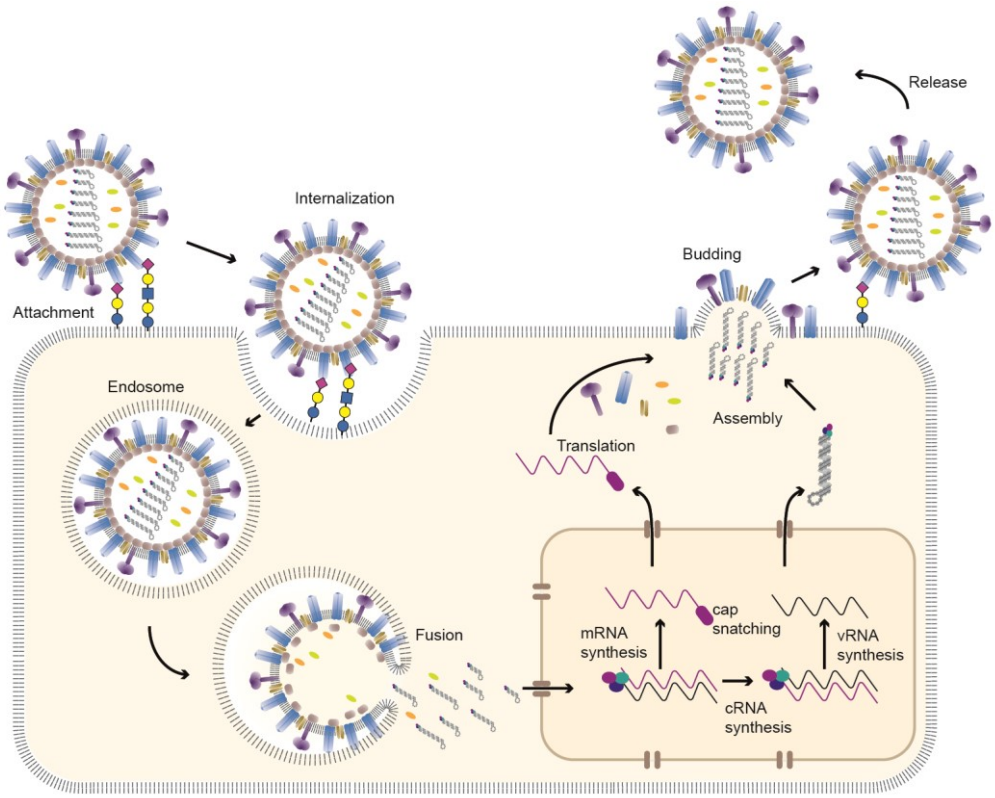

Figure 2: Replication cycle of IAV.
Virus particles attach to cell surface glycoproteins via HA-SA interactions and are subsequently internalized. Upon maturing of the endosome, the pH in the lumen drops driving HA-mediated fusion of the endosomal with the viral membrane. Consequently, vRNPs are released and enter the nucleus, where the viral polymerase complex transcribes viral mRNA and replicates the viral genome. Viral proteins are translated in the cytoplasm. Progeny virions assemble and bud from the plasma membrane and are ultimately released by NA cleaving cell-surface SA.

The viral genome is replicated by generation of a positive sense RNA lacking a 5' cap from the vRNA template and the subsequent synthesis of new genomic vRNA from the positive sense RNA template[61]. This process does not require priming and proceeds without host cell factors[70]. Newly synthesized genomic vRNA assembles into vRNP with newly synthesized polymerase and NP proteins and can in turn serve as template for replication or mRNA transcription. Finally, vRNPs are exported to the cytosol and trafficked to the plasma membrane. Re-entering of newly synthesized vRNPs into the nucleus is prevented by masking the nuclear localization signal on NP[4]. Segments contain a packaginging signal to ensure one copy of each segment is packaged into each budding progeny virion[71]. Other viral proteins align at the plasma membrane below patches of viral membrane proteins. Accumulation of viral proteins in the membrane enlarges the lipid raft domains and probably causes membrane deformation and curvature. HA, NA, M1, M2 are thought to concertedly recruit vRNPs and the necessary virus proteins and establish the virion structure[72]. Budding viruses are retained by HA interacting with SA on cell-surface glycoproteins and depend on NA cleavage of SA for release of progeny virus[66].

1.1.4. Hemagglutinin

HA is the most abundant membrane protein on an IAV virion. A spherical virion carries around 290-340 HA trimers and 24-50 NA tetramers[25, 27].

Initially, the HA protein is synthesized as precursor H0 and is cleaved protolytically into HA1 and HA2, which are linked by disulfide bonds[73]. Cleavage is conducted by intra- and extracellular proteases depending on the IAV subtype[74]. The HA structure is divided into the globular HA head (HA1 and some of HA2) and the HA stem (HA2), with the head carrying the receptor binding site (RBS) and being responsible for attachment and the stem harboring the fusion peptide [73] (Figure 3). The receptor binding pocket is formed by the 130 loop (amino acids 134-138) and 220 loop (amino acids 224-228) to the sides and the 190 helix (Glu 190 and Leu 194), His 183 and Thr 155 to the rear(Figure 3). The bottom of the binding grove is built by Tyr 98 and Trp 153(Weis et al., 1988). The amino acids in the RBS and the SA receptor interact via hydrogen bonds and van der Waals contacts(Weis et al., 1988). Amino acids in the vicinity stabilize the RBS without direct interaction with the receptor[43].

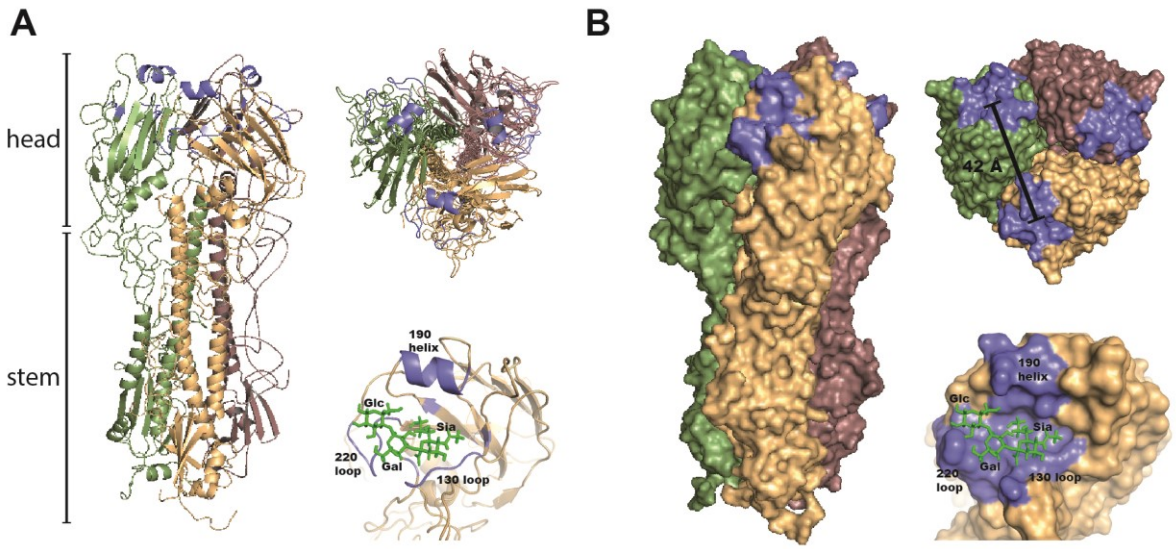

Figure 3: Structure of the HA protein.
(A) Crystal structure of the whole HA trimer (left), the top view (upper right) and the RBS with bound receptor analog (lower right). (B) Surface representation of the whole HA trimer (left), the top view (upper right) and the RBS with bound receptor analog (lower right). Images of the HA protein of influenza A/X31 virus (PDB, 1HGG) [2] were generated using PyMOL [3]. Individual monomers are colored separately, the binding pocket is marked in purple and the receptor analogue is displayed as green sticks.

HA undergoes cotranslational and posttranslational modifications in the ER and Golgi apparatus like host cell proteins. Hence, the oligosaccharides attached to HA depend on the host cell as well as the virus strain[75-77]. HA glycosylation is essential for correct folding and trimerization of the protein and for intracellular transport to the cellular membrane[78]. Furthermore, glycans shield antigenic sites from the host immune system but can also hamper receptor binding, which the virus then needs to compensate for by additional mutations[79-81]. Glycosylations also affect IAV virulence. Deletion of glycosylation sites in the HA head has led to increased virulence of IAV in mice, whereas additional glycosylation sites in the HA head resulted in attenuation[82]. In general, the number of N-

glycosylations on the HA head have increased over time[83-85]. Among H3N2 viruses, influenza A/X31 virus has two glycosylation sites in the globular head domain whereas A/Panama/2007/1999 has 5 glycosylation sites in the head domain [79]. In contrast, glycosylations of the HA stem domain remain mostly conserved across different strains.

IAV HAs are divided into Group 1 or Group 2 HAs depending on the HA sequence (Figure 4). Intersubtype variations range from 30 to 70 % sequence identity[86]. Despite being subtyped and grouped according to HA sequence, the intrasubtype variations are high as well, especially for the HA surface. The HA1 surface of an H3 HA from 2012 shares only around 70% sequence identity with the HA1 surface of an H3 HA from 1968[87]. There are some conserved residues in the HA RBS resulting in a conserved general structure, but the overall variability of the RBS within H3 HAs is high with only 52% sequence identity between the RBS of an 2012 HA compared to 1968[87]. This can be attributed to antigenic drift, which results in the accumulation of mutations especially in HA[88, 89].

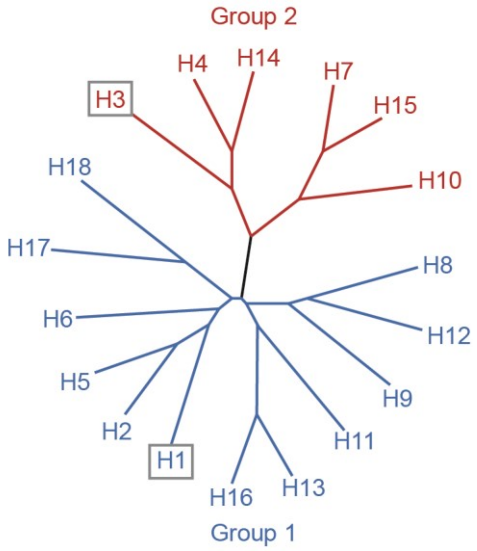

Figure 4: IAV HA phylogeny.
Based on the amino acid sequence, two groups (group 1 and group 2) of IAV HAs are distinguished. Only H1 of group 1 and H3 of group 2 (highlighted by rectangle) currently circulate in humans. Image modified from Wu and Panté [4]

Individual HA-SA interactions are weak[90]. IAV engages in multiple receptor binding events and stabilizes the attachment through high avidity, though the exact valency is still unknown[91-93]. In simulations, bimodal binding of receptors to RBS on the same HA, which are 42Å apart, resulted in the highest binding affinity, indicating a role of bimodal binding during attachment[94]. This notion is further supported by glycan array data suggesting preferred bidendate binding to glycans[95]. The interaction of IAV with living cells is highly dynamic. Unbinding events accompany attachment[93] and this off-rate depends on valency and NA activity[92]. The RBS does not show deformation upon receptor binding or unbinding[93]. The possibility of a secondary SA binding site on HA has been discussed, but its relevance to an infection has not been clearly proven[94, 96]. NA binds SA more strongly than HA and this bond is more stable. However, due to HAs higher abundancy and valency it is mainly responsible for attachment[97]. In fact, there is no clear correlation between high affinity binding of HA to its receptor and high infectivity of a virus[98, 99].

1.1.5. Hemagglutinin receptor

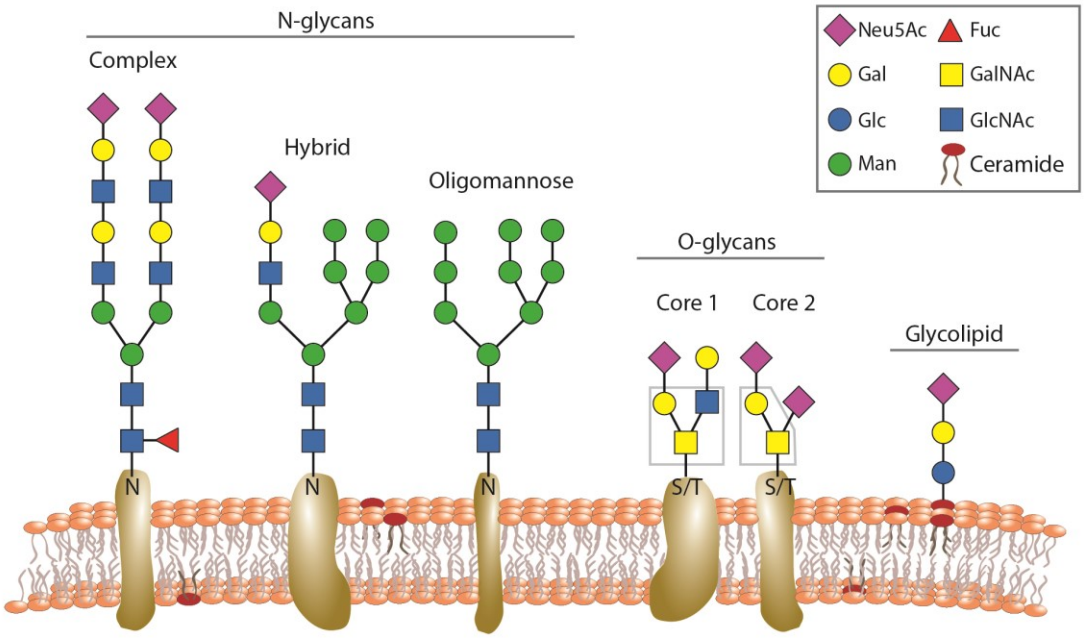

Figure 5: Major types of glycans on the cell surface.
Complex, hybrid and oligomannose N-glycans as well as core 1 and core 2 O-glycans and a glycolipid are depicted by one example each. The common cores of the O-glycans are boxed in grey. Image modified from de Graaf and Fouchier [100].

The mammalian cell surface is covered by a glycocalyx. The genome does not directly encode glycan structures. As such, glycan structures rely on a variety of factors and even small changes in external factors can cause a cell to produce vastly different glycans. Even without a change in any cue, the glycans may vary in their structure or even be absent entirely, a phenomenon called microheterogenity[101, 102]. The major types of glycans are distinguished according to whether they are attached to lipids, or to proteins either through an oxgen atom (O-glycans) or a nitrogen atom (N-glycans) (Figure 5). N-glycans are synthesized and covalently linked to an asparagine residue of the glycosylation motif Asn-X-Ser/Thr in the ER or Golgi network[101, 103]. Eukaryotic N-glycans share a core structure and are further divided into groups depending on how the structure extends from the core. Oligomannose N-glycans extend with only mannose residues, complex N-glycans feature multiple N-acetyllactosamine repeats and hybrid N-glycans consist of both[102]. Sialic acids are highly diverse sugars usually located at the termini of glycans. They have a nine-carbon backbone with a variety of linkages to the 2-position and various substitutions at the 4, 5, 7, 8 and 9 position. N-acetylneuraminic acid (Neu5Ac) and N-glycolylneuraminic acid (Neu5Gc) are common SAs found in mammals[104, 105].

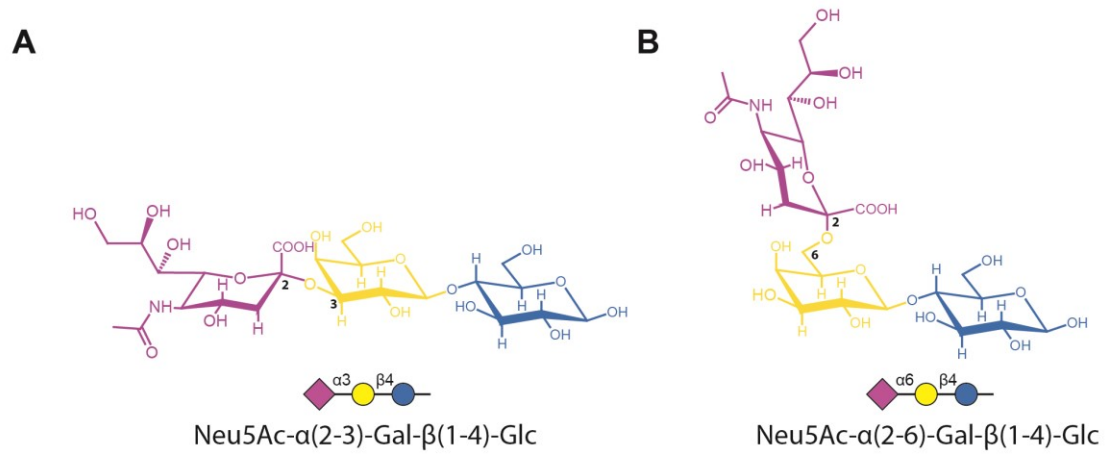

Figure 6: The typical IAV receptor Sialyllactose.
The difference between the α2,3-linkage (A) and the α2,6-linkage (B) of N-acetylneuraminic acid (Neu5Ac) to galactose (Gal) is visualized. The C-Atoms involved in the linkage of Neu5Ac to Gal are numbered in black. α2,3- and α2,6-Sialyllactose are presented in a chemical structure and given as symbol and word representation below. Sugars are colored to match the symbol representation.

Avian IAV preferentially bind to terminal Neu5Ac linked to a penultimate galactose via α2,3-linkage, whereas human IAV prefer α2,6-linkage[106, 107] (Figure 6). The amino acids primarily determining receptor specificity are located at positions 226 and 228[108, 109]. In the human lung and bronchus, a broad spectrum of both α2,6-linked and α2,3-linked SAs is expressed abundantly. This includes large bi-, tri- and tetra-antennary complex N-glycans with varying numbers of N-acetyllactosamine repeats, core fucosylated glycans, oligomannose glycans and diverse O-glycans. There is a higher degree of sialylation in glycans in the lung than in the bronchus and more. In the nasopharynx, glycans are less diverse and contain fewer N-acetyllactosamine repeats[99]. The upper respiratory tract contains predominantly α2,6-linked SA, whereas in the lower respiratory tract more α2,3-linked SA is found[110]. In birds, both α2,3-linked SA and α2,6-linked SA are found in the respiratory tract and the intestinal tract[111]. This differential distribution may be involved in determining the severity of an IAV infection.

However, there is emerging evidence that the linkage of the terminal SA to the penultimate galactose alone is too simplistic to characterize binding preferences. Instead, the specific receptor environment including the underlying glycans, fucosylation and sulfation determines host cell specificity[112, 113]. Shape and topology appear to be more important to the binding than the SA itself[114-116]. In fact, the avidity of H3N2 virus to the representative α2,6-linked trisaccharide receptor has decreased 4-fold between 1968 and 2001 and another 200-fold from 2001 to 2010 [117]. H3N2 viruses have evolved from binding a large breadth of glycans including short glycans to a more restricted binding profile with preferred binding of long, branched glycans with possible bidendate binding[87, 95, 117, 118]. Only α2,6, not α2,3-linked Neu5Ac can adopt conformations that enable bidendate binding[119]. The entropic penalty of α2,6-linked Neu5Ac binding to HA is larger than that of α2,3-linked Neu5Ac, because it has one rotable bond more, allowing for multiple conformations and more contact points with HA[115]. To overcome the entropic penalty and facilitate binding, a higher binding affinity is necessary[119]. Rather than canonical sialylated glycans recent H3N2 viruses increasingly bind mannose-rich phosphorylated glycans [118]. Neu5Acα2–8Neu5Acα

substructures, Neu5Gc and terminal galactose or GlcNAc have also been identified as receptors for viruses of different host species. An additional fucose on those glycan structures introduces a turning angle possibly leading to human-origin virus binding[116]. Addition of further glycosylations to the HA head also impacts receptor binding. Without HA glycosylation, HA receptor binding is much stronger[81, 120]. HA head glycosylations might also contribute to the evolving binding preference of longer glycan structures that are not sterically hindered by HA glycosylation[118]. Changes in receptor specificity driven by antigenic drift result in influenza viruses with a highly diverse receptor binding profile. Gulati et al.[121] tested 45 influenza virus strains but did not identify one single glycan that bound to all of them. When conducting binding analysis it important to keep in mind that there is no clear link between binding and replication, rendering it impossible to predict infectivity from glycan array binding profiles[99]. Along the same lines, changes in receptor binding specificity or affinity do not necessarily result in reduced viral fitness[121].

1.1.6. Neuraminidase

Next to HA, NA is the second major viral surface protein. NA is a sialidase and enzymatically cleaves the α-ketosidic linkage between terminal Neu5Ac and the penultimate sugar residue[122]. Therefore, the main function traditionally attributed to NA is the release of progeny virus from the cell surface during virus budding[66]. However, NA activity is not only important for the release of progeny virus, but also for penetrating the mucus barrier[123]. This mucus layer features an enormous number of sialylated O-glycans acting as decoy receptors for IAV. The virus needs HA/NA interplay for movement until it reaches functional N-glycan receptors on the cell surface that facilitate internalization[124].

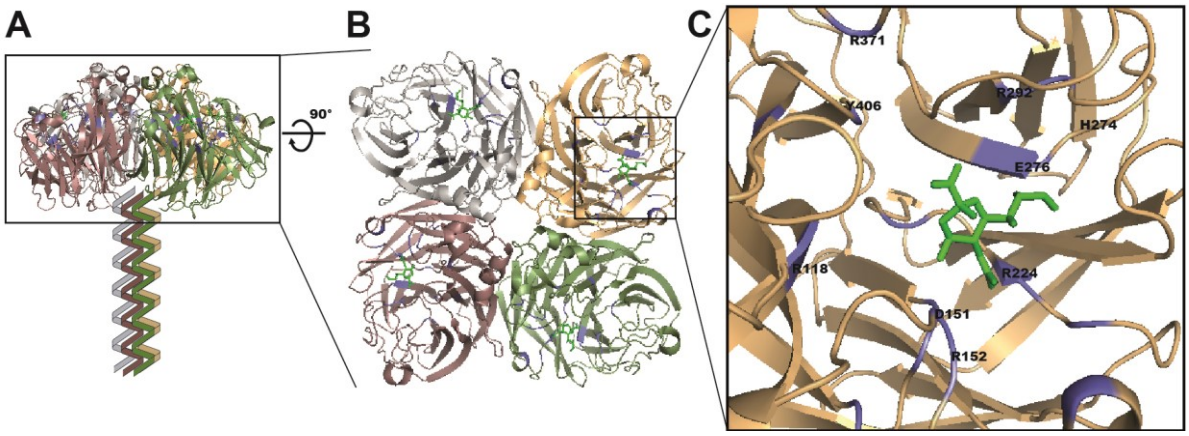

Figure 7: Crystal structure of the NA protein.
Images of the N2 NA protein (PDB, 2BAT)[125] as side view (A), top view (B) and SA binding site close up (C) were generated using PyMOL [3]. The structure of the stem has not been resolved yet and is depicted as helices here. Individual monomers are colored separately, the binding pocket including the active site is marked in purple and the sialic acid substrate is displayed as green sticks. Amino acids essential for NA activity[126] are given in black numbers.

Like HA, NAs are also subtyped according to their amino acid sequence with a total of 11 subtypes (N1-N11) described to date[18]. Intrasubtype homology is as high as 90%, whereas intersubtype homology is around 50%. Still, the overall structure is conserved among all NA subtypes[126]. NA is a homotetrameric protein with a box-shaped globular head that is connected to the viral membrane

through a thin stalk (Figure 7A). Each monomer harbors an active site that fits the substrate SA(Figure 7B). The main residues involved in the catalytic cleavage of the SA linkage are the highly conserved R118, D151, R152, R224, E276, R292, R371, and Y406 (Figure 7C)[126]. A second SA binding site that is not catalytically active has been described for the avian NA subtypes N6 and N9. The function of this second binding site is yet to be elucidated completely[127]. Curiously, in some H3N2 isolates after 1994 NA-dependent hemagglutination was noticed that was druggable with NA inhibitors, indicating a receptor binding function in the catalytic site[128]. Affinity of NA to the sialylated receptor was actually higher than that of HA[129]. This adds another layer of complexity to the balance between NA and SA that is required for efficient virus replication[123].

1.2. Influenza prevention and treatment

To date, annual vaccination is the most effective way to prevent seasonal influenza infection. Since the first inactivated monovalent vaccine preparation in 1942 influenza vaccines have been continuously improved and modified to yield the current vaccines containing either split virus or viral subunits[130]. In addition, live-attenuated influenza vaccines administered intranasally are available for children[131]. IAV subtypes H3N2 and H1N1 and IBV lineages Victoria and Yamagata cause most human illnesses of seasonal influenza[132]. A quadrivalent vaccine aiming at protecting from all four is recommended in Germany since 2018, replacing the former recommendation of a trivalent vaccine containing only one IBV component[133]. Vaccination is only recommended for risk groups and people with high exposition such as medical staff[134], which is in line with the WHO recommendations[6].

HA is the main antigen. Most antibodies conferring immunity target one of the five major antigenic sites on the HA head to impede the RBS and thus attachment or the HA stem and thus hamper fusion[135]. Influenza viruses mutate to escape neutralization by antibodies, sometimes also introducing glycosylation sites in or near antigenic sites to prevent antibody binding. As a result of this antigenic drift, the antigenic sites on the HA head vary considerably between strains although the overall structure remains conserved[135, 136]. Since influenza viruses evolve rapidly, the vaccine components need to be matched to the strains circulating. Thus, recommended vaccine strains are updated by the WHO twice a year. Still, vaccine effectiveness between 2004 and 2015 was only 33% for IAV H3N2, 54% for Influenza B and 61-67% for IAV H1N1[137]. Especially in patients aged 65 and older, the main vaccine target group, effectiveness against IAV H3N2 viruses is suboptimal[138].

In the case of an influenza pandemic, the situation is even more problematic. It takes approximately 5-6 month until the first vaccine supply is available once a new pandemic flu stain is identified[139] possibly resulting in high economic loss due to measurements like social distancing that need to be in place during this delay[140]. Therefore, additional tools to fight influenza virus infection are urgently needed.

1.2.1. Antiviral inhibitors

Anti influenza drugs can be directed at many steps of the influenza virus replication cycle, either by targeting the virus directly or by targeting host factors essential for viral replication[141]. Globally

licensed anti influenza inhibitors fall into three classes: M2 inhibitors, NA inhibitors and polymerase inhibitors[142]. Development of resistance against existing antivirals, especially when being used in the clinics, require frequent development of derivates and stress the need for new antiviral substances[143]. In the following, an overview of licensed inhibitors and promising inhibitor candidates currently in development is given.

1.2.1.1. Host directed inhibitors

One way to prevent influenza virus infections is to block host cell components essential for viral replication[141]. Since influenza virus entry is mediated by attachment to SA receptors in the airway epithelium, these receptors were targeted by the inhalation drug candidate DAS181, a recombinant fusion protein with sialidase activity. DAS181 cleaves avian and human SA receptors in the airway epithelium and thereby inhibits virus replication in the nM range[144]. This strategy proved to be very effective against influenza A and B viruses including H5N1 and NA inhibitor resistant strains in both mouse and ferret models[145, 146]. However, concluding from a phase I trial, adverse respiratory effects occur when DAS181 is applied for more than seven days and the induction of antibodies against DAS181 drastically limits the dosing as well as repeated application[147]. Resistance can occur also to this inhibitor, as serial passaging selected for mutations in HA (G137R, S136T, S186I) and NA leading to increased receptor binding and decreased NA activity[148]. A different host directed inhibitor aims at impeding maturation of viral HA. Thiazolides like Nitazoxanine impair intracellular transport of HA from the ER to the golgi network, resulting in HA not being trafficked to the host cell membrane as required for virus budding[149]. The reduction in symptoms duration was comparable to NA inhibitors in one clinical trial[150] in contrast to no clinical benefit in other trial[151], so further investigations in this regard are required.

1.2.1.2. M2-inhibitors

The first class of anti influenza inhibitors was developed in the 60ties and directed against the viral ion channel M2. Adamantane derivates Amantadine and Rimantadine bind to the influenza A virus M2 ion channel and block its function by physically occluding the channel[152, 153]. Adamantanes are specific to influenza A virus M2 and therefore not effective against influenza B virus. M2-inhibitors shorten the duration of influenza symptoms by one day, but can have adverse effects on the central nervous system[154]. This eventually led to amantadine gaining an indication for Parkinson's disease[155]. In addition to the toxic side effects, the development of resistance against adamantanes dramatically limits their applicability for the treatment of influenza. A single point mutation in one of five positions in the sequence of the M2 protein is sufficient to render the virus resistant[156, 157]. During the 2005/2006 influenza season, 92.3% of influenza isolates carried a mutation conferring resistance to adamantanes, so the CDC recommended against the use of adamantanes for the treatment of influenza[158]. Albeit the use of adamantanes being limited to the Parkinson's Disease indication since 2006, influenza viruses currently circulating are still resistant[159].

1.2.1.3. NA-inhibitors

Influenza virus membrane protein NA cleaves sialic acid to release virus progeny from the host cell surface and also to penetrate the host mucus barrier. The design of inhibitors against NA was enabled by the determination of the crystal structure of the SA binding pocket[160]. NA evolves continuously and – like HA – is highly variably between influenza viruses. Still, the active site of NA contains 8 conserved residues including residues directly contacting the SA substrate[161]. This knowledge was exploited for drug design. Specifically, two modifications were made to SA to generate Zanamivir, an SA analogue with higher binding affinity to the NA receptor binding pocket then SA and thus inhibiting NA activity[162-164]. Firstly, the negatively charged hydroxy-group on the C4 position of SA aligned with a negatively charged part in the NA active site and was therefore exchanged to a positively charged amino-group. Additionally, a guanidino group was introduced for another charge-based favorable interaction[162-164]. To allow oral administration, modifications to Zanamivir were made, resulting in a second NA inhibitor, Oseltamivir[165]. First Zanamivir and then also Oseltamivir were both approved by the FDA in 1999. However, they are only licensed for treatment of uncomplicated influenza, as no controlled trial data exists on serious infections[166]. The therapeutic benefit of NA inhibitors in uncomplicated influenza is modest and reduces symptom duration only by 17 to 25 hours[167], but the risk of death is reduced by half, indicating a great benefit for treatment of serious influenza in adults[168]. Despite being approved for all age groups, it is still unclear whether NA inhibitors also reduce mortality in children[169, 170]. NA inhibitors are less effective against influenza B viruses than influenza A viruses[171] and can even be without clinical benefit in uncomplicated influenza B virus infections[172].

Resistance to NA inhibitors can arise due to mutations in structural and catalytic residues of the active site of NA, even in residues that were previously considered conserved[161]. To fit Oseltamivir with its hydrophobic pentyloxy side chain in the NA active site, residue E276 (N1 numbering) needs to turn so its carboxyl group is oriented away, subsequently allowing hydrophobic interaction of Oseltamivir with the underlying methylene of E276[173, 174]. This turn of E276 is prevented by the mutation H274Y, one of the most common mutations conferring Oseltamivir resistance. Zanamivir does not have this bulky side chain and thus does not need rearrangement of the active site. Instead, it interacts via hydrogen bonds with the carboxyl group of E276 like the natural substrate SA[173, 174]. As a result, cross-resistance between zanamivir and Oseltamivir is limited despite both compounds being SA analogues, highlighting the fact that small changes can impact binding greatly. In addition to mutations in NA, mutations in HA can also confer resistance to NA inhibitors. In fact*, in vitro* selections of resistant variants have predominantly generated mutations in HA, specifically in the RBS. Mutations like T155A, V223I, R229I, K222T, S186F and S165N in the H1 HA RBS decrease the affinity for SA, resulting in mutant viruses less dependent on NA activity[161, 175]. Often, two or three mutations in HA are selected upon serial passaging with Oseltamivir, such as G135E in combination with N248T in H3 HA, although each mutation individually proved to be associated with resistance, probably by altering receptor specificity or SA affinity[176]. HA mutations conferring Oseltamivir resistance are diverse and have not been limited to the RBS but can occur in many different regions of HA[161]. HA mutant viruses are cross-resistant to all NA inhibitors, since the

effect does not depend on how NA is inhibited. Technically, their NA activity is not resistant to inhibition though, the HA mutations just balance the NA inhibition.

A loss of fitness is associated with the single NA mutation H274Y (N1 numbering), leading to the emergence of resistance against NA inhibitors being underestimated for a long time, but compensatory mutations enable the virus to retain full infectivity[177]. Oseltamivir resistance occurs in all age groups if treated but at the highest frequency in very young children age 1-5 [178]. However, Oseltamivir resistant viruses can emerge and persist even without Oseltamivir usage[179]. Widespread resistance to Oseltamivir developed in pre-pandemic H1N1 viruses[180, 181], which were then replaced by the mostly Oseltamivir susceptible pandemic H1N1 viruses in 2009[182]. However, increasing cases of Oseltamivir resistant viruses in the 2010/2011 season demonstrate the potential of also pandemic H1N1 viruses to emerge and circulate[183].

Apart from Oseltamivir and zanamivir, other SA analogues acting as NA inhibitors have been developed. One of them is peramivir, which is also licensed in the USA since 2015[184] and in Europe since 2018[185]. Peramivir shares features with Oseltamivir and zanamivir, such as a hydrophobic side chain requiring rearrangement of the NA active site for binding like Oseltamivir and the guanidino substitution of zanamivir[186]. Therefore, resistance mutations against either zanamivir or Oseltamivir can confer cross-resistance to peramivir. Another zanamivir-based compound is the long-acting laninamivir, which is licensed in Japan for therapeutic and prophylactic treatment[187].

Recent NA inhibitor development efforts mainly focused on improving zanamivir or Oseltamivir. Derivates of Oseltamivir with improved pharmacokinetic properties aiming to minimize resistance mechanisms were generated[188, 189] as well as covalent NA inhibitors based on zanamivir and Oseltamivir[190]. Another approach is the construction of zanamivir dimers[191], trimers and tetramers[192], which inhibited NA activity more effectively than zanamivir.

1.2.1.4. Polymerase-inhibitors

Another strategy to inhibit influenza viruses is to interfere with viral RNA transcription. Several drugs that interfere with different subunits of the viral polymerase have been developed.

Favipiravir is a purine nucleoside analogue acting as a competitive inhibitor of influenza PB1 and also other viral RNA polymerases. Phase II and III studies have been completed[193], leading to its approval in Japan in 2014 for the treatment of infections with influenza viruses resistant to other available inhibitors[194]. Since viral RNA is replicated inaccurately or not at all under favipiravir treatment, it has been suggested to have a high threshold for resistance mutations[195]. Indeed, resistant variants have proven difficult to isolate in cell culture[196, 197], but resistance conferred by the combination of one mutation in PB1 and PA each has been described[198]. Major drawbacks of favipiravir are its teratogenicity and modest clinical benefit of only a few hours of illness alleviation if applied in monotherapy. Furthermore, varying efficacy in clinical phase III studies warrant further studies[199].

Pimodivir inhibits influenza A PB2 cap-snatching and thus RNA transcription[200]. It was well tolerated in a phase II study and showed virologic improvements over the placebo control[201]. However, a phase III study in hospitalized and high-risk outpatients was prematurely terminated[202], underlining the difficulty of translating the antiviral potential of drug candidates in pre-clinical studies to clinical applications.

A more successful inhibitor of the influenza polymerase is baloxavir marboxil, which was approved for the treatment of influenza in Japan and the USA in 2018[203, 204]. Baloxavir marboxil binds to PA and selectively inhibits the cap-dependent endonuclease activity, which reduced the viral load one day after treatment and accelerated alleviation of symptoms[205]. The viral load was reduced more effectively with baloxavir marboxil than with Oseltamivir, but the time to symptoms reduction of influenza A virus infection was comparable for both inhibitors[172]. A single point mutation in PA, namely I39T/M/F, confers resistance to baloxavir marboxil[206, 207]. Resistance emerges rapidly during treatment of uncomplicated influenza[172] and resistant variants can be transmitted[208].

1.2.1.5. HA inhibitors

Inhibitors targeting HA mainly use one of two mechanisms: They either interfere with HA attachment to its receptor, or with fusion of the viral and the endosomal membrane, thus preventing escape into the cytoplasm. Therefore, they impede early steps of the viral replication cycle. Blocking viral entry has proven to be a successful strategy before. In the treatment of human immunodeficiency virus (HIV), for example, Maraviroc and Fostemsavir bind CCR5 and gp120, respectively, and thus interfere with attachment[209, 210].

The most prominent inhibitor of influenza virus HA fusion is the small molecule compound Arbidol, which has been licensed for the treatment of influenza A and B infections in Russia for decades and also in China since 2006[211]. Arbidol is an indole derivative that binds at the interface of HA2 from different monomers in the upper stem region of the HA trimer (Figure 8). It interacts mainly by hydrophobic interactions, but also forms salt bridges accompanied by conformational rearrangements. This network of interactions stabilizes the prefusion conformation of HA, thus preventing the conformational change required to expose the fusion peptide and ultimately fusion[1]. Consequently, resistance mutations were detected in the HA stem. The four single point mutations K51N, K117R, Q27N and Q42H in the HA2 subunit of the HA stem confer

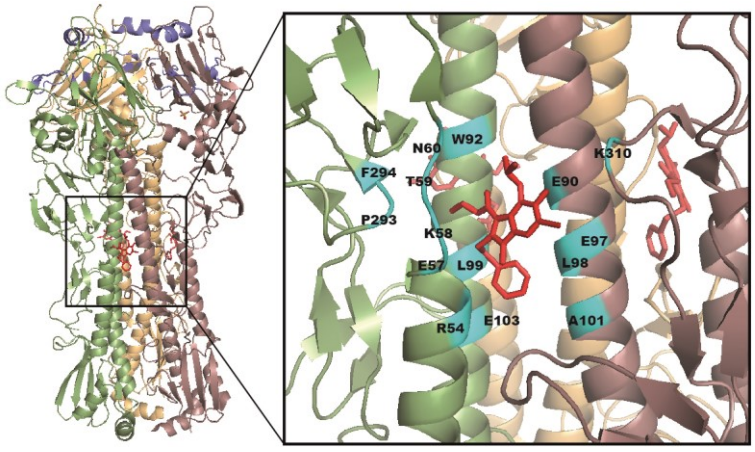

Figure 8: Structure of the HA protein in complex with the small molecule inhibitor Arbidol.
Images of the HA protein of A/X31 (PDB, 5T6N)[1] were generated using PyMOL [3]. Individual monomers are colored separately, the Arbidol binding pocket is marked in cyan and Arbidol is displayed as red sticks. Arbidol binds at the interface of two HA monomers in the HA stem region.

resistance to arbidol[212]. Though curiously, those mutations are not directly at the arbidol binding site[1]. IC_{50} values determined range from 4.4 to 12.1 µM depending on the influenza strain and with an TC_{50} of around 60 µM[212, 213], the therapeutic window may be too narrow. Despite being proposed as a broad inhibitor of several different viruses[211], arbidol has so far failed to become an approved drug for any viral infection outside Russia and China[214].

Passive immunization using broadly neutralizing antibodies is another approach targeting the HA protein. Several monoclonal antibodies targeting conserved regions of the HA protein have been developed. CR6261/CR8020 and MEDI8852 target different HA stem epitopes were being evaluated in phase II studies[215] but have since been withdrawn. MHAA4549A, another monoclonal antibody directed at the HA stem, was an efficient inhibitor of influenza virus infections in pre-clinical studies, but showed no improvement of clinical outcome in a phase II trial[216]. CT-P27 is a mix of two antibodies shown to be effective in vitro and in vivo[217], but results on the clinical phase I and II studies conducted have not been published even years later[218]. There is some hope for a successful monoclonal antibody in VIS410, which was well tolerated and efficient in a phase IIa trial, which will be followed up by a phase IIb trial[219]. These examples underline the difficulty of translating pre-clinical success into functional antiviral drugs. Monoclonal antibodies face an additional hurdle, because they were not deemed cost efficient. However, they may still bridge the time between the discovery of a new pandemic virus and the long development of a potential vaccine[218]. In preparation for future pandemics, especially monoclonal antibodies effective at inhibiting avian influenza viruses are of interest. Several antibodies have been shown to inhibit H5N1 viruses *in vivo*, including the above mentioned MEDI8852[220, 221]. Despite several monoclonal antibodies against influenza virus HA being in development, none has been approved yet[218] and as a consequence, monoclonal antibodies are not part of the pandemic preparedness plan in Germany[222]. Nonetheless, this does not imply that therapy with monoclonal antibodies cannot be successful. Monoclonal antibodies can be a powerful tool to combat viral diseases, as shown by their contribution in the fight against other viral infections. As early as 1998, the monoclonal antibody Palivizumab was approved as a prophylaxis for respiratory syncytial virus (RSV) in high-risk infants[223]. As Palivizumab requires monthly administration, an improved monoclonal with longer half-life is currently in clinical phase II/III trials[224]. Moreover, INMAZEB, a cocktail containing three monoclonal antibodies directed against Zaire ebolavirus glycoprotein improved survival in a clinical trial[225] and was since approved by the FDA for treatment of Ebola virus disease[226]. Antibody cocktails aiming at pan-Ebolavirus protection are also in development[227]. Furthermore, two monoclonal antibody cocktails directed against the RBD of SARS-CoV-2 spike glycoprotein were shown to reduce hospitalizations in COVID-19 patients and were therefore given an emergency use authorization by the FDA[228, 229]. However, antibody resistance can develop, as has happened in SARS-CoV-2 variants B.1.351, P1 and B.1.617.2, limiting the effectivity of monoclonal antibodies[230-232].

A variety of peptides both of natural origin and designed in silico have shown promise as anti influenza HA inhibitors[233]. Several peptides target the conserved HA stem region and inhibit fusion[234-236]. The peptide Flufirvitide-3 binding to the HA stem made it into clinical trials. However,

no benefit compared to placebo could be observed[237]. Antibodies have also been widely used as starting point for the design of peptides. Peptides derived from antibodies binding to the HA RBS efficiently inhibited virus infection in vitro and peptide binding was easily optimized by substitution of amino acids[238]. The best binder, termed PeB, matched best the conserved HA RBS. Along the same lines, peptides mimicking antibody loops were designed to limit the possibility of escape mutations[239]. Peptides based on broadly neutralizing stem antibodies were able to inhibit H1N1 and H5N1 strains[240]. The same group also developed a small molecule mimicking the binding mode of a different broadly neutralizing stem antibody that protected mice against challenge with a influenza H1N1 virus[241]. The peptide FluPep is blocking viral attachment to cells as well[242]. A different approach involves the design of peptides to mimic the carbohydrate receptor and thus provide an easy to prepare competitive inhibitor[243].

There is also a variety of small molecules that interfere with the attachment of HA to its receptor. N-cyclohexyltaurine for example, was found to bind to the RBS of both group 1 and group 2 HAs by mimicking the SA binding mode[244]. However, whether this translates to inhibition of infection *in vitro* and *in vivo* still remains to be investigated. Another candidate, Neoechinulin B, inhibited attachment of influenza viruses to cells but a lot of compound was required to achieve an effect[245]. Individual HA-SA interactions are weak[90], so IAV engages in multiple receptor binding events and stabilizes the attachment through high avidity[91, 93]. This might explain why it has so far proven difficult to inhibit HA attachment using monovalent inhibitors like monovalent SA[246]. A way to overcome this is either by employing high affinity binders, which in turn face the challenge of limited broad activity, or to apply the principle of multivalency. The latter is further discussed in the section below.

1.2.1.6. Multivalent HA inhibitors

Individual HA-SA interactions are weak[90] and therefore influenza viruses rely on the cooperative binding of multiple HA proteins to multiple cell-surface receptors for attachment. This principle is called multivalency and is not restricted to influenza viruses but applies to numerous biological systems such as other viruses or bacteria attaching to cells or cell-cell contacts[91]. The valency of an interaction corresponds to the number of same interactions between two particles. The exact valency with which influenza viruses bind their SA receptors is still unknown[92]. As virus attachment to cells is highly dynamic and accompanied by many binding and unbinding events[93], it is conceivable that the valency of the interaction between an influenza virus particle and a cell may be dynamic as well. In case the valency is unknown, Whitesides et al. introduced the enhancement factor β to describe the increased binding strength of a multivalent interaction in contrast to the monovalent counterpart[91].

Several distinct effects can contribute to the overall binding strength of a multivalent interaction between virus particle and cell. Binding of a ligand to its receptor comes at an entropic cost that is made up of translational, rotational and conformational entropies. Rotational and translational entropic cost comes from the degrees of freedom being lost upon binding. The translational entropic cost additionally depends on particle concentration and increases with decreasing

interaction partners. A conformational entropic cost is payed due to reduced number of conformations a ligand can assume after binding. The higher the constraint inflicted on the ligand compared to the unbound state, the higher the conformational entropic cost. Therefore, conformational entropic cost depends on the flexibility of the multivalent system. The more flexible the system, the higher the entropic cost[91]. Given that the conformational entropic cost is smaller than the translational and rotational entropic cost, the first binding event, in example the first viral HA RBS interacting with the first cellular SA receptor, needs to pay the highest entropic penalty, while all following binding events face lower entropic costs. This results in the entropic barrier being lower for multivalent systems, enhancing their overall affinity[247] and was termed the chelate effect. Furthermore, the first binding event can enthalpically enhance or diminish the consecutive binding events. Rigid polyvalent systems are more likely to be subject to enthalpically diminished binding due to spatial mismatches[91]. This means, enthalpy and entropy have counteracting and compensating effects on the affinity of an interaction depending on flexibility. Flexible systems favor enthalpic enhancement at the cost of higher entropic penalty and conversely, rigid systems pay lower entropic penalty but may face enthalpic diminishment[91, 248]. Another relevant phenomenon is statistical rebinding. Due to the first HA-SA interaction, other HA trimers are in proximity to the cell surface with more SA receptors. If the first HA releases its receptor, other HA-SA interactions restore the overall bound state of the virus, leading to slower off-rates[249].

A variety of multivalent systems that compete with HA receptor binding have been evaluated as influenza virus inhibitors so far. Some of the first multivalent inhibitors were based on polyacrylamide or polyacrylate backbones functionalized with SA, demonstrating early on that the inhibition of influenza virus was more efficient compared to monovalent versions of those compounds[250-253]. These pioneering studies showed that both entropically enhanced competitive inhibition[251] and steric shielding[254] contribute to the observed inhibition of hemagglutination. Unfortunately, acrylamide-based constructs are highly toxic[255, 256] and have low biocompatibility[257]. Thus, they are not suited for *in vivo* applications. Another widely studied material is sialylated PAMAM scaffolds[258-261]. However, this backbone is associated with toxicity concerns as well[262]. Improved biocompatibility has since been addressed by a variety of other sialylated constructs, such as chitosan[263, 264], liposomes[265-268], gold nanoparticles[269, 270], phage capsids[271], erythrocyte membrane coated nanostructures[272, 273] and polyglycerol[274, 275]. Whether toxic or not, all constructs contribute to understanding the parameters essential in successful scaffold design, which will be discussed in the following paragraphs.

Major factors relevant to the design of sialylated systems are scaffold size, flexibility, ligand density and the linker or spacer between SA and the backbone. Scaffold size was shown to be important as a determinant of steric shielding and multivalency effects[276]. Virus infection was more potently inhibited by compounds of larger sizes, an effect that can in part be attributed to cross-linking of virions by larger compounds[270, 274] as well as shielding effects[94]. Further addition of ligands to a scaffold does not increase binding inhibition infinitely. The ligand density, also called degree of functionalization, reaches a saturation point after which further addition of ligands does not

increase binding inhibition[260, 274]. This may be explained by the steric repulsion of unbound ligands from the surface, which increases with increasing ligand density, counteracting the decrease in Gibbs free energy also caused by the increased ligand density[275]. An optimum degree of functionalization therefore needs to be determined for each multivalent system[277]. Another important factor is scaffold flexibility. A flexible scaffold one the one hand can access and bind more receptors due to more attainable conformations[277]. On the other hand, a rigid scaffold reduces possibly undesired degrees of freedom that can hamper binding due to entropic penalties, as discussed above. Bhatia et al. assessed the effect of scaffold flexibility in a study comparing a linear, flexible polyglycerol scaffold to a dendritic, rigid polyglycerol scaffold. They were able to demonstrate that the linear constructs were more efficient at inhibiting influenza virus infection in vitro and in vivo than the dendritic constructs[275]. However, this result is specific to the exact scaffold configuration and may differ in other multivalent systems. Another factor that proved essential is the linker or spacer between the SA functionalization and the scaffold backbone. Several groups have evaluated linkers in their systems. Lauster et al. used ethylene glycol linkers of different length to link SA to a phage capsid scaffold, of which the shortest one, monoethylene glycol, yielded the compound most effective at inhibiting influenza virus binding independent of subtype[271]. Similarly, glycopolymers inhibited influenza virus binding best with a medium length linker, which was also ethylene glycol[278], and sialylated gold nanoparticles were more effective with shorter linkers as well[279]. In contrast, shorter linkers and shorter ligand moieties resulted in higher IC_{50} values for trivalent constructs[280] and brush polymers[281]. As it was predicted that the free energy of a multivalent binding not necessarily depends strongly on linker length, the optimum linker is not thermodynamically obvious[282]. Molecular modeling revealed that the optimum linker length is slightly longer than the distance between the ligand and the receptor, and that in a suboptimal linker it is preferable to have longer rather than shorter linker length[283]. In result, the linker is another component highly dependent on the exact scaffold configuration and needs to be optimized for each system.

All scaffolds can be divided into two different groups depending on whether the functional unit is distributed statistically or whether the system is defined. Most scaffolds fall into the former group, since high valency is easier to realize in statistically distributed systems. The latter group has the advantage that precise design can match the target surface optimally while simultaneously reducing unnecessary degrees of freedom that can inflict entropic penalties on the binding. Such constructs are more difficult to realize with high valency[284] and thus often are limited to bi-, or trivalent systems[285-287]. Larger defined systems were achieved by PAMAM dendrimers[260, 261]. The most sophisticated defined system to date is sialylated bacteriophage capsids engineered to match the geometry of HA binding sites (Figure 9). The capsid of Qβ phages consists of 180 copies of the coat protein assembled into an icosahedral structure, with each copy of the coat protein being functionalized with SA to serve as a multivalent inhibitor. Sialylated phage capsids were able to inhibit influenza virus infection with a subnanomolar IC_{50} value and showed the potential to alleviate symptoms of disease in mice[271]. However, synthesis and purification of phage capsids at larger quantities still pose a challenge, thus limiting their potential for therapeutic applications.

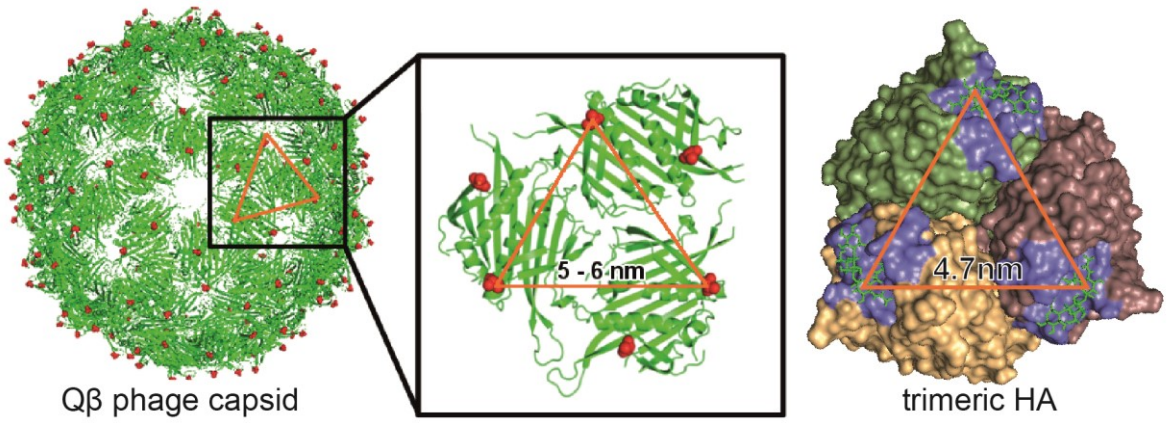

Figure 9: Functional Qβ phage capsids that match the distances between HA RBSs structurally.
Red dots one the phage capsid represent position K16 of the coat protein that was functionalized with SA. The distance between SA attachments on the capsid geometrically matches the three RBS on one HA trimer, as visualized by the orange triangle. Image modified from Lauster et al.Lauster, Klenk, Ludwig, Nojoumi, Behren, Adam, Stadtmüller, Saenger, Zimmler, Hönzke, Yao, Hoffmann, Bardua, Hamann, Witzenrath, Sander, Wolff, Hocke, Hippenstiel, De Carlo, Neudecker, Osterrieder, Budisa, Netz, Böttcher, Liese, Herrmann and Hackenberger [271].

Aside from SA only, longer sialylated sugar chains have also been incorporated into multivalent scaffold systems. One such example is conjugation of the biantennary sialyllactosamine with an α2,6-linkage of the SA to the penultimate galactose to a polyacrylic acid (PAA) backbone, which was able to bind a variety of human influenza viruses and reduce symptoms of disease in mice[257]. The same group also conjugated the trisaccharide sialyllactosamine to the PAA backbone and were thus able to protect mice from lethal challenge with influenza virus[288]. Similarly, sialyllactose conjugated to PAMAM dendrimers show inhibitory potential towards human and avian influenza viruses depending on the linkage of the terminal SA to the penultimate galactose employed in the sialyllactose-functionalization[260, 261]. Understandably, a polyacrylamide or polyacrylic acid-based carrier is not recommended for human applications due to the lack of safety data, but the incorporation of sugars extending beyond the terminal SA into multivalent systems is a promising prospect in biocompatible polymers[257]. As a more biocompatible approach, liposomes carrying sialyllactosamine successfully neutralized influenza virus[289] and liposomes carrying the oligosaccharide LSTc have achieved inhibition of influenza virus infection at nanomolar concentrations[268]. Furthermore, scaffolds made of polyglutamic acid carrying sialyllactosamine with multiple lactosamine repeats protected MDCK II cells from infection at IC50 values in the nM range[290].

Multivalent systems for inhibition of HA can also be functionalized with components other than the sialylated receptor, such as HA binding peptides. The first report in this regard was the multivalent presentation of PeB[238] on dendritic polyglycerol scaffolds, which showed more efficient inhibition of influenza virus infection[291]. Another example is FluPep[242], which had 10-fold higher antiviral activity when conjugated to gold and silver nanoparticles compared to monovalent FluPep[249].

Many characteristics render multivalent sialylated polyglcerols (PG) advantageous as anti-influenza virus inhibitors, which is why they were studied in the work at hand. Importantly, they are low molecular weight, water-soluble, chemically stable and highly biocompatible[292-294]. Some esters of

oligoglycerols have even been approved by the FDA for use as food or pharmaceutical additives, underlining their safety[295]. Furthermore, hydroxyl groups on the PG backbone allow a broad range of modifications that are easily realized. This is especially important when considering that the exact scaffold configuration is fundamental in the design of effective inhibitors as discussed earlier in this section. The thiol-ene linker between the SA functionalization and the PG is hydrolytically stable, rendering it unsusceptible to cleavage by viral NA[275].

Bhatia et al. synthesized linear and dendritic polyglycerols (LPG and dPG) to determine the which scaffold was more efficient at inhibiting influenza virus infection (Figure 10)[275]. They also synthesized both LPG and dPG at different degrees of functionalization (DF) in order to optimize SA density. Compounds are named according to the following pattern: $PG_{MW\ scaffold}SA_{DF}$. The optimum degree of sialylation was revealed to be different for linear and dendritic PGs. The most potent LPG compounds were $LPG_{10}SA_{0.40}$ and $LPG_{10}SA_{0.70}$, which have 40% and 70% SA functionalization, respectively, and the most potent dPG compound was $dPG_{10}SA_{0.15}$, which has 15% SA functionalization. Overall, the optimized LPG was more effective at inhibiting influenza virus A/X31 (H3N2) than the optimized dPG. SA is linked differently to dPGs and LPGs originating in the preparation by copper-catalyzed Sharpless-Huisgen click reaction and thiol-ene coupling, respectively. To control for this difference, $LPG_{10}SA_{0.20}$ with a DF at the dPG optimum and the corresponding linkage was prepared by copper-catalyzed click reaction. This compound was able to prove that the better performance of the optimized LPG compared to the optimized dPG was indeed due to the different scaffold[275].

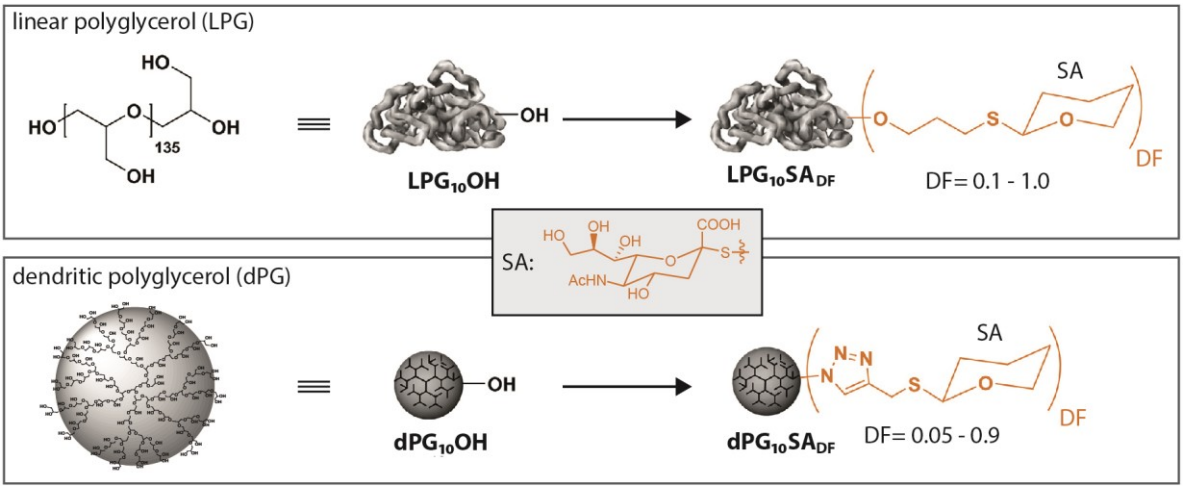

Figure 10: Structure of linear and dendritic polyglycerol (PG).
The hydroxyl groups are functionalized with SA at different degrees of functionalization (DF) using thiol-ene coupling (LPG) or copper-catalyzed Sharpless-Huisgen click reaction (dPG). The SA functionalization is statistically distributed on the scaffold. Control compounds are not functionalized. Images modified from Bhatia et al.[275] and Bhatia, Dimde and Haag [296].

While optimized LPG and dPG were very effective at inhibiting influenza virus A/X31 (H3N2) infection with IC_{50} values in the nanomolar range, their potential for broad activity against a variety of IAV strains remains to be fully explored. Influenza viruses evolve and accumulate mutations especially in HA[88, 89]. Especially the RBS of HA is highly variable, with a sequence identity on the amino acid level that can be as low as 52% between two H3H2 viruses[87]. The change of receptor binding profile toward long, branched glycans[95, 117, 118] discussed in section 1.1.5 is a result of this

variability. It cannot be assumed that a compound raised against HA of one influenza strain is also effective against other influenza strains, because receptor binding properties can be considerably different. With these considerations in mind, many groups have tested their compounds for broad activity against different influenza subtypes and strains[253, 261, 297, 298], but it still remains a problem often neglected[252, 281, 286, 288, 299-301]. Another problem is posed by the fact that often just the binding of a compound to virus particles or even just HA is investigated[279, 286, 300, 302]. However, the best binder might not be the best inhibitor, since there is no clear link between virus binding and replication[99].

Despite several viruses besides IAV binding to SA (refer to section 1.1.6), the usage of multivalent systems incorporating SA for inhibition of viruses other than influenza virus has not been as extensively explored so far. However, some advances in this regard have been reported. A scaffold of human serum albumin functionalized with α2,3-linked sialyllactose or with SA inhibited adenovirus type 37 infection sucessfully[303, 304]. Furthermore, the importance of sulfated polysaccharides to the SARS-CoV-2 spike glycoprotein was demonstrated[305] and inhibition of infection by multivalent polysaccharides was shown *in vitro*[306]. In addition, spike protein also bound to sialic acid derivates multivalently displayed on gold nanoparticles[307], so it is conceivable that both multivalency and sialic acids might be employed to design inhibitor candidates against SARS-CoV-2.

1.3. Aim of Study

The current tools to fight influenza virus infections consist of vaccines with somtiems disappointing effectiveness[137] and small molecule inhibitors, against which resistance emerges rapidly[143]. Therefore, additional antiviral agents to combat influenza virus infections are needed urgently.

The viral surface protein HA is involved in virus attachment to host cells and thus poses a promising drug target, as inhibiting attachment and consequently cell entry can abrogate infection completely[308]. As individual HA-SA bonds are weak[2], multivalent compounds presenting SA units on their surface are employed to inhibit virus binding competitively[250-253, 309].

Sialylated polyglycerols (PGs) are effective multivalent inhibitors with advantageous properties, such as their low molecular weight, biocompatibility and easy modification[275]. However, their effectivity has so far been only explored against few influenza virus strains. As influenza viruses evolve, the HA RBS and the receptor binding profile evolve as well[88, 89, 95]. Therefore, it is key to investigate any potential new inhibitor for broad activity against a variety of influenza virus subtypes and strains. The aim of this study is to evaluate and characterize multivalent sialylated PGs as anti-influenza virus inhibitors. Early in this study it became apparent that the inhibitory capacity of PGs functionalized with SA was restricted to a limited number of IAV strains. Therefore, the majority of this study focused on elucidating the molecular basis for this restriction. For this purpose, resistance to a SA-functionalized PG was induced in a susceptible IAV strain. The resulting virus variants were characterized and analyzed for their receptor binding properties. The underlying objective was to modify PGs strategically to broaden the spectrum of susceptible IAV strains.

2. Material

Virus strains		
A/X31	H3N2	allantoic fluid
A/Udorn/1972	H3N2	MDCK II supernatant
A/Panama/2007/1999	H3N2	MDCK II supernatant
A/Mallard/439/2004	H3N2	allantoic fluid
A/Bremen/5/2017	H3N2	MDCK II supernatant
A/NewCaledonia/20/1999	H1N1	MDCK II supernatant
A/PR/8/1934	H1N1	allantoic fluid
A/Bayern/ 63/2009	H1N1pdm	MDCK II supernatant
A/Sachsen/1816/2002	H1N2	allantoic fluid
A/turkey/Italy/472/ 1999	H7N1	MDCK II supernatant

Mutant viruses			
X31 WT	A/X31	none	serial passaging
L1	A/X31	G135E	serial passaging
L2	A/X31	K140N	serial passaging
L3	A/X31	P99F/G144D	serial passaging
O1	A/X31	N188D/N286T	serial passaging
O2	A/X31	G135E/N188D/N286T	serial passaging
O3	A/X31	S228G	serial passaging
P1	A/Panama/2007/1999	T135G	reverse genetics
P2	A/Panama/2007/1999	N144G	reverse genetics

Cell lines		
MDCK II	Madin-Darby Canine Kidney cells	MEM
HEK 293T	Human Embryonic Kidney cells	DMEM

Bacteria			
Escherichia coli (E.coli), strain XL1-Blue	recA1 endA1 gyrA96 thi-1 hsdR17 supE44 relA1 lac [F`proAB lac Iq ZδM15 Tn10 (Tetr)]	2x YT medium	Stratagene/Agilent (Santa Clara, USA)

Compounds					
multivalent polyglycerols[1]	Ligands	number of residues		MW [kDa]	
$LPG_{10}SA_{0.40}$	SA	60	PBS	30	
$LPG_{10}SA_{0.70}$	SA	99	PBS	45	
$dPG_{20}SA_{0.15}$	SA	26	PBS	20	
LPG_{10}-(6'-SLN_3)$_{0.35}$	SL	37	PBS	33,8	
LPG_{10}-(6'-SLN_3)$_{0.50}$	SL	88	PBS	74,18	
LPG_{10}-(3'-SLN_3)$_{0.20}$	SL	24	PBS	24,7	
LPG_{10}-(6'-SLN_3)$_{0.30}$ (3'-SLN_3)$_{0.30}$	SL	67	PBS	54,7	
LPG_{10}-(6'-SLamide)$_{0.50}$	SL	67	PBS	56	
dPG_{10}-(6'-SLamide)$_{0.15}$	SL	20	PBS	24	
$LPG_{10}ZA_{0.10}$	Zanamivir	13	PBS	15,0	
$LPG_{10}ZA_{0.40}$	Zanamivir	54	PBS	30	
$dPG_{10}ZA_{0.10}$	Zanamivir	13	PBS	15	
$LPG_{10}ZA_{0.15}SA_{0.30}$	Zanamivir/SA	16/40	PBS	30	
$LPG_{10}ZA_{0.40}SL_{0.40}$	Zanamivir/SL	54/60	PBS	65	
LPG_{10}	none		PBS	10	
dPG_{10}	none		PBS	12	
Cy3-labeled multivalent PGs[1]					Cy3/Polymer [mg/g]
Cy3-$LPG_{10}SA_{0.40}$	SA	60	PBS	30	0.45
Cy3-LPG_{10}	none		PBS	10	0.13
multivalent phage capsids[2]					
qß Capsid [sia1]	SA	144	PBS		
qß Capsid [HPG]	none		PBS		
small molecules				MW [g/mol]	
Arbidol			DMSO	513,9	
Oseltamivir			DMSO	284,4	
Zanamivir			DMSO	332,31	

[1] All multivalent polyglycerols and Cy3-labeled PGs were synthesized by the AG Haag (Freie Universität Berlin), namely Sumati Bhatia, Pallavi Kiran and Padri Parshad.

[2] All multivalent phage capsids were synthesized by the AG Hackenberger (Leibniz-Forschungsinstitut für Molekulare Pharmakologie, Berlin), namely Lutz Adam and Simon Klenk.

Kits	
ReliaPrep RNA Cell Mini Prep System	Promega (Wisconsin, USA)
Super Script III One-Step RT-PCR System with Platinum Taq High Fidelity	Invitrogen by Life Technologies (Darmstadt, Germany)
MSB SPIN PCRapace	Stratec Molecular GmbH (Berlin, Germany)
Qubit dsDNA BR Assay	Life Technologies (Darmstadt, Germany)

QIAamp MinElute Virus Spin	Qiagen (Hilden, Germany)
RevertAid RT Reverse Transcription Kit	Thermo Fisher Scientific (Bonn, Germany)
BigDye® Terminator 3.1 Kit	Applied Biosystems (Darmstadt, Germany)
Platinum® Taq DNA Polymerase	Thermo Fisher Scientific (Bonn, Germany)
RayBio® Glycan Array 100	RayBiotech (Norcross, USA)
LYNX Rapid Plus Biotin (Type 1) Antibody Conjugation Kit	Bio-Rad (Hercules, USA)
CellTiter 96® AQueous One Solution Cell Proliferation Assay (MTS)	Promega (Wisconsin, USA)
QuikChange II Site-Directed MutagenesisKit	Agilent (Santa Clara, USA)
Invisorb® Spin Plasmid Mini Two	Stratec Molecular GmbH (Berlin, Germany)
QIAfilter Plasmid Maxi Kit	Qiagen (Hilden, Germany)
Pierce BCA Protein Assay Kit	Thermo Fisher Scientific (Bonn, Germany)

Enzymes	
DpnI	Fermentas (St. Leon-Rot, Germany)
RNAsin	Promega (Wisconsin, USA)

Antibodies			
Primary antibodies			
anti-IAV NP	mouse	1:1000	AbD Serotec/Bio-Rad (Hercules, USA)
anti-NS1	rabbit	1:500	BioGenes (Berlin, Germany)
Na,K-ATPase alpha 1 subunit	mouse	1:100	Millipore/Merck (Darmstadt, Germany)
Secondary antibodies			
Alexa Fluor™ 488 anti-mouse IgG	donkey	1:1000	Invitrogen™/Thermo Fisher Scientific (Bonn, Germany)
Alexa Fluor™ 647 anti-mouse IgG	goat	1:1000	
Alexa Fluor™ 488 anti-rabbit IgG	goat	1:1000	
Alexa Fluor™ 568 anti-mouse IgG	goat	1:1000	
Alexa Fluor™ 647 anti-rabbit IgG	donkey	1:1000	

Primer	
MBTuni-12	ACGCGTGATCAGCAAAAGCAGG
MBTuni-13	ACGCGTGATCAGTAGAAACAAGG
MBTuni-12-G	ACGCGTGATCAGCGAAAGCAGG
X31-HA EcoRI-F	CGTAGAATTCCATCATTGCTTTGAGCTACATTTT
X31-HA XbaI_R	CGTATCTAGATGCACCTAATGTTGCCTCTCT

X31 WT HA Seq F	CGTA TGAGGGTTTCACTTGGACTG
X31 WT HA Seq R	CGTA TGATTTTCCAGAGCGACAAG
PanHA T135G_F	GTCGCTCAGAATGGAGGAAGCTCTGCTTGCAAAAG
PanHA T135G_R	CTTTTGCAAGCAGAGCTTCCTCCATTCTGAGCGAC
PanHA N144G_F	CTGCTTGCAAAAGGAGATCTGGTAACAGTTTCTTTAGTAG
PanHA N144G_R	CTACTAAAGAAACTGTTACCAGATCTCCTTTTGCAAGCAG
pHW2000_2895f	AGCTCTCTGGCTAACTAGAG
pHW2000_342r	TGGCAACTAGAAGGCACAG
X31-HA_F2	CACGAACCAAGAACAAACCA

Plasmids	
pHW2000-A/Panama/2007/1999-NP	Andrea Martini, FG17, RKI, Berlin
pHW2000-A/Panama/2007/1999-PA	Andrea Martini, FG17, RKI, Berlin
pHW2000-A/Panama/2007/1999-PB1	Andrea Martini, FG17, RKI, Berlin
pHW2000-A/Panama/2007/1999-PB2	Andrea Martini, FG17, RKI, Berlin
pHW2000-A/Panama/2007/1999-M	Andrea Martini, FG17, RKI, Berlin
pHW2000-A/Panama/2007/1999-NA	Andrea Martini, FG17, RKI, Berlin
pHW2000-A/Panama/2007/1999-HA	Andrea Martini, FG17, RKI, Berlin
pHW2000-A/Panama/2007/1999-NS1	Andrea Martini, FG17, RKI, Berlin
pHW2000-A/Panama/2007/1999-HA (T135G)	Marlena Stadtmüller, FG17, RKI, Berlin
pHW2000-A/Panama/2007/1999-HA (N144G)	Marlena Stadtmüller, FG17, RKI, Berlin

Equipment	
Microscopes	
CKX41 inverse bright field microscope	Olympus (Tokyo, Japan)
Leica DM IL	Leica (Wetzlar, Germany)
Confocal laser scan microscope LSM 780	Zeiss (Oberkochen, Germany)
Zeiss Observer.D1	Zeiss (Oberkochen, Germany)
Centrifuges	
centrifuge Sorvall LYNX 4000 superspeed	Sorvall/Thermo Fisher Scientific (Bonn, Germany)
Heraeus™ Pico™ 17 microcentrifuge	Heraeus/Thermo Fisher Scientific (Bonn, Germany)
5417R cooling centrifuge	Eppendorf (Hamburg, Germany)
Multifuge 1S-R (rotor: 75002000)	Heraeus/Thermo Fisher Scientific (Bonn, Germany)
Optima™-L 100K ultracentrifuge with 70-Ti rotor	Beckman coulter (Brea, USA)
Sprout™	Heathrow Scientific (Vernon Hills, USA)
Microcentrifuge SD	Carl Roth (Karlsruhe, Germany)
Mixing devices	
Shaker Roto-Shake Genie®	Scientific Industries (Bohemia, USA)
Shaker Vortex Genie® 2	Scientific Industries (Bohemia, USA)

Thermomixer compact	Eppendorf (Hamburg, Germany)
IKA® Vortex 1	IKA (Staufen im Breisgau, Germany)
Heidolph MR 3001	Heidolph (Schwabach, Germany)
Blockthermostat TCR 100	Carl Roth (Karlsruhe, Germany)
Ecotron	ifors MT (Bottmingen, Switzerland)
Other Devices	
Cell culture incubator	Binder GmbH (Tuttlingen, Germany)
Water bath DC10	Thermo Haake GmbH (Karlsruhe, Germany)
Sterile work bench Herasafe™ KS12	Thermo Fisher Scientific (Bonn, Germany)
Qubit 2.0 (Fluorometer)	invitrogen
NanoDrop™ 8000 UV/Vis Spectrophotometer	Thermo Fisher Scientific (Bonn, Germany)
Mastercycler gradient (thermocycler)	Eppendorf (Hamburg, Germany)
Personal Cycler (thermocycler)	Biometra (Göttingen, Germany)
FLUOstar® Omega Plate Reader	BMG Labtech (Ortenberg, Germany)
GenePix 400B (microarray reader)	Molecular Devices (San José, USA)
Tecan Fluorometer Infinite F200 Pro	Tecan (Männedorf, Switzerland)

media			
cell culture media			
complete MEM/DMEM	MDCK II	MEM/DMEM	
		FBS	10%
		Pen/Strep	50 mg/ml
		L-glutamine	2 mM
complete infection MEM/DMEM	MDCK II	MEM/DMEM	
		BSA	0.2 %
		Pen/Strep	50 mg/ml
		L-glutamine	2 mM
		TPCK-treated trypsin	100 µg/ml
Avicel Overlay Medium	MDCK II	2x MEM	
		Avicel RC-581 in H2O	1.25 %
		BSA	0.2 %
		DEAE-Dextran	0.01 %
		$NaHCO_3$	0.05 %
		TPCK-treated trypsin	100 µg/ml
Agar Overlay Medium	MDCK II	2x MEM	
		Oxoid agar	2%
		BSA	0.2 %
		DEAE-Dextran	0.01 %
		$NaHCO_3$	0.05 %
		TPCK-treated trypsin	100 µg/ml
transfection DMEM	HEK 293T	DMEM	

	FBS	10%
	L-glutamine	2 mM
media for bacteria		
2x YT-medium	Trypton	16 g/l
	yeast extract	10 g/l
	NaCl	10 g/l
SOC medium	Trypton	20 g/l
	yeast extract	5 g/l
	NaCl	10 mM
	KCl	2.5 mM
	$MgCl_2$	20 mM
2x YT-agar	2x YT-medium	
	bacto-agar	1.5 % (w/v)
	ampicillin	100 g/l

Buffer and solutions		
PBS	NaCl	137 mM
	KCl	2.7 mM
	Na_2HPO_4	80.9 mM
	KH_2PO_4	1.5 mM
	in ddH_2O	
PBS++	$MgCl_2$	1 mM
	$CaCl_2$	1 mM
	BSA	0.2 %
	in PBS	
Crystal violet stock solution, 10x	ethanol	20 % (v/v)
	crystal violet	1 % (w/v)
	in ddH_2O	
Crystal violet solution, 1x	formaldehyde	10 % (v/v)
	crystal violet stock solution, 10x	10 % (v/v)
	in ddH_2O	
GA sterile binding buffer	BSA	1%
	Tween 20	0.05 %
	in PBS	
GA washing buffer	Tween 20	0.1 %
	in PBS	
GA blocking buffer	BSA	1%
	in PBS	
GA permeabilization solution	Tween 20	0.1 %
	Triton-X100	0.3 %
	in PBS	
50x TAE buffer	Tris	2 M
	acetic acid	1 M
	EDTA (pH 8)	10 mM

	in ddH_2O	
10x NTE	Tris	0.1 M
	NaCl	1 M
	EDTA (pH 8)	0.01 M
	in ddH_2O	
MES assay buffer	MES	32.5 mM
	$CaCl_2$	4 mM
	in ddH_2O	
stop solution	glycin	0.1 M
	ethanol	25 % (v/v)
	in ddH_2O	

Chemicals and Consumables	
1.5 ml reaction tubes	Sarstedt (Nürnbrecht, Germany)
12-well plates	TPP (Trasadingen, Switzerland)
15 ml reaction tubes	Roth (Karlsruhe, Germany)
2 ml reaction tubes	Sarstedt (Nürnbrecht, Germany)
24-well plates	TPP (Trasadingen, Switzerland)
2-Morpholinethansulfonsäure MES	Sigama-Aldrich (Taufkirchen, Germany)
48-well plates	Greiner (Solingen, Germany)
4-Methylumbelliferone, sodium salt	Sigama-Aldrich (Taufkirchen, Germany)
50 ml reaction tubes	TPP (Trasadingen, Switzerland)
6-well plates	TPP (Trasadingen, Switzerland)
96-well plates	BRAND (Wertheim, Germany)
96-well plates	TPP (Trasadingen, Switzerland)
96-well plates, black, flat bottom	Nunc (Roskilde, Denmark)
acetic acid	Carl Roth (Karlsruhe, Germany)
Acrylamide/Bis-acrylamide solution 30% (29/1)	Carl Roth (Karlsruhe, Germany)
Agarose NEEO Ultra Quality	Carl Roth (Karlsruhe, Germany)
Ampicillin	Roche (Mannheim, Germany)
Avicel microcrystalline cellulose	FMC Corporation (Philadelphia, USA)
Bacto-Agar	Becton-Dickenson (Heidelberg, Germany)
Bovine Albumin Fraction V	Carl Roth (Karlsruhe, Germany)
$CaCl_2$	Merck (Darmstadt, Germany)
Cell culture flasks	TPP (Trasadingen, Switzerland)
Cell culture flasks	TPP (Trasadingen, Switzerland)
Crystal Violet	Merck (Darmstadt, Germany)
DAPI	Merck (Darmstadt, Germany)
DEAE-dextran	Merck (Darmstadt, Germany)
DMSO	Sigama-Aldrich (Taufkirchen, Germany)
DNA 6x loading buffer	Fermentas (St. Leon-Rot, Germany)
EDTA	Carl Roth (Karlsruhe, Germany)
Ethanol, ≥99.9 %	Carl Roth (Karlsruhe, Germany)
Fetal bovine serum (FBS)	Merck (Darmstadt, Germany)
Formaldehyde, 37 %	Carl Roth (Karlsruhe, Germany)

GelRed	Genaxxon bioscience (Ulm, Germany)
GeneRuler™ 100 bp Plus DNA-ladder	Thermo Fisher Scientific (Bonn, Germany)
glycin	VWR international (Darmstadt, Germany)
KCl	Merck (Darmstadt, Germany)
KH_2PO_4	Thermo Fisher Scientific (Bonn, Germany)
L-glutamine	Carl Roth (Karlsruhe, Germany)
Lipofectamine® 2000	Invitrogen by Life Technologies (Darmstadt, Germany)
Methanol	Carl Roth (Karlsruhe, Germany)
$MgCl_2$	Carl Roth (Karlsruhe, Germany)
Midori Green Advance	Biozym Diagnostics (Oldendorf, Germany)
MUNANA(2´-(4-Methylumbelliferyl)-a-D-N-acetylneuraminic acid, sodium salt	Biosynth (Thal, Switzerland)
Na_2HPO_4	Thermo Fisher Scientific (Bonn, Germany)
NaCl	Carl Roth (Karlsruhe, Germany)
$NaHCO_3$	Merck (Darmstadt, Germany)
$NaHCO_3$	Merck (Darmstadt, Germany)
NaOH	VWR international (Darmstadt, Germany)
Opti®-MEM	Thermo Fisher Scientific (Bonn, Germany)
oxoid agar	Thermo Fisher Scientific (Bonn, Germany
Parafilm	American National Can (Chicago, USA)
PBS	Thermo Fisher Scientific (Bonn, Germany)
Penicillin/Streptomycin, 10 000 U/ml	Thermo Fisher Scientific (Bonn, Germany)
Succrose	Merck (Darmstadt, Germany)
Succrose	Merck (Darmstadt, Germany)
TPCK-treated trypsin	Merck (Darmstadt, Germany)
Tris	Carl Roth (Karlsruhe, Germany)
Triton X-100	SERVA Electrophoresis (Heidelberg, Germany)
Trypsin (cell culture)	Gibco® (Darmstadt, Germany)
Tryptone	Becton-Dickenson (Heidelberg, Germany)
Tween-20	Carl Roth (Karlsruhe, Germany)
Yeast extract	Becton-Dickenson (Heidelberg, Germany)

Software	
GraphPad Prism 8.4.0	GraphPad Software, Inc.
Zen 2.6 (blue/black)	Carl Zeiss Microscopy GmbH
Geneious Prime 2020.2.3	Biomatters Ltd.
Microsoft Office 2010/2013	Microsoft Corporation
Adobe Illustrator CS6	Adobe Systems Inc.
Endnote X7.7.1	Thomson Reuters
PyMol 1.7.2.1	Schrödinger, LLC
GenePix Pro 7.2	Molecular Devices, LLC

3. Methods

3.1. Cell culture and infectious work

All cell culture and infectious work was conducted in an appropriate BSL-2 environment.

3.1.1. Cell culture

All cell culture work was conducted under sterile conditions and at room temperature (RT). Cells were maintained in T75 or T175 cell culture flasks in their specific culture medium as specified in section 2 (cell lines) in a humidified environment at 5% CO_2 and 37°C. The absence of mycoplasma was confirmed using polymerase chain reaction (PCR). When 90% confluency was reached, cells were sub-cultured by removing the cell culture medium and washing once with phosphate buffered saline (PBS). Subsequently, Trypsin-EDTA solution was added and the flask incubated at 37°C until the adherent cells detached from the flask's surface. Cells were then resuspended in fresh medium and the fraction required was transferred to a new flask.

3.1.2. Cell viability assay

Cytotoxicity of compounds was assessed using the CellTiter 96® AQueous One Solution Cell Proliferation Assay (Promega). The assay relies on the reduction of the tetrazolium compound 3-(4,5-dimethylthiazol-2-yl)-5-(3-carboxymethoxyphenyl)-2-(4-sulfophenyl)-2H-tetrazolium (MTS) to formazan in active mitochondria. Mitochondrial activity correlates to the number of cells and therefore cell viability can be inferred. 15 000 MDCK II cells were seeded into each well of a 96-well plate on the day before the experiment. Cells were washed once with PBS and then supplemented with a 2-fold serial dilution of compounds in complete MEM. After 24 h at 37°C and 5 % CO_2, 20 µl MTS reagent was added to each well and incubated at 37°C for 1 h. Subsequently, the reduction to formazan was assessed by reading the absorbance at 490 nm with a FLUOstar® Omega Plate Reader. Background from blank wells without cells was substracted from all data. Cell viability of treated cells is given as % of cell viability of mock treated cells.

3.1.3. Virus preparation

Virus stocks were either produced in the allantoic cavity of embryonated chicken eggs or in MDCK II cells as indicated for each virus strain in section 2 (virus strains). For virus production in chicken eggs, 10 day old eggs were inoculated with 1000 PFU of virus in 100 µl of PBS++ and incubated at 37°C for 48 h in a humidified environment. Eggs were cooled at 4°C over night before opening the eggshell. The allantoic fluid was harvested without damaging the yolk sac and clarified by centrifugation at 3000 rpm for 5 min at 4°C. The HA titer (refer to section 3.1.5) of each preparation was determined and allantoic fluids containing the same virus strain with similar HA titers were pooled before storing aliquots at -80°C. For virus production in MDCK II cells, MDCK II cells at 80-90 % confluency were washed with PBS and then infected with MOI 0.01 of a virus solution diluted in PBS++ for 45 min at RT with occasional gentle shaking. Afterwards, the inoculum was removed, cells washed with PBS and supplemented with complete infection MEM. Infected cells were incubated at 37°C and 5% CO_2 for two or three days depending on the cytopathic effect

(CPE), which was monitored using a light microscope. When most cells showed CPE, cell culture supernatants were harvested and clarified by centrifugation at 3500 rpm for 5 min at 4°C. Aliquots were stored at -80°C until use. Exact virus titers of all stocks were determined using plaque assay (refer to section 3.1.4).

3.1.4. Virus titration by Plaque forming assay

Most influenza viruses cause a cytopathic lytic effect, which is visible as plaques in infected confluent cell monolayers. This effect is utilized for virus titration, as plaques can be counted to determine the number of infectious virus particles in a solution.

To this end, MDCK II cells were seeded in 12-well plates the day before infection. A confluent cell monolayer on the day of infection is important to obtain easily visible plaques. A ten-fold dilution series of the virus solution to be titrated was prepared in 135 µl PBS++. Cells were washed once with PBS, followed by infection with 125 µl of virus dilution for 45 min at RT with intermittent gentle shaking. Subsequently, the inoculum was suctioned off, cells washed with PBS and overlaid with semi-viscous Avicel Overlay Medium, which prevents the virus from spreading via the medium and thus enables plaque formation. After 48 h at 37°C and 5% CO_2, the Avicel Overlay Medium was removed and residual avicel particles washed off with PBS. Crystal violet solution was added for at least 30 min at RT to fix and stain the cells. The crystal violet solution was then removed and the stained plates washed with water. Plates were air-dried before plaques were counted. The number of infectious particles are given in plaque forming units (PFU) per ml and were calculated by the following formula:

$$PFU/ml = \frac{number\ of\ plaques * 1\ ml}{dilution\ factor * infection\ volume\ [ml]}$$

3.1.5. Hemagglutination assay

Mediated by HA, influenza virus binds to sialylated glycans on the cell surface to attach and initiate cell entry. When influenza HA binds to sialylated glycans on erythrocytes, it functions as a cross-linker and causes agglutination. This effect can be used to estimate virus titers quickly, the so-called HA titers. However, as hemagglutination does not discriminate between infectious and non-infectious virus particles and the hemagglutination ability between different influenza virus strains can differ, the hemagglutination assay cannot be used for a precise determination of virus titers.

To determine the HA titer, serial two-fold dilutions of the virus solution to be titrated were prepared in PBS in a 96-well plate with V-bottom. Equal volume of 1% chicken erythrocyte solution was added and the plate then sealed and incubated at 4°C for 30 – 60 min. Afterwards, the plate was tilted to visualize hemagglutination. In case there is enough virus in a well, agglutinated erythrocytes will appear as a diffuse red staining. Otherwise, the erythrocytes, which have sunken to the bottom of the well during incubation, will stream down upon tilting resulting in a red line. The highest dilution at which hemagglutination can still be observed represents the HA titer of a solution.

3.1.6. Hemagglutination Elution assay

Influenza viruses attach to and agglutinate erythrocytes mediated by HA binding to surface glycans and dissociate again mediated by NA cleaving SA off the glycans. At 4 °C, NA is inactive and does therefore not interfere with the hemagglutination assay described in section 3.1.5. At 37°C, NA is active and elutes the virus from erythrocytes. The speed of virus elution depends on the HA/NA balance. In case the NA activity is the same, virus elution depends on the HA binding strength only and the HA elution assay thus presents a measure for HA binding strength.

NA activity was measured using the MUNANA assay (refer to section 3.2.6) prior to the HA elution assay. Input virus was adjusted to the same relative fluorescence units (RFU) to assure the same NA activity in all samples in the HA elution assay. A serial two-fold dilution of the virus solution was prepared in PBS in a 96-well plate with V-bottom. Equal volume of 1% chicken erythrocyte solution was added and the plate then sealed and incubated at 4°C for 60 min. The plate was then tilted and the starting HA titer recorded. Afterwards, the plate was incubated at 37°C to facilitate NA mediated virus elution. The plate was tilted every 30 min and the new HA titer recorded each time. Results are given as relative HA titers [%] compared to the starting HA titer recorded before elution.

3.1.7. Measuring Infection Inhibition

To determine whether a compound is able to inhibit virus infection, a therapeutic approach was employed, in which a compound is added after an infection has been established, and is in contrast to a prophylactic approach, which relies on preincubation of virus or cells with a compound. MDCK II cells at 80-90 % confluency were washed with PBS and then infected with MOI 0.01 of the indicated virus solution diluted in PBS++ for 45 min at RT with occasional gentle shaking. Afterwards, the inoculum was removed, unbound virus washed off with PBS and cell supplemented with complete infection MEM. Compounds or PBS were added to the medium at the indicated concentrations within 5 min after infection. Infected cells were incubated at 37°C and 5% CO_2 for 24 h. The duration of 24 h enables two to three rounds of infection. Therefore, the effect on a specific step in the viral replication cycle cannot be distinguished but rather the effect on multicyclic infection is assayed. After the 24 h incubation, virus titers in the supernatant were determined using plaque titration (refer to section 3.1.4). For growth curves, cell culture supernatants were titrated after 8, 16, 24, 48 and 72 h. For determination of IC_{50} values, a 5-fold dilution series of compound was applied and IC_{50} values then calculated by fitting normalized and transformed data with nonlinear regression using GraphPad Prism 8.4.0. All data represent at least three independent experiments in duplicates.

3.1.8. Serial passaging

Viruses adapt to external selection pressure by accumulating mutations. Inhibitors exert such a selection pressure on the virus and continuous exposure will therefore most likely result in virus variants resistant to the inhibitor given the adaptive mutations result in replication competent virus. To generate resistant virus variants *in vitro*, serial passaging can be employed. Serial

passaging is an iterative process during which cell culture supernatant of infected cells treated with inhibitor is used to infect the following passage. Inhibitor concentrations are escalated from passage to passage, thus increasing the selection pressure and promoting replication of the best adapted virus variants (Figure 11).

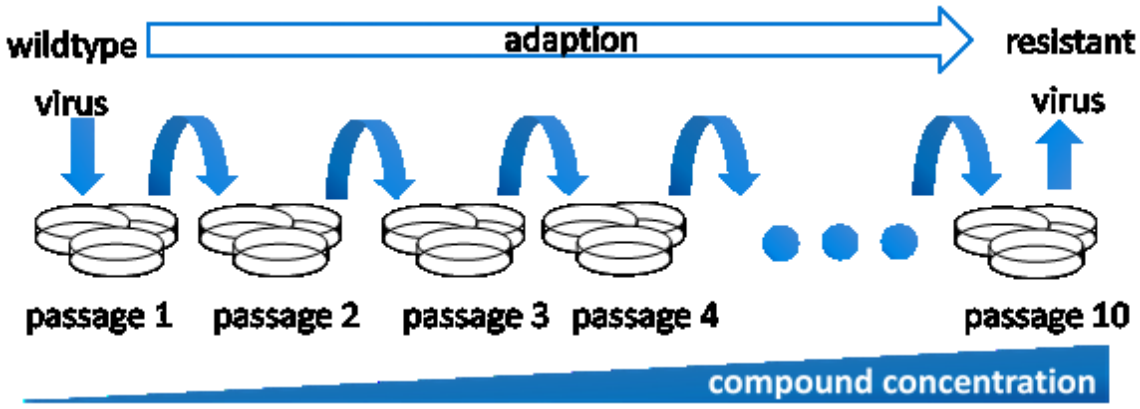

Figure 11: Principle of induction of resistant virus variants using serial passaging.
WT virus is used to infect the initial passage at MOI 0.01 and treated with compound in the medium or left untreated. After 24 h, infectious particles in the supernatant are titrated using plaque assay and then used to infect the next passage at MOI 0.01. Escalating compound concentrations are used for subsequent passages in order to subject the virus to increasing selection pressure and consequently adaption.

Here, variant viruses of influenza A virus A/X31 (H3N2) were generated against $LPG_{10}SA_{0.40}$, the licensed NA inhibitor Oseltamivir and the partially licensed fusion inhibitor arbidol. MDCK II cells at 80-90% confluency were washed with PBS and infected with the parental influenza A/X31 WT virus at MOI 0.01 for 45 min at RT with occasional gentle shaking. Afterwards, the inoculum was removed, unbound virus washed off with PBS. The cells were supplemented with complete infection MEM containing either the initial concentration of $LPG_{10}SA_{0.40}$, Oseltamivir or arbidol or left untreated and incubated at 37°C and 5% CO_2. After 24h, supernatants were titrated with plaque assay and used to infect the next passage at MOI 0.01, which then contained a higher concentration of compound in the medium. All compound concentrations are specified in Table 2. Three replicates of each treatment were conducted in separate wells on the plate, resulting in three different virus variants. Supernatants from passage 4, 7 and 10 and the parental WT virus were processed for next generation sequencing as detailed in section 3.2.1.

Table 2: Compound concentrations used at each passage of serial passaging. Concentrations of LPG10SA0.40 are given relating to SA and PG concentration both.

Passage	1	2	3	4	5	6	7	8	9	10	
$LPG_{10}SA_{0.40}$	0.1	0.1	0.2	0.3	0.8	2	4	20	100	100	µM [SA]
	1,67	1,67	3,33	5,00	13,33	33,33	66,67	333,3	1666,7	1666,7	nM [PG]
Oseltamivir	0,005	0,01	0,01	0,015	0,015	0,02	0,06	0,1	0,4	0,8	µM
Arbidol	20	30	40	40	40	40	40				µM

The stocks of the mutant viruses obtained from the initial serial passaging experiment (see also section 0 for generation of the stocks) were then subjected to serial passaging without selection pressure to test for possible revertants. The experiment was conducted analogously by using the

supernatant from infected cells to inoculate the subsequent passage with the difference that no compound was added to the medium. To check for presence or absence of mutations in HA, supernatants were then processed for sanger sequencing of the HA gene as detailed in section 3.2.2.

3.1.9. Plaque-purification of mutant viruses

The cell culture supernatants of serial passaging contain a mixed virus population consisting of mutant viruses carrying adaptive mutations but also viruses without the identified mutations. To obtain more homogenous virus stocks for further analyses, the heterogenous virus populations were plaque purified. One individual plaque is the result of one infectious particle and plaque-picking therefore facilitates purification. To this end, a ten-fold dilution series of the serial passaging cell culture supernatants was prepared in 135 µl PBS++. MDCK II cells at confluency were washed once with PBS, followed by infection with 125 µl of virus dilution for 45 min at RT with intermittent gentle shaking. Subsequently, the inoculum was suctioned off, cells washed with PBS and overlaid with Agar Overlay Medium, which prevents the virus from spreading via the medium and thus enables plaque formation. After 48 h at 37°C and 5% CO_2, single plaques were picked from wells with distinguishable, well separated plaques, dissolved in PBS and used to infect fresh flasks of MDCK II cells according to the virus preparation protocol (refer to section 3.1.3). The existence of the specific HA mutations identified by NGS and the absence of further mutations was confirmed by NGS of the plaque-purified virus stocks.

3.1.10. Immunofluorescence staining

Immunofluorescence staining was performed on coverslips, of which one was placed into each well of a 24-well plate. MDCK II cells were seeded directly onto the coverslips and infected on the next day with MOI 0.1 or 0.01 according to the protocol detailed in section 3.1.6. After incubation for the indicated time (6 h or 24 h) with Cy3-labeled compounds at the indicated concentration, cells were washed with PBS and fixed with 2.5 % paraformaldehyde for 15 min, followed by permeabilization with 0.2% Triton X-100 for 10 min. Next, coverslips were washed three times with PBS and then incubated with 30 µl of primary antibody diluted appropriately in 3 % BSA for 2 h at RT in a humid environment. Afterwards, coverslips were washed three times with PBS and incubated with 30 µl secondary antibody diluted appropriately in 3 % BSA for 1 h at RT in a humid environment. After another three washing steps with PBS, cell nuclei were stained with 30 µl of DAPI solution for 10 min. Coverslips were washed again three times with PBS and once with ddH_2O before finally mounting them with Mowiol. Fluorescence was visualized under a Zeiss Axio Observer D1 inverted epifluorescence microscope or Zeiss LSM 780 confocal laser scanning microscope and images generated with Zeiss ZEN imaging software.

3.1.11. Rescue of recombinant viruses

Amino acid changes were introduced to A/Panama/2007/1999 HA using reverse genetics. As influenza viruses have a negative sense RNA genome, cDNA is required to generate recombinant viruses by transfection without helper viruses. Here, an established eight plasmid cDNA system

(pHW-2000) was used, which relies on synthesis of both positive-sense mRNA and negative-sense vRNA from the plasmid template[310]. This is facilitated by the opposing orientation of the two transcription units on the plasmid. The full set of pHW-2000 plasmids containing the segment information of A/Panama/2007/1999 were constructed by Andrea Martini (formerly at Unit 17 at the RKI). In the study at hand, recombinant viruses were generated by first introducing the desired mutation into the HA-encoding plasmid pHW-2000-A/Panama/2007/1999-HA (refer to section 2: plasmids, for details) and then transfecting cells with the whole plasmid system including the mutated HA as described in the following.

For transfection, Lipofectamine® 2000 was diluted in 125 µl of Opti®-MEM at a ratio of 1.5 µl/1 µg plasmid DNA and incubated at RT for 5 min. 500 ng of each of the 8 pHW-2000 plasmids containing the genome information of influenza virus A/Panama/2007/1999 were diluted in Opti®-MEM to a total volume of 25 µl. The DNA - Opti®-MEM mixture was added to the Lipofectamine® 2000 - Opti®-MEM mixture and incubated for 20 min at RT to allow the formation of positively charged liposomes with integrated DNA. Meanwhile, a T75 flask of HEK 293T cells, which had been subcultured on the day before to ensure they were in dividing stage, were washed with PBS and detached with Typsin-EDTA solution. Cells were resuspended in 10 ml transfection DMEM, pelleted at 800g for 3 min and again resuspended in 10 ml transfection DMEM. 6-well plates were prepared with 1.2 ml transfection DMEM per well before adding 800 µl of cell suspension, resulting in around $0.7*10^6$ cells per well. The transfection solution containing the plasmid DNA and Lipofectamine® 2000 was added dropwise to the cells and distributed by shaking carefully. Cells were incubated at 37 °C and 5 % CO_2 for 48 h. After 6 h, the medium was replaced with fresh transfection DMEM.

The supernatant of the transfected HEK 293T cells contains newly generated recombinant virus und was further propagated on MDCK II cells. MDCK II cells in 6-well plates were washed with PBS and infected with 250 µl of transfected HEK 293T cell culture supernatant for 45 min at RT with occasional gentle shaking. Afterwards, input virus was removed, cells washed two times with PBS++ and supplemented with 2 ml complete infection MEM. Cells were incubated at 37 °C and 5 % CO_2 for 48 h, after which virus titers in the supernatant were determined using plaque assay. Finally, stocks of the rescued viruses were prepared in MDCK II cells according to the virus preparation protocol described in section 3.1.3.

3.1.12. Purification of virus by ultracentrifugation

To purify and concentrate virus solutions, ultracentrifugation was applied. 5 ml of 25 % sucrose in 1x NTE in ultracentrifugation tubes was carefully overlayed with 33 ml of cell culture supernatant containing virus (refer to section 3.1.3 for preparation details) without perturbing the interface between sucrose solution and virus solution. Centrifugation was performed at 24 000 rpm at 10 °C for 90 min. The liquid fraction was discarded and the virus-containing pellet resuspended in 100-500 µl PBS according to approximate pellet size. The resuspended virus solution was left in the ultracentrifugation tube over night at 4 °C to facilitate complete dissolving of the pellet. On the next day, the virus solution was aliquoted and stored at -80°C. Protein content of the purified virus

solution was determined using the Pierce BCA Protein Assay Kit (Thermo Fisher Scientific) according to the manufacturers' instructions and virus titers were determined by plaque assay (3.1.4).

3.2. Molecular biology methods

3.2.1. Next Generation Sequencing

To identify virus variants generated by serial passaging in section 3.1.8, next generation sequencing (NGS) was employed. For this purpose, viral RNA was extracted from serial passaging cell culture supernatants, amplified using a one-step whole genome RT-PCR, purified and then subjected to NGS. The detailed procedure is described in the following.

Total RNA was extracted from the cell culture supernatants using the ReliaPrep RNA Cell Miniprep System (Promega) according to the manufacturers' instructions. Viral RNA was then amplified using a one-step whole genome RT-PCR as previously described[311]. The influenza virus genome is segmented into eight genomic segments encoding for the different viral proteins, with each protein varying from strain to strain. Therefore, amplification of the influenza virus genome can be complicated and require multiple primer pairs. However, the promoter region of each segment contains a conserved hairpin structure, which was exploited to design a set of three primers that amplify all eight segments irrespective of influenza virus strain or subtype (Figure 12A,B), thus simplifying specific amplification greatly[311].

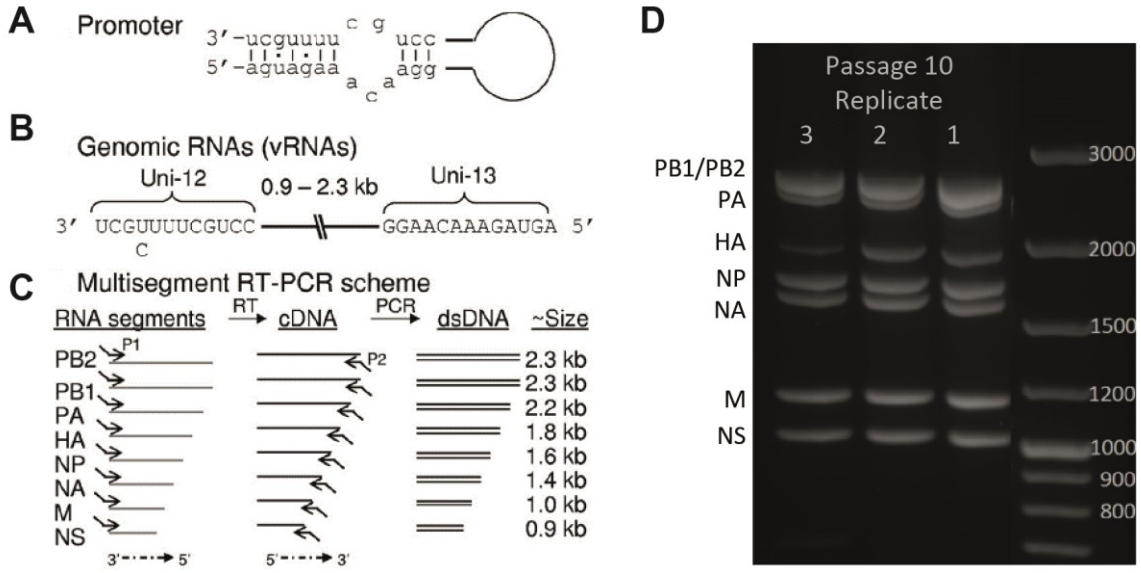

Figure 12: Principle of the one-step whole genome RT-PCR for influenza viruses.
(A) Promoter region with panhandle structure, (B) design of primers against the promoter region, (C) multisegment PCR scheme with expected product sizes and (D) agarose gel image of PCR products obtained from amplifying RNA extracted from cell culture supernatants of passage 10 of the $LPG_{10}SA_{0.40}$-treated cells of the passaging experiment. Seven distinct bands at the correct size can be observed. PB1 and PB2 cannot be distinguished as they are the same size. A, B and C modified from Zhou, Donnelly, Scholes, St George, Hatta, Kawaoka and Wentworth [311].

To perform one-step whole genome RT-PCR, the Super Script III One-Step RT-PCR System with Platinum Taq High Fidelity (Invitrogen by Life Technologies) was used with the parameters listed in

Table 3. Viral RNA was linearized to allow primer annealing to the promoter region before adding the enzyme mix and starting the reaction. The cycler program includes two sets of cycles with different annealing times to allow optimal amplification of all eight segments despite their different sizes.

Table 3: Protocol for one-step whole genome RT-PCR with PCR mixture composition and cycler program.

	Component	Volume
Primer Mix		
	10 µM MBT Uni12	0.5 µl
	10 µM MBT Uni12-G	0.5 µl
	10 µM MBT Uni13	1 µl
	Sample RNA	14 µl
	RNA linearization 72°C 2min, 0°C 2 min	
Enzyme Mix		
	2R-Mix	25 µl
	$MgSO_4$	8 µl
	HiFi Taq Polymerase	1 µl
	Primer Mix with Sample	16 µl

temp	time		
42°C	60 min		initial
94°C	2 min		denaturation
94°C	30 sec		denaturation
45°C	30 sec	5 cycles	annealing
68°C	3 min		elongation
94°C	30 sec		denaturation
57°C	30 sec	35 cycles	annealing
68°C	3 min		elongation
4°C	∞		cooling

PCR products were purified using the MSB SPIN PCRapace Kit (Stratec) according as per the manufacturers' protocol 1a and eluted in 20 µl ddH_2O. Successful amplification of all segments was confirmed via gel electrophoresis. 50 ml 1x TBE buffer containing 1.5% agarose were boiled in a microwave at 600 W for 1 min to dissolve the agarose completely. After cooling, 2.5 µl GelRed was added to facilitate DNA staining. Samples were diluted 1:10 in ddH_2O and supplemented 1:5 with loading buffer before loading on the gel. GeneRuler™ 100 bp Plus DNA-ladder was loaded as well for determination of fragment sizes by comparison. Samples were first allowed to enter the gel at 50 V for 5 min. Then, separation of fragments was performed at 30 V for 6-7 h until the dye front almost reached the far end of the gel. For further separation of PB1/PB2 and PA, the gel was subjected to 10 V for another 2 h. Finally, DNA bands were visualized using UV light in a transilluminator (Figure 12D). DNA concentration in the samples was measure using the Qubit dsDNA BR Assay Kit and a Qubit 2.0 Fluorometer. All samples were diluted to a DNA concentration of 86.9 ng/µl, which was the lowest concentration measured in any sample. Sequencing was conducted in the Robert Koch-institute in-house sequencing facility using an Illumina MiSeq.

3.2.2. Sanger sequencing

To confirm the existence or absence of HA mutations, Sanger sequencing was employed. To this end, viral RNA was extracted, reverse transcribed, amplified using standard PCR, purified and finally sequenced. The detailed procedure is described in the following.

RNA was extracted from cell culture supernatant virus stocks using the QIAamp MinElute Virus Spin kit (Qiagen) as per the manufacturers' instructions. cDNA was generated from the RNA using the RevertAid RT Reverse Transcription kit (Thermo Fisher Scientific) according to the protocol specified in Table 4. In the next step, cDNA was amplified using the parameters listed in Table 5.

Table 4: Components and heating protocol of reverse transcription.

	Component	Volume
Primer Mix		
	ddH_2O	7.5 µl
	10 µM MBT Uni12	0.5 µl
	10 µM MBT Uni12-G	0.5 µl
	10 µM MBT Uni13	1 µl
	Sample RNA	3 µl
	RNA linearization 65°C 5min, 0°C 2 min	
Enzyme Mix		
	Buffer	4 µl
	dNTPs	2 µl
	RNAsin	0.5 µl
	RevertAid RT	1 µl
	Primer Mix with Sample	12.5 µl
	Reverse transcription 42°C 50 min, 70°C 10 min	

Table 5: Protocol for standard PCR mixture composition and cycler program.

Component	Volume
ddH_2O	13.55 µl
10x Buffer	2.5 µl
50 mM Mg	2.5 µl
10 mM dNTPs	2.0 µl
X31-HA EcoRI-F	0.75 µl
X31-HA Xbal_R	0.75 µl
X31-HA_F2	0.75 µl
Taq polymerase	0.2 µl
Sample cDNA	2 µl

temp	time		
94°C	2 min		initial denaturation
94°C	30 sec		denaturation
59°C	30 sec	35 cycles	annealing
72°C	2 min		elongation
72°C	300 sec		final elongation
4°C	∞		cooling

PCR products were purifed using the MSB SPIN PCRapace Kit (Stratec) according to the manufacturers' protocol 1a and eluted in 20 µl ddH_2O. DNA content was measured using a NanoDrop™ 8000 UV/Vis spectrophotometer and samples diluted 1:10 in ddH_20 before sequencing with the BigDye® Terminator 3.1 sequencing kit (Applied Biosystems) according to the manufacturers' instructions and the parameters specified in. Finally, the sequence was determined at the Robert Koch-institute in-house sequencing facility.

Table 6: Protocol for Sanger sequencing PCR mixture composition and cycler program.

Component	Volume
ddH_2O	6 µl
5x ABI reaction buffer	1.5 µl
Primer 10 µM	0.5 µl
BigDye® 3.1 mix	1.0 µl
Sample DNA	1 µl (10-20 ng)

temp	time		
96°C	2 min		initial denaturation
96°C	10 sec		denaturation
59°C	5 sec	25 cycles	annealing
60°C	4 min		elongation
4°C	∞		cooling

3.2.3. Antibody biotinylation

Anti-IAV NP antibody was biotinylated using the LYNX Rapid Plus Biotin (Type 1) Antibody Conjugation Kit according to the manufacturers' instructions. Briefly, 1 µl of Rapid Modifier was added to 10 µl of Anti-IAV NP antibody. The mixture was then added to Lynx Rapid Plus and mixed carefully by pipetting up and down. After 15 min of incubation at RT, 1 µl of Lynx Rapid Quencher was added to stop the biotinylation reaction. Biotinylated Anti-IAV NP antibody was used without purification and stored at 4 °C until use. Successful biotinylation was verified using western blot.

3.2.4. Glycan microarray analysis

Glycan arrays are tools to investigate carbohydrate interactions of particularly but not exclusively lectins, antibodies and pathogens. Glycans are printed in a defined spatial arrangement on a microscopy slide, with one microarray slide containing a number of identical subarrays that can be loaded independently (Figure 13A). Samples to test for glycan binding, such as virions in this case, are incubated with the array to allow binding. Unbound virus is washed off, whereas bound virus is subsequently detected by consecutive primary and fluorophore-labeled secondary antibody (Figure 13B). Fluorescence signal can then be read out by a microarray reader.

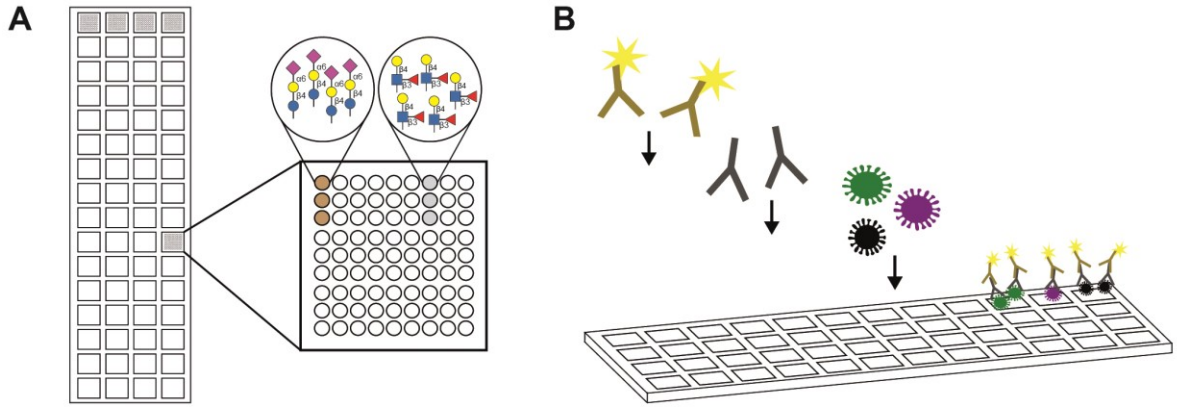

Figure 13: Glycan microarray analysis with a low-density microarray.
(A) Schematic layout of the low-density glycan microarray. 64 identical sub-arrays each containing 25 spots with distinct glycans in triplicates were printed on a microscopy slide. (B) Detection principle of glycan-bound molecules. Virus samples are incubated on the array to allow binding. Bound virus is then detected by an antibody against viral NP, which in turn is detected by a secondary antibody carrying carrying a fluorophore. Afterwards, the slide is scanned using a microarray reader (not depicted).

In this study, two different glycan arrays were employed: a low-density array and a commercial array. The low-density array contains 25 distinct, mostly sialylated glycans in 64 subarrays per slide. In contrast, the commercial array contains 100 distinct glycans covering a larger variety of glycan species albeit in 4 subarrays per slide. The protocol differs for both arrays and will thus be described separately in the following paragraphs.

The low-density microarray was kindly provided by Prof. Peter Seeberger of the Max-Planck-Institute of Colloids and Interfaces and handled according to a previously described protocol[112]. Briefly, dry array slides were washed once with 50 µl PBS and incubated with 30 µl of virus solution in GA sterile binding buffer containing $2*10^6$ PFU in a moist chamber at 4°C over night with continuous gentle shaking. Then, slides were washed three times with 50 µl GA washing buffer, followed by fixation with 50 µl 2.5 % formaldehyde for 15 min at RT and permeabilization with 50 µl GA permeabilization solution for 10 min at RT, after which slides were washed again three times with 50 µl GA washing buffer. Next, slides were blocked with GA blocking buffer for 2h at RT with continuous gentle shaking and subsequently incubated with anti-IAV NP primary antibody diluted 1:1000 in GA blocking buffer in a moist chamber at 4°C over night with continuous gentle shaking. Residual primary antibody was removed by washing three times with 50 µl GA washing buffer. Then, slides were incubated with Alexa Fluor™ 568 anti-mouse secondary antibody 1:200 in GA blocking buffer for 1h at RT with continuous gentle shaking. Slides were washed again three times with 50 µl GA washing buffer. Finally, slides were disassembled, dipped into distilled water for 1 min and scanned using a GenePix microarray scanner. Fluorescence images were analyzed with the GenePix pro 7.2 software. Spots containing irregular signals originating from dust or small damages to the slide surface were excluded from the analysis. Signal intensities of individual array slides were normalized using binding data of $2*10^6$ PFU of influenza A/X31 WT virus, which was applied on each slide to allow comparison, and background signal was subtracted. A concentration dependent effect was excluded in this setting by analyzing different virus concentrations.

The commercial array (RayBio® Glycan Array 100) was obtained from RayBiotech (Norcross, USA). Glycan-binding was analyzed using the sandwich-based approach of the manufacturers' instructions. First, slides were allowed to equilibrate to RT for 2 h and air-dryed for 30 min before usage. 400 µl of virus solution containing 125 µg/ml of virus in GA binding buffer were incubated on the array at 4°C over night with continuous gentle shaking, after which slides were washed three times for 5 min with 800 µl GA washing buffer. Virus were fixed with 2,5 % formaldehyde in PBS for 15 min and permeabilized with GA permeabilization buffer for 10 min. Afterwards, slides were washed with washing buffers from the array kit (5x 5 min WB I and 2x 5 min WB II) and blocked for 3 h with sample diluent. The remaining protocol was conducted according to the manufacturers' instructions. Briefly, slides were incubated with biotinylated anti-IAV NP primary antibody (for biotinylation protocol, refer to section 3.2.3) diluted 1:1000 in sample diluent at 4°C over night with continuous gentle shaking. Slides were washed again thoroughly (5x 5 min WB I and 2x 5 min WB II) before incubation with streptavidin-coupled Cy3 equivalent dye with continuous gentle shaking for 1h in the dark. Next, slides were washed (5x 5 min WB I), disassembled carefully and washed further (1x 15 min WB I and 1x 5 min WB II). Finally, slides were washed with distilled

water for 1 min and air-dried before scanning using a GenePix microarray scanner. Fluorescence images were analyzed with the GenePix pro 7.2 software and processed using the Raybio Analysis Tool Excel Spreadsheet. In the Analysis Tool, data wa normalized to positive controls and background signal substracted.

3.2.5. Plasmid mutagenesis and preparation

Mutagenesis of the pHW-2000-A/Panama/2007/1999-HA plasmid was conducted using the QuikChange II Site-Directed Mutagenesis Kit (Agilent) according to the parameters detailed in Table 7. The primers were designed to generate the mutations T135G (PanHA T135G_R/F) or N144G (PanHA N144G_R/F) in the HA segment (section 2, Primer). To avoid incorporation of the input plasmid without mutations during transformation, the input plasmid was digested by addition of 1 µl DpnI (10 U/µl) to the PCR product for 1 h at 37°C. DpnI specifically degrades methylated DNA and therefore only the input plasmid, which is of bacterial origin and therefore methylated.

Table 7: Protocol for mutagenesis PCR mixture composition and cycler program.

Component	Volume
5x Buffer	5 µl
Plasmid DNA	5 ng
dNTP-Mix	1.0 µl
Primer F	125 ng
Primer R	125 ng
ddH_2O	Ad 50 µl
Pfu turbo DNA polymerase	1 µl

temp	time		
95°C	1 min		initial denaturation
95°C	30 sec		denaturation
55°C	1 min	12 cycles	annealing
68°C	2 min		elongation
4°C	∞		cooling

Competent *E.coli* XL1-Blue cells were thawed on ice for transformation. 50 µl of competent cells were carefully mixed with 1 µl of PCR-product from above and incubated on ice for 30 min. DNA uptake was induced by a heat-pulse of 42 °C for 45 sec followed by another 2 min on ice. Subsequently, cells were supplemented with 500 µl super optimal broth with catabolite repression (SOC) medium and incubated at 37°C for 1 h at 220 rpm. The plasmid contains an ampicillin resistance gene, so cells were plated on 2x YT agar plates containing 100 µg/ml ampicillin and incubated at 37°C over night to select for cells which have successfully taken up the plasmid.

Single clones were picked and incubated in 5 ml 2x YT medium containing 100 µg/ml ampicillin at 37°C and 200 rpm overnight. Of 4 ml of this culture, Bacteria were pelleted and plasmid DNA isolated using the Invisorb® Spin Plasmid Mini Two (Stratec Molecular GmbH) according to the manufacturers' instructions. The DNA concentration was determined with a NanoDrop™ 8000 UV/Vis spectrophotometer and the HA gene from the plasmid sequenced with sanger sequencing as detailed in the last paragraph of section 3.2.2 and using primer pHW2000_2895f. The remaining 1 ml of the mini cultures of clones corresponding to DNA carrying the desired mutation as determined by sanger sequencing was incubated in 200 ml 2x YT medium containing 100 µg/ml ampicillin at 37°C and 200 rpm overnight. Bacteria were pelleted and plasmid DNA isolated using the QIAfilter Plasmid Maxi Kit (Qiagen) according to the manufacturers' instructions. The DNA

concentration was determined with a NanoDrop™ 8000 UV/Vis spectrophotometer and the HA mutations confirmed again with sanger sequencing as detailed in the last paragraph of section 3.2.2 and using primers pHW2000_2895f and pHW2000_342r.

3.2.6. Determination of NA activity with MUNANA

NA activity was determined using the 2'-(4-Methylumbelliferyl)-α-D-*N*-acetylneuraminic acid (MUNANA) assay, which relies on cleavage of MUNANA by NA to release the fluorescent 4-methylumbelliferone (4-MU). For determination of NA activity, a 2-fold serial dilution of virus solution was prepared in MES assay buffer. To each well 30 µl of 85 µM MUNANA substrate in MES assay buffer were added. Assay plates were then sealed and incubated in the dark at 37°C for 2 h. Cleavage of MUNANA by NA was terminated by adding 150 µl of stop solution to each well. The amount of released 4-MU was measured at 365 nm excitation and 460 nm emission using a Tecan Fluorometer Infinite F200 Pro.

4. Results

4.1. Measuring infection inhibition using a two-step inhibition analysis

To measure effectivity of antiviral agents targeting the HA, most often the hemagglutination inhibition assay (HAI), cytotoxicity inhibition assay or the plaque reduction assay (PRA) are employed. These assays have advantages in their simplicity but also limitations in their informative value. The HAI assay measures the ability of an inhibitor to prevent virus-mediated hemagglutination of red blood cells. However, successful hemagglutination or hemagglutination inhibition does not always translate to infection of cells or prevention thereof[312]. Cytotoxicity inhibition measures the viability of infected cells in relation to drug concentration. Therefore, it doesn't directly detect the impact on virus propagation. PRA often incorporates a preincubation step of virus solution with compound, which is a prophylactic setting and counter to the therapeutic approach this study is pursuing. Furthermore, PRA is not flexible. Samples need to be stained after a fixed time, which renders some analyses e.g. growth curve analysis impossible.

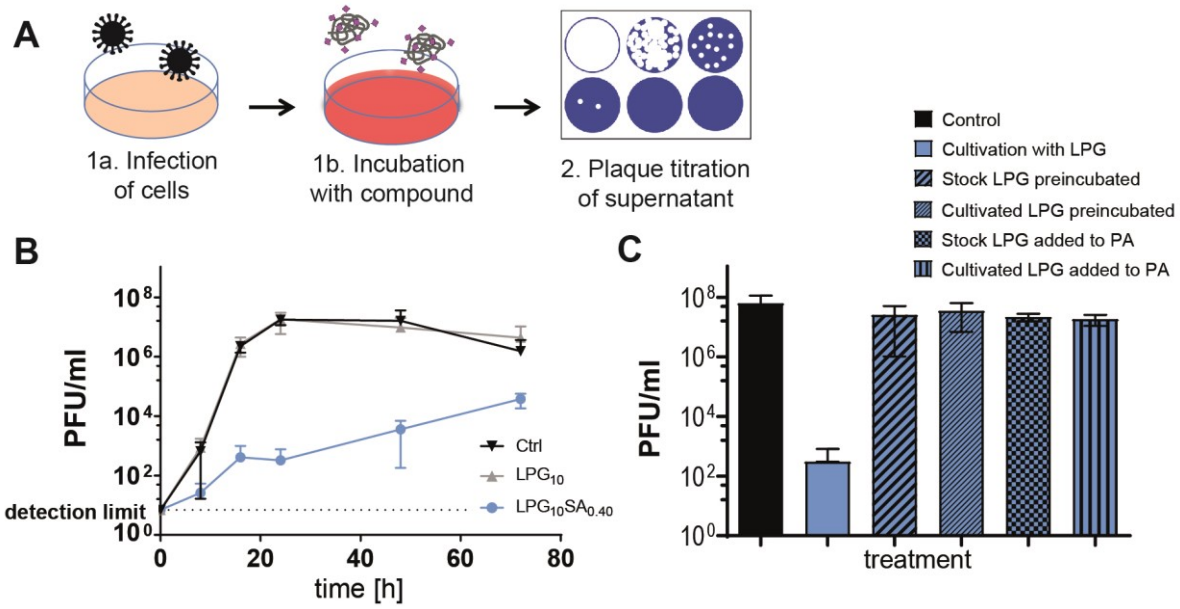

Figure 14: Design of the two-step assay for measuring inhibition of infection.
(A) Procedure of the two-step assay for measuring inhibition of infection. (B) Growth curve of influenza A/X31 virus on MDCK II cells infected with MOI 0.01 and treated with 1,67 µM [PG] of compound or left untreated (Mean ± SD, N=3 in duplicates). (C) Impact of residual compound from the first step on the result of the second step of the two-step inhibition analysis. 167 nM [PG] of compound was either incubated in culture medium on cells for 24h (cultivated LPG) or applied directly from the stock solution (stock LPG). Additionally, both versions were either preincubated with the supernatant directly before step 2 (preincubated) or added into the avicel medium of step 2 (added to PA) (Mean ± SD, N=2 in triplicates).

For the reasons stated above, a two-step inhibition analysis was employed. This comprises infection of cells and incubation with or without compound for a set time and then analyzing the supernatant for infectious particles using plaque assay (PA) (Figure 14A). Initially, this setup was evaluated in two analyses. First, a growth curve analysis of influenza virus A/X31 with or without a prototypic LPG ($LPG_{10}SA_{0.40}$) conducted according to the two-step procedure revealed that the difference between treated and untreated samples increased until 24 hpi and did not change much

at later time points (Figure 14B). Therefore, 24 h was selected as standard incubation time of the first step. Untreated, influenza A/X31 virus grows to a titer of 10^7-10^8 PFU/ml (Figure 14C, black). Treated with $LPG_{10}SA_{0.40}$ the titer is reduced by 4-5 orders of magnitude (Figure 14C, blue, no pattern). Since there is no dialysis step between step one and step two, the effect of residual compound on the plaque assay result was assessed in a second experiment by spiking samples with $LPG_{10}SA_{0.40}$ (Figure 14C, blue, patterned). 167 nM [PG] of compound were applied, because this is the maximum concentration present in the first 1:10 dilution of a 1,67 µM [PG] test sample in the plaque assay during the usual assay procedure. Either stock LPG was added or LPG cultivated in culture medium on cells for 24 h to control for possible cell- or medium- related effects, but no difference was observed between the two versions. Compound was spiked in in two different ways. Firstly, it was added to the supernatants of infected cell culture taken after the 24h incubation of step one. After preincubation for 30 min the solution was used to infect the cells for plaque assay. No significant difference to untreated virus was observed here. Secondly, the compound was spiked in to the Avicel Overlay Medium used in step two, so the compound was present in the medium during the whole 48 h incubation of the PA. No significant difference to untreated virus was observed here as well. This suggests that most of the residual compound present in the supernatant after step one is washed off together with any unbound virus right after the infection step of the PA. In the PA itself, the compound is probably just as limited in its mobility through the medium as the virus and therefore has little effect on the infection. These data suggest that the two-step inhibition analysis with a 24 h incubation in step one is suitable to measure the inhibitory potential of compounds.

4.2. Sialylated PGs inhibit influenza A/X31 virus propagation

With the two-step inhibition assay established, the next step was to apply this assay using influenza A/X31 virus and to generally gain more insights into the function of the compounds. This comprises determining the PG most effective at inhibiting influenza A/X31 virus, tracking labeled PGs in immunofluorescence and investigating possible synergy with Oseltamivir.

4.2.1. $LPG_{10}SA_{0.40}$ is most effective at inhibiting influenza A/X31 virus propagation

Polylgycerol (PG) was chosen as the basic scaffold material due to its excellent carrier properties (refer to section 1.2.1.6). However, there are many possibilities of how to configure the scaffold exactly and the optimal geometry has to be determined, especially in order to obtain a potent inhibitor. The first scaffold configurations analyzed were that of linear PG (LPG) and dendritic PG (dPG) and the optimal degree of functionalization (DF) with SA. Scaffold configuration is reflected in compound names, which follow the pattern $scaffold_{MW}SA_{DF}$. Bhatia et al.[275] tested a range of LPGs and dPGs with different SA density regarding their potential to raise cell viability upon influenza A/X31 virus infection. All functionalized compounds were able to increase cell viability and thus inhibit infection. High SA densities were not necessary for effective inhibition of IAV propagation. The most effective LPGs were $LPG_{10}SA_{0.40}$ and $LPG_{10}SA_{0.70}$and the most effective dPG was $dPG_{10}SA_{0.15}$. Therefore, in the study at hand, these three compounds were further compared in

the therapeutic two-step infection assay and IC_{50} values calculated from the results (Table 8). The LPGs have lower IC_{50} values than the dPG compound, confirming the findings of Bhatia et al.[275]. $LPG_{10}SA_{0.40}$ had the lowest IC_{50} in this setting. Notably, the IC_{50} of $LPG_{10}SA_{0.40}$ was more than 100-fold lower than that of Oseltamivir.

Table 8: IC50 values of several compounds against influenza A/X31 virus.

IC_{50} [µM P/SA]*	$LPG_{10}SA_{0.40}$	$LPG_{10}SA_{0.70}$	$dPG_{10}SA_{0.15}$	Oseltamivir
IC_{50} [µM P]	0,01513	0,01840	0,09132	2,735
IC_{50} [µM SA]	0,9078	1,8216	2,37432	

*Concentrations are given in relation to particle (P) or ligand (SA)

4.2.2. $LPG_{10}SA_{0.40}$ associates with virus infected cells in immunofluorescence staining

The inhibition of influenza A/X31 virus propagation with sialylated PG was confirmed in immunofluorescence imaging using Cy3-labeled PGs (Figure 15). For this purpose, MDCK II cells grown on cover slips were infected with influenza A/X31 virus and treated with Cy3-labeled $LPG_{10}SA_{0.40}$ or LPG_{10} for 24h or for 6h. Afterwards, cells were fixed, permeabilized and stained for viral antigen as well as cell nuclei and imaged using indirect fluorescence microscopy.

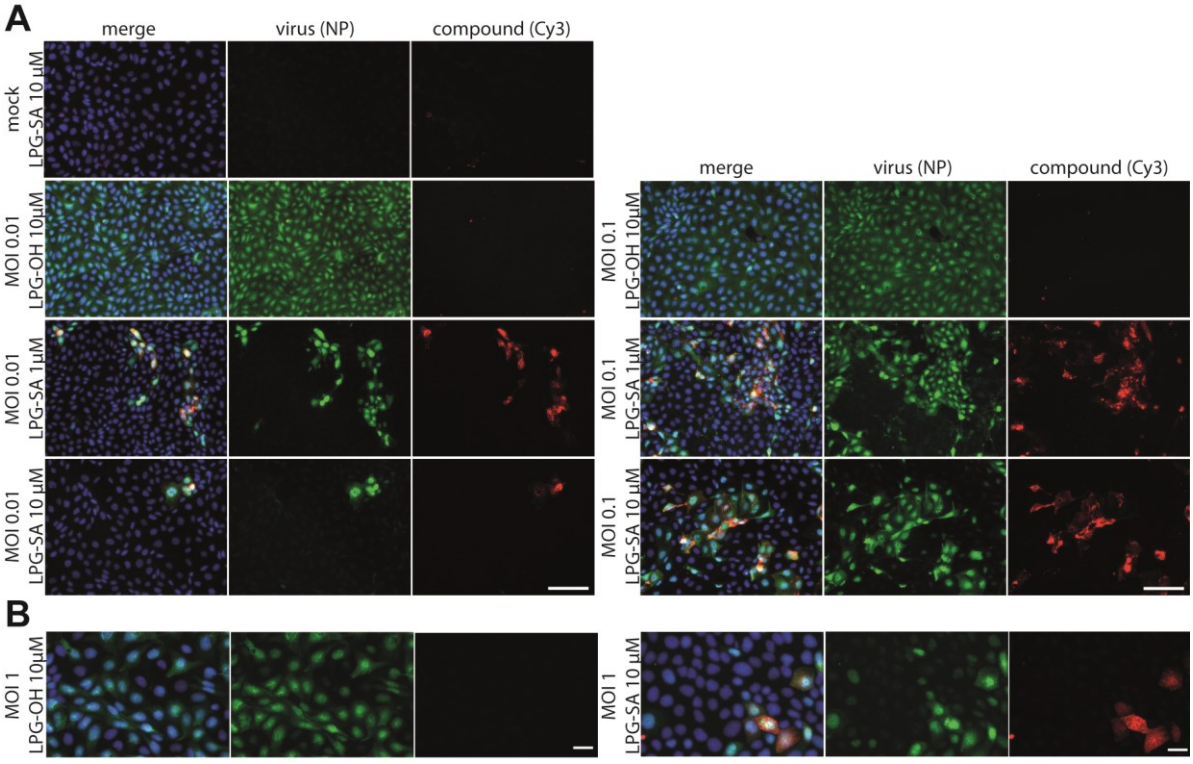

Figure 15: Immunofluorescence staining visualizing inhibition of influenza A/X31 virus propagation.
MDCK II cells were infected with influenza A/X31 virus at MOI 0.1 or 0.01 and treated with the indicated compound at the indicated concentration for 24 h (A) or infected with A/X31 virus at MOI 1 and treated with the indicated compound for 6h (B). Cells were fixed, permeabilized and stained with an antibody against viral NP (green). Nuclei were stained with DAPI (blue) and compounds are labeled with Cy3 (red) (A: scale bar: 100 µM, B: scale bar: 20 µM). LPG-SA refers to Cy3-labeled $LPG_{10}SA_{0.40}$ and LPG-OH refers to Cy3-labeled LPG_{10}.

Cy3-$LPG_{10}SA_{0.40}$ associated with virus signal and was only detected in infected cells (Figure 15). This association supports binding of the compound to a viral component, as per the assumed mechanism of inhibition. Almost no Cy3-$LPG_{10}SA_{0.40}$ was detectable in mock infected cells. This is probably due to the absence of its binding partner. Therefore, it was washed off while preparing the slides. This also means that $LPG_{10}SA_{0.40}$ does not detectably bind any cellular components. Cy3-LPG_{10} was not detected, presumably because it was not retained and thus washed off while preparing the slides. Cy3-$LPG_{10}SA_{0.40}$ inhibited virus propagation in a concentration-dependent manner, with 10 µM of compound reducing the number of infected cells more than 1 µM of compound (Figure 15A). However, there was also some level of virus replication that escaped the compound. This can be more easily observed when infecting cells with a higher MOI (Figure 15A, right panel, and Figure 15B). There is a number of infected cells without associated compound, even at 10 µM of compound. Still, robust inhibition of multicyclic infection by Cy3-$LPG_{10}SA_{0.40}$ can be observed (Figure 15A). In addition, there is also an inhibitory effect observed after a period of time allowing for only one cycle of infection (Figure 15B).

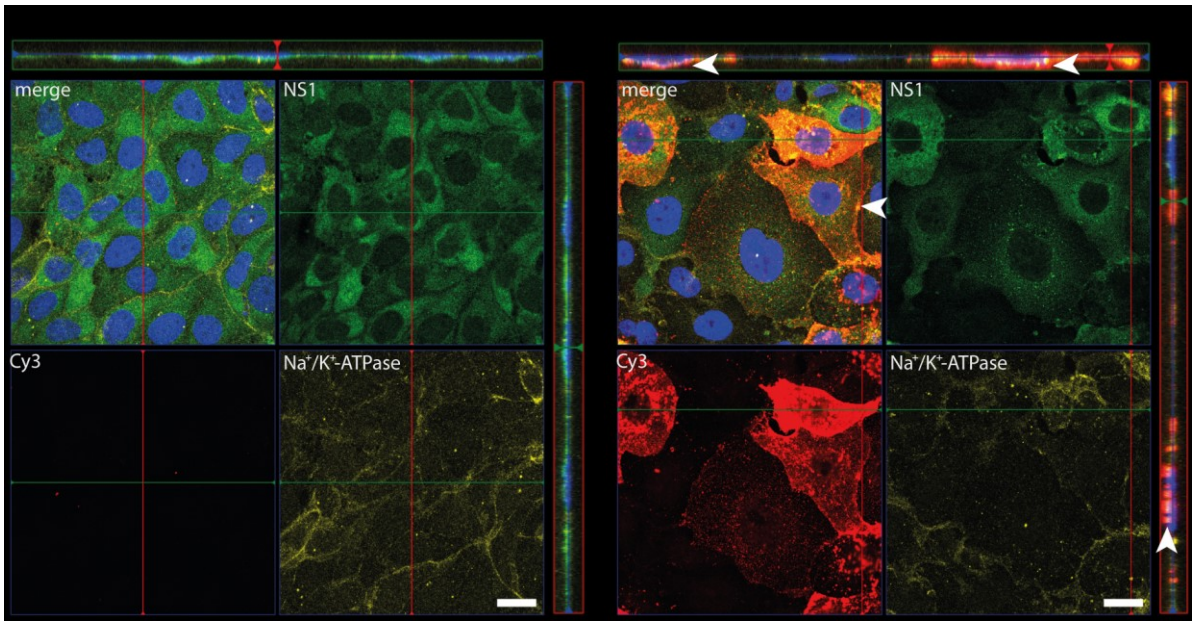

Figure 16: Immunofluorescence Z-stack analysis to track compound localization.
MDCK II cells were infected with influenza A/X31 virus at MOI 0.1 and treated with 10 µM of Cy3-labeled LPG_{10} (left panel) or $LPG_{10}SA_{0.40}$ (right panel) for 24 h. Cells were fixed, permeabilized and stained with an antibody against viral NS1 (green). Nuclei were stained with DAPI (blue), cellular membrane protein Na^+/K^+-ATPase is shown in yellow and compounds are labeled with Cy3 (red) (scale bar: 20 µM). LPG-SA refers to Cy3-labeled $LPG_{10}SA_{0.40}$ and LPG-OH refers to Cy3-labeled LPG_{10}. White arrowheads indicate some of the numerous areas where compound accumulated at the cell membrane.

In order to investigate the association of compound with viral components, most likely HA, more closely, Z-stack analysis of immunofluorescence slides was done (Figure 16). The membrane protein sodium-potassium-ATPase (Na+/K+-ATPase) was stained to visualize the cell membrane. Here we can see that Cy3-labeled $LPG_{10}SA_{0.40}$ indeed associated with infected cells. It appears to have mainly stayed at the cell surface and accumulated in many spots at the cell membrane (Figure 16, white arrowheads). There was also some compound in the cytoplasm, so it seems to have been taken up by cells sporadically, probably together with virus. However, the majority of compound

stayed at the membrane. The compound could be bound to virus attached to the membrane at the infection step, or to progeny virus about to bud from the membrane.

4.2.3. There is no synergy between $LPG_{10}SA_{0.40}$ and Oseltamivir

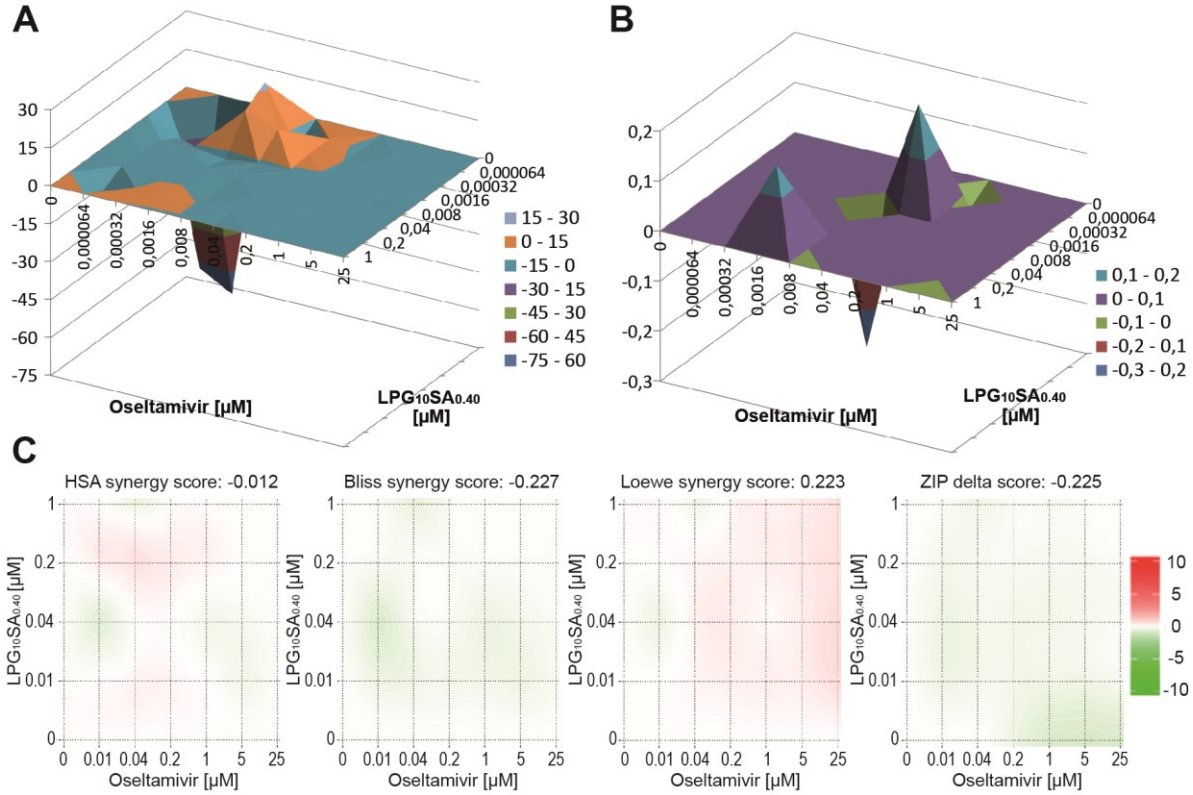

Figure 17: Analysis of Synergism between $LPG_{10}SA_{0.40}$ and Oseltamivir carboxylate.
Shown are synergy plots (A) and synergy plots at 95% confidence (B) for combinations of the two drugs against A/X31 virus. Synergy plots were calculated using MacSynergy II[313]. The Y-axis represents the amount (%) the effect of the drug combination that exceeds the additive effect. (C) Synergy analysis using SynergyFinder[314]. Four different calculation approaches were used. N=3 in duplicates.

If the combination of two drugs results in a greater effect than the expected additive effect, this is called a synergistic effect[315]. In case the effect is smaller than the expected additive effect, it is called antagonism. The balance between HA and NA is important for viral fitness[123]. Therefore, it is conceivable that attacking both HA and NA at once by using sialylated PG together with Oseltamivir might result in drug synergy, as was the case with other inhibitors targeting HA[316, 317]. To test for synergy between $LPG_{10}SA_{0.40}$ and Oseltamivir, serial dilutions of both drugs were combined against influenza A/X31 virus in the two-step inhibition assay. This means, the infection was first established before both compounds were added to the medium together. Synergy was analyzed using MacSynergy II[313], which bases its calculations on the Bliss independence model[315]. The results are shown in Figure 17. Moderate synergy can be observed for low concentrations of both compounds (Figure 17A). However, if a confidence interval of 95% was applied, only minor levels of synergy remained (Figure 17B). Data from the combination study was also analyzed using SynergyFinder[314], which allows the direct comparison of the calculation methods highest single agent (HSA), Loewe and zero interaction potency (ZIP) in addition to Bliss (Figure 17C). All four methods yielded similar results in that the combination of $LPG_{10}SA_{0.40}$ and Oseltamivir resulted in an effect that is less than 1 % above the expected additive effect over a range of concentrations.

For comparison, much higher synergy of around 100% above the expected additive effect has been reported for combinations of Baloxavir with Oseltamivir, Zanamivir, Laninamivir or Peramivir in cell culture[318]. Combination of Oseltamivir and Amantadine even resulted in an effect of around 1000 % above the expected additive effect[319]. Therefore, the combination of $LPG_{10}SA_{0.40}$ and Oseltamivir here is neither considered strong synergy nor antagonism. This is in agreement with the MacSynergy II analysis. Based on this data, synergy between sialylated PGs and Oseltamivir seems unlikely.

4.3. Sialylated PGs are not broadly active

Since IAV HA is highly variable[320] and many amino acid changes also occur at the RBS[87], antiviral agents targeting the HA need to be tested for broad activity. The therapeutic two-step inhibition assay was employed to test the best two LPGs ($LPG_{10}SA_{0.40}$ and $LPG_{10}SA_{0.70}$) against a broad panel of influenza strains, including older and recent H3N2, pre-pandemic and pandemic H1N1 and also an H1N2 and an H7N1 strain (Figure 18A). $LPG_{10}SA_{0.40}$ and $LPG_{10}SA_{0.70}$ were able to inhibit influenza A viruses A/X31 (H3N2) and A/Mallard/439/2004 (H3N2) by several orders of magnitude and influenza A viruses A/Udorn/1972 (H3N2) and A/turkey/Italy/472/1999 by around one order of magnitude. In contrast, the propagation of influenza A viruses A/Panama/2007/1999 (H3N2), A/PR/8/34 (H1N1), A/NewCaledonia/20/1999 (H1N1), A/Bayern/63/2009 (H1N1pdm) and A/Sachsen/1816/2002 (H1N2) was not inhibited by the tested LPGs. Virus treated with control compound LPG_{10} without functionalization grew to titers comparable with untreated virus.

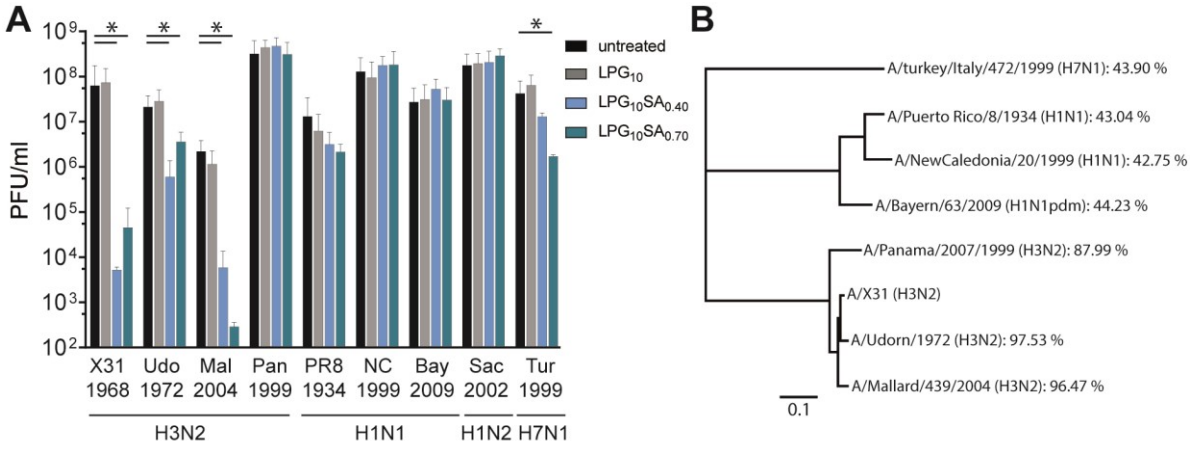

Figure 18: Inhibition of various strains of influenza virus using SA-functionalized LPG.
(A) MDCK II cells were infected with influenza viruses A/X31 (X31 1968), A/Udorn/1972 (Udo 1972), A/Mallard/439/2004 (Mal 2004), A/Panama/2007/1999 (Pan 1999), A/PR/8/1934 (PR8 1934), A/NewCaledonia/20/1999 (NC 1999), A/Bayern/63/2009pdm (Bay 2009), A/Sachsen/1816/2002 (Sac 2002) or A/turkey/Italy/472/1999 (Tur 1999) at MOI 0.01 and treated with1,67 µM [PG] of compound or left untreated for 24h (Mean ± SD, N=3 in duplicates, *p<0.05). The data of influenza viruses A/X31, A/Mallard/439/2004 and A/turkey/Italy/472/1999 have been published[275] (B) Phylogenetic Tree of the HA protein sequence of the different strains generated using Geneious Prime 2020.0.5[321]. Percentages represent the sequence identity of the HA protein on the amino acid level compared to HA of influenza A/X31 virus.

Among the influenza virus strains that got inhibited, A/X31, A/Udorn/1972 and A/Mallard/439/2004 virus share a high sequence similarity of the HA protein. They are all H3 viruses and, as well as H7 virus A/turkey/Italy/472/1999, belong to group 2 HAs (refer to section 1.1.4). In this panel of viruses, the tested LPGs were not able to inhibit H1N1 viruses, which are representatives of the group 1 HAs. Notably, influenza A/Panama/2007/1999 virus was also not

inhibited albeit being an H3N2 virus and more closely related to influenza A/X31 virus than the H7 virus. However, the amino acid sequence of A/Panama/2007/1999 virus HA does not cluster as closely as the amino acid sequence of the HAs of the other H3N2 viruses tested here (Figure 18B). Taken together, these results indicate that SA-functionalized PGs are sensitive to subtle differences in the HA RBS.

To address the question whether the lack of susceptibility of a virus strain towards $LPG_{10}SA_{0.40}$ originates in a lack of HA binding, non-susceptible strains A/Panama/2007/1999 (H3N2) and A/PR/8/34 (H1N1) were analyzed for association of Cy3-labeled compound in immunofluorescence stainings (Figure 19). As shown before in Figure 15, the propagation of susceptible strain A/X31 was reduced from infection of the whole cell layer when treated with unfunctionalized control compound Cy3-LPG_{10} to a few isolated infected cells when treated with 5 µM [PG] of Cy3-$LPG_{10}SA_{0.40}$ and Cy3-$LPG_{10}SA_{0.40}$ was only detected in infected cells. In contrast, propagation of A/Panama/2007/1999 and A/PR/8/34 viruses was not affected by Cy3-$LPG_{10}SA_{0.40}$ treatment, which was expected as both viruses had not been inhibited by SA-LPGs in the two-step inhibition assay (Figure 18A). Curiously, however, Cy3-$LPG_{10}SA_{0.40}$ was detected in many cells infected with A/Panama/2007/1999 virus, but not in cells infected with A/PR/8/34 virus. A lack of susceptibility of a virus strain towards $LPG_{10}SA_{0.40}$ is therefore not necessarily due to a complete lack of binding of viral components, presumably HA. It is likely that intrasubtype differences in the HA RBS, which are subtle compared to intersubtype differences, reduce the affinity for SA and thus render inhibition by SA-functionalized PGs ineffective without necessarily abolishing SA-binding completely. This concept is discussed in detail in Section 5.2.

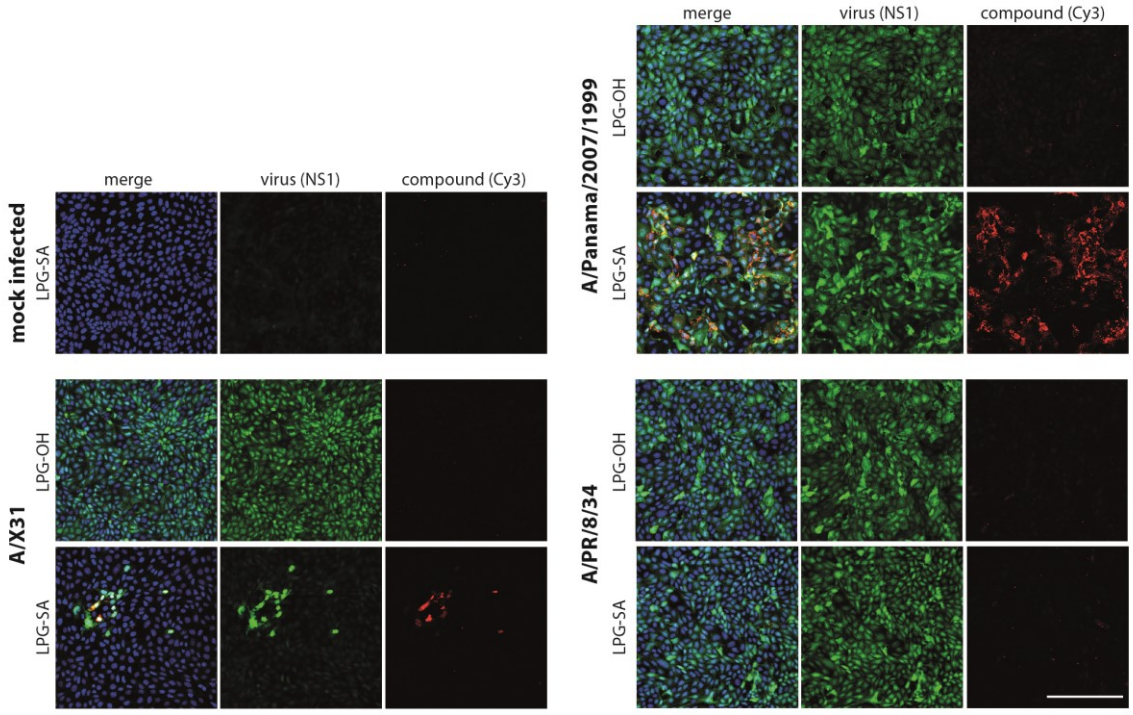

Figure 19: Association of PGs with virus in immunofluorescence stainings.
MDCK II cells were infected with the indicated virus at MOI 0.01 and treated with 5 µM of the indicated compound for 24 h. Cells were fixed, permeabilized and stained with an antibody against viral NS1 (green). Nuclei were stained with DAPI (blue) and compounds are labeled with Cy3 (red) (scale bar: 200 µM). LPG-SA refers to Cy3-labeled $LPG_{10}SA_{0.40}$ and LPG-OH refers to Cy3-labeled LPG_{10}.

4.4. Generating $LPG_{10}SA_{0.40}$ - resistant mutant viruses

Even though there have been many amino acid changes in the H3 RBS of seasonal H3N2 viruses over time, all different virus strains still have in common that they mainly bind to sugars with terminal SA[87]. For example, A/Panama/2007/1999 virus binds to terminal SA on a glycan array[87] and also associates with Cy3-$LPG_{10}SA_{0.40}$ in immunofluorescence analysis (Figure 19). This warrants the question which structural elements determine whether a virus strain is inhibited by SA-functionalized PGs and which is not. This was addressed with the following experiments.

4.4.1. Resistance develops rapidly

In order to determine the molecular basis of resistance or susceptibility as well as the threshold of resistance to SA-functionalized PGs, we induced resistance to $LPG_{10}SA_{0.40}$ in the susceptible strain A/X31 by serial passaging with increasing concentrations of compound. Resistance against commercial inhibitors Oseltamivir and Arbidol was induced in parallel as a control for the process. MDCK II cells were infected with influenza A/X31 virus at MOI 0.01 and treated with inhibitor or left untreated for 24 h. Supernatants were titrated using plaque assay before infecting subsequent passages at MOI 0.01. Each treatment was applied to three independent wells. Compound concentrations a little higher than the IC_{50} were applied in the first passage and were then increased continuously (Figure 20B). The concentration of $LPG_{10}SA_{0.40}$ was escalated up to several 100-fold of the initial concentration at passage 10 (Figure 20B). Even at passage 2 of $LPG_{10}SA_{0.40}$-treatment virus grew to 1-2 orders of magnitude higher titers with the same concentration of 1.67 nM [PG] (Figure 20A). Virus titers continued to rise with each passage even though the LPG concentration was raised at the same time. By passage ten 1.67 µM of $LPG_{10}SA_{0.40}$ were not able to substantially reduce virus titers anymore, which is 1000-fold of the initial concentration at passage 1.

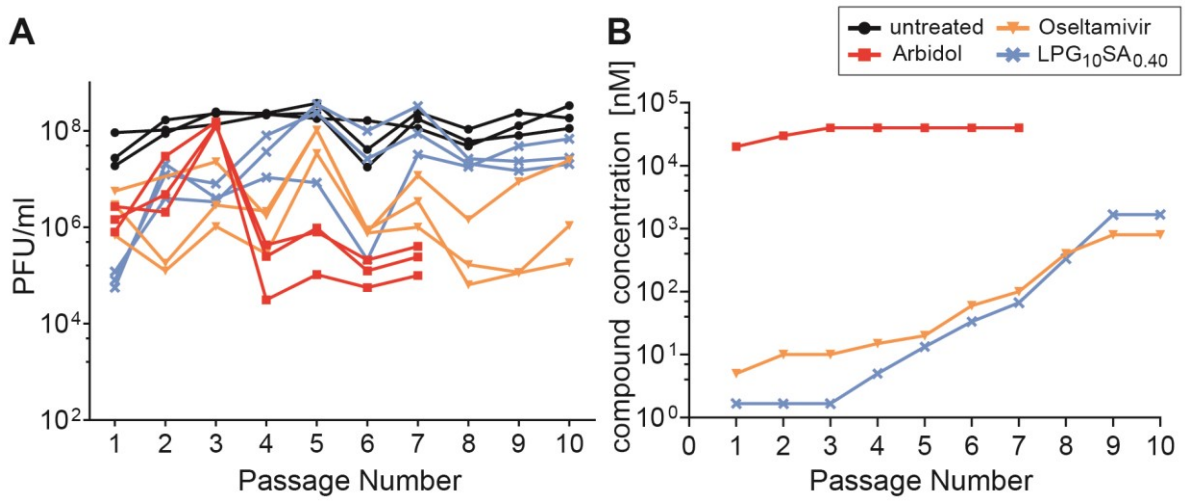

Figure 20: Inducing resistance in influenza A/X31 virus by serial passaging.
(A) MDCK II cells were infected at MOI 0.01 and treated with the indicated compound for 24h or left untreated. Supernatants were titrated with plaque assay und used to infect fresh MDCK II cells at MOI 0.01, which were treated with escalating concentrations of compound. This procedure was iterated for 10 passages in three independent wells each, and results from each well are depicted separately to visualize the differences. (B) Concentration of each compound used at each passage.

RNA of supernatants of passages 4, 7 and 10 and the initial virus stock (passage 0) was extracted, amplified with a one-step whole genome RT PCR and subjected to next generation sequencing. All mutations were the result of single nucleotide substitutions. The resulting amino acid changes and their variant frequency are listed in Table 9.

Table 9: Variant frequency of mutations induced by $LPG_{10}SA_{0.40}$, Oseltamivir or Arbidol compared to WT.

mutation	Passage 0	Passage 4			Passage 7			Passage 10		
	Reference[1]	Replicate			Replicate			Replicate		
		1	2	3	1	2	3	1	2	3
HA mutations										
$LPG_{10}SA_{0.40}$										
P99F	0.1%	0.0%	0.1%	0.0%	0.0%	20.6%	0.0%	0.0%	0.1%	94.8%
G135E	0.1%	89.8%	0.0%	0.0%	98.5%	0.0%	0.0%	98.4%	0.0%	0.0%
K140I	0.0%	0.0%	0.0%	60.9%	0.0%	0.0%	1.9%	0.0%	0.0%	0.0%
K140N	0.0%	0.0%	0.1%	29.5%	0.0%	0.0%	97.3%	0.0%	99.0%	0.0%
G144D	0.0%	0.2%	38.4%	0.0%	0.0%	98.6%	0.0%	0.0%	0.0%	99.6%
R224M	0.3%	0.1%	43.9%	0.0%	0.4%	74.3%	0.3%	0.5%	0.3%	2.3%
Oseltamivir										
G135E	0.1%	0.0%	0.0%	0.0%	0.1%	68.4%	0.1%	0.0%	98.5%	0.1%
N188D	0.1%	35.5%	82.0%	0.1%	50.9%	99.2%	0.1%	26.7%	99.4%	0.0%
S228G	0.0%	0.0%	0.0%	0.6%	0.0%	0.0%	10.0%	0.0%	0.1%	90.4%
N296T	0.5%	35.1%	79.5%	1.6%	47.5%	99.4%	0.1%	28.6%	99.5%	0.1%
A495T	0.1%	0.4%	0.9%	41.2%	0.3%	0.0%	87.8%	0.0%	0.0%	6.7%
Arbidol										
K380N	0,0%	1,8%	0,0%	0,0%	70,4%	0,0%	0,0%			
D438V	0,0%	0,0%	0,0%	16,0%	0,0%	0,0%	64,5%			
E443R	0,0%	0,0%	61,4%	0,0%	0,0%	78,5%	0,0%			
PB2 mutations										
$LPG_{10}SA_{0.40}$										
G76R	0,1%	0,0%	0,1%	0,5%	0,0%	0,0%	2,0%	0,0%	70,0%	0,0%
Oseltamivir										
E160G	0,1%	0,1%	0,3%	0,1%	5,9%	0,1%	3,3%	71,0%	0,1%	0,1%
P304S	0,0%	0,0%	0,0%	0,7%	0,1%	0,0%	28,8%	0,0%	0,1%	74,6%
I506V	0,1%	0,1%	0,0%	0,0%	0,0%	0,0%	22,8%	0,0%	0,1%	67,6%

[1] Reference corresponds to the sequence of the initial virus used to infect passage 1

Each of the three replicates per treatment had different mutations and is therefore listed separately. Notably, the sequence of the initial virus used to infect passage 1 was identical to the

sequence of the untreated passaged virus. Influenza A/X31 virus, the virus used for this experiment, is a laboratory strain with a high passaging history. Therefore, it can be assumed that the virus is stably adapted to MDCK II cell culture that its genome is in principle stable during further passage in MDCK II cells. In all treated samples mutations occurred mostly in HA. There were no mutations in other segments. Most mutations that were present in passage 10 already appeared at an earlier passage (Table 9). G135E appeared in $LPG_{10}SA_{0.40}$-treated replicate 1 already at passage 4 with high variant frequency, which was stabilized in subsequent passages. In $LPG_{10}SA_{0.40}$-treated replicate 2 mutations K140I and K140N were detected at passage 4 in 60.9% and 29.5% of the sequences, respectively. By passage 7 the K140N mutation proved dominant at 97.3% of the sequences. $LPG_{10}SA_{0.40}$-treated replicate 3 had mutations G144D and R224M at 38.4% and 43.9% respectively at passage 4, though by passage 10 only the former was present at 99.6%. Additionally, P99F occurred at 20.6% in this replicate at passage 7 and solidified to 94.8 % at passage 10. This coincides with an increase in virus titer of this replicate starting from passage 7 (Figure 20A).

Titers of Oseltamivir-treated samples reflected changes in compound concentration more closely (Figure 20A). A steep increase in concentration, for example from 20 nM at passage 5 to 60 nM at passage 6, resulted in decreased virus titers, whereas a low increase in concentration resulted in increased virus titers. The propagation of two of the three replicates was still inhibited by Oseltamivir by more than one order of magnitude at a compound concentration 160-fold of the initial concentration at passage 10. This suggests that while the virus adapted, it retained some sensitivity to Oseltamivir. Furthermore, the three replicates within the Oseltamivir- or $LPG_{10}SA_{0.40}$-treated groups displayed differences in titers at times exceeding one order of magnitude, indicating that virus adapted to treatment non-uniformly in each well. The HA mutation G135E, which developed in $LPG_{10}SA_{0.40}$-treated replicate 1, also appeared upon Oseltamivir-treatment, albeit not as early as passage 4 (Table 9). Further HA mutations induced by Oseltamivir are N188D, S228G, N296T and A495T, most of which were already present at passage 4. Notably, no NA mutations were detected despite Oseltamivir being an NA inhibitor. The HA/NA balance is very important for viral fitness[123] and some alterations in NA activity can be compensated by alterations in HA or vice versa. As such, resistance to NA inhibitors conferred by mutations in HA that decrease receptor affinity has been detected *in vitro* before[175, 322].

Increasing the Arbidol concentration was not possible after passage three because higher concentrations resulted in widespread cell death even in the absence of infection. The CC_{50} of Arbidol has been shown to be 40 µg/ml in MDCK cell culture[323]. The highest concentration used here is 40 µM and corresponds to 20.6 µg/ml. Higher concentrations are well within the concentration range exhibiting high cell toxicity. Furthermore, Arbidol is not soluble in water and therefore solved in DMSO. Adding more DMSO together with more Arbidol might have contributed to cell death. After four passages at the same Arbidol concentration and without changes in the resulting virus titer, serial passaging was stopped at passage 7 for Arbidol-treated samples (Figure 20A). Arbidol-treated samples displayed a rise in virus titers over the first 3 passages indicating adaption. However, there was a drop of more than two orders of magnitudes in virus titer in

passage 4 that continues to passage 7, although the compound concentration was not increased anymore. Since the Arbidol concentration was not increased from passage 3 to passage 4 it is unlikely that the virus is struggling due to the presence of the inhibitor. A possible explanation could be reduced viral fitness due to an acquired Arbidol-resistance. Without treatment, viral titers stayed roughly the same over the course of ten passages. Arbidol – adapted mutants were not analyzed further due to the cytotoxicity problems with Arbidol in cell culture.

Single additional mutations in the PB2 gene were detected in one $LPG_{10}SA_{0.40}$-selected variant (L2) and two Oseltamivir-selected variants (O1 and O3), but were not investigated further (Table 9). It is conceivable that a PB2 mutation may result in increased polymerase activity, and therefore contribute to compensation of attenuation of virus propagation due to inhibitors. This might especially be relevant to the Oseltamivir-induced mutations. Oseltamivir-selected Variant 2 (O2) has three HA mutations and no PB2 mutation. In contrast, Oseltamivir-selected variants 1 and 3 (O1 and O3) have two and one HA mutation, respectively, and in addition one and two PB2 mutations, respectively. It is conceivable that the three HA mutations of O2 were sufficient to confer resistance to Oseltamivir, whereas less HA mutations in the other variants were compensated by the PB2 mutations. However, further analysis is required to draw conclusions in this regard.

Plaques from passage 10 were picked and the sequence of mutant virus stocks confirmed with NGS, resulting in $LPG_{10}SA_{0.40}$ – adapted mutant viruses L1 (G135E), L2 (K140N) and L3 (P99F/G144D) and Oseltamivir – adapted mutant viruses O1 (N188D/N296T), O2 (G135E/N188D/N296T) and O3 (S228G).

4.4.2. $LPG_{10}SA_{0.40}$-induced mutations map to the RBS

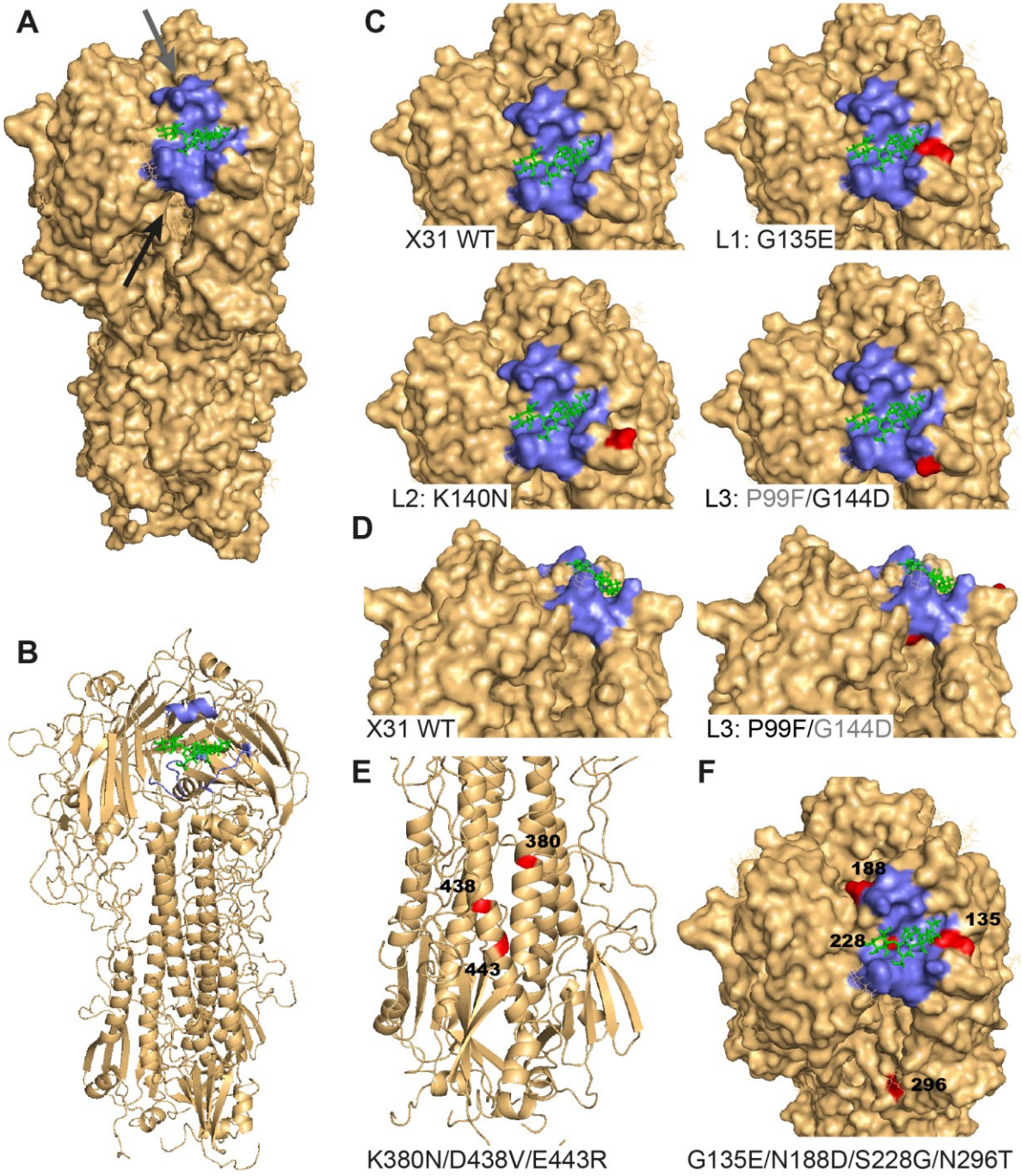

Figure 21: Crystal structure of WT and variant HAs.
Images of the HA protein of influenza A/X31 virus (PDB, 1HGG)[2] were generated using PyMOL[3]. HA structure is depicted with RBS (blue), SL (green) and mutated amino acids (red). (A) Whole WT HA trimer as a surface representation. The arrows indicate the approximate angle the RBS close-ups are viewed with the gray arrow corresponding to top view and the black arrow corresponding to down view. (B) Whole WT HA as a structure motif representation. (C) Close-ups of the top view of the RBS of WT and $LPG_{10}SA_{0.40}$-resistant mutant HAs. WT, L1, L2 and L3 are each displayed separately. (D) Down view of the RBS of WT and L3. (E) HA stem with Arbidol-induced mutations from all three independent variants. (F) HA head with Oseltamivir-induced mutations from all three independent variants.

Most mutations induced by serial passaging in the presence of either $LPG_{10}SA_{0.40}$, Oseltamivir or Arbidol occurred in HA, which is visualized in Figure 21. $LPG_{10}SA_{0.40}$-induced mutations map in or close to the RBS (Figure 21C, D). Because $LPG_{10}SA_{0.40}$ is a competitive inhibitor of receptor binding,

mutations at the RBS conform to expectations. Mutations induced by Arbidol map to the stem region of the HA (Figure 21E), which is close to where Arbidol binds (compare to section 1.2.1.5). These mutations are not visible clearly in the surface representation and are therefore displayed as structure motif representation. Other mutations conferring resistance to Arbidol that have been described before also map to regions in the HA stem in proximity but not directly in the Arbidol binding site[1]. The reason has been speculated to be due to the complexity of the structural HA rearrangements during fusion, but in essence remains to be elucidated. Oseltamivir induced mutations in the HA head region, most of which are located in the RBS (Figure 21). This is in agreement with previous findings of HA mutations reducing receptor binding affinity to confer resistance to NA inhibitors[175, 322].

4.4.3. Resistance confers cross-resistance to other sialylated PGs

Serial Passaging in the presence of $LPG_{10}SA_{0.40}$ or Oseltamivir resulted in virus variants L1 (G135E), L2 (k140N), L3 (P99F/G144D), O1 (N188D/N296T), O2 (G135E/N188D/N296T) and O3 (S228G). In order to confirm resistance to $LPG_{10}SA_{0.40}$ or Oseltamivir, respectively, the mutant viruses were analyzed in the two-step inhibition assay (Figure 22). As expected, influenza A/X31 WT virus propagation was inhibited by sialylated PGs and Oseltamivir but not by unsialylated control PGs. Interestingly, all influenza A/X31 virus variants grew to slightly higher titers than influenza A/X31 WT virus. Virus titers of the mutants L1, L2 and L3 were not reduced by $LPG_{10}SA_{0.40}$, confirming resistance to this compound.

Apart from $LPG_{10}SA_{0.40}$, there are several other multivalent PG inhibitors that differ in SA density and scaffold flexibility and thus, ultimately, in the topological presentation of their SA residues to the viral HA. In order to investigate the significance of this topology of SA presentation for resistance or susceptibility, we analyzed inhibition of the selected virus variants by two classes of multivalent SA-functionalized inhibitors effective against the parental influenza A/X31 virus. The first class is comprised of two previously described PG inhibitors: the linear $LPG_{10}SA_{0.70}$ which differs from $LPG_{10}SA_{0.40}$ in the degree of functionalization, and the dendritic $dPG_{10}SA_{0.15}$, which differs in scaffold flexibility (compare Figure 10, section 4.2.1 and Bhatia et al.[275]). The second class is SA-functionalized capsids derived from the Qβ bacteriophage. Qβ capsids were engineered to present SA in a way matching the HA trimer spatially (for details, refer to section 1.2.1.6). Sialylated Qβ phage capsids with ethylene glycol (EG) linkers of different lengths have been recently shown to be promising multivalent inhibitors of IAV HA by Lauster et al.[271]. Qβ[sia1], which has the shortest EG linker among the tested compounds, was especially effective against H3N2 viruses and therefore selected for analysis here.

Strikingly, L1, L2 and L3 were completely cross-resistant to the other PG-based compounds $LPG_{10}SA_{0.70}$ and $dPG_{10}SA_{0.15}$, despite those compounds not being used to induce adaption (Figure 22A). In contrast, the phage capsid-based compound Qβ[sia1][271] was able to reduce virus titers of mutant viruses by one to four orders of magnitude in the two-step inhibition assay, even if the inhibition was not as pronounced as for the parental influenza A/X31 virus. Taken together, these results suggest that despite their differences in SA presentation, the three PG-based compounds

target overlapping structural elements of the HA RBS. The phage capsid compound on the other hand, seems to interact with the HA RBS in a different manner that facilitates inhibition.

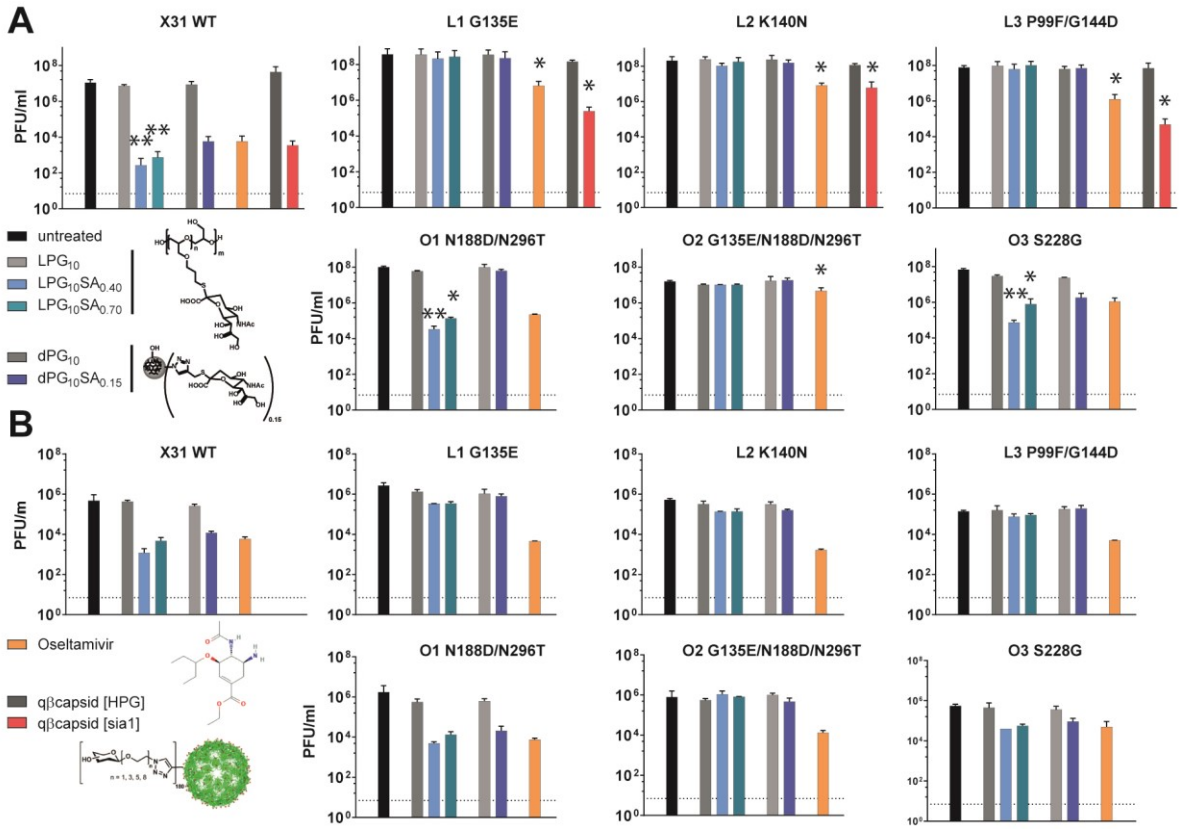

Figure 22: Cross-resistance of mutant viruses against other SA-functionalized compounds.
(A) MDCK II cells were infected with MOI 0.01 and treated with 1.67 µM [PG] of PG-compound, 0.8 µM of Oselamivir, 7 nM of capsid-compound or left untreated for the indicated time (Mean ± SD, N=2-3 in duplicates, *p<0.0332, **p<0.0021 compared to untreated). (B) Calu3 cells were infected with MOI 0.01 and treated with 1.67 µM [PG] of PG-compound, 0.8 µM of Oselamivir or left untreated for the indicated time (Mean ± SD, N=1 in duplicates). The dotted line depicts the detection limit. The structure of each compound group is illustrated in the figure legend. The capsid structure was obtained from Lauster et al.[271], Oseltamivir structure was obtained from PubChem (CID 65028) and the PG structures were kindly provided by Sumati Bhatia (group of Prof. Haag, Freie Universität Berlin).

Oseltamivir was able to inhibit L1, L2 and L3 propagation by more than one order of magnitude confirming that NA inhibition was not greatly affected by $LPG_{10}SA_{0.40}$-induced resistance (Figure 22). Oseltamivir also reduced virus titers of O1, O2 and O3, indicating that the virus variants retained some Oseltamivir-sensitivity, a notion that was also suggested earlier (4.4.1). Notably, O2 propagation was not affected by any of the sialylated PGs. This is most likely due to the presence of the mutation G135E, which was also induced by $LPG_{10}SA_{0.40}$ and conferred resistance in L1. Titers of O1 and O3 were reduced by 2-3 orders of magnitude by $LPG_{10}SA_{0.40}$ and $LPG_{10}SA_{0.70}$, which is less reduction compared to WT virus titers. Adaption in the presence of Oseltamivir resulted in mutations in HA, mostly in the RBS. It is therefore possible that the Oseltamivir-induced mutations also affect susceptibility to sialylated PGs, which act at the RBS. Curiously, O1 and O3 were only marginally affected by $dPG_{10}SA_{0.15}$. This is especially unexpected, as the three PG-based compounds were found to behave similarly towards the mutant viruses L1, L2 and L3. The HA mutations in O1 and O3, namely N188D, N296T and S228G, might be part of structural elements of the HA RBS that are targeted only by the dendritic PG for inhibition. However, it is also entirely feasible that this is

just an effect resulting from the lower efficacy of $dPG_{10}SA_{0.15}$ against influenza A/X31 WT virus propagation compared to the LPG compounds. $LPG_{10}SA_{0.40}$ and $LPG_{10}SA_{0.70}$ inhibited O1 and O3 less efficiently than influenza A/X31 WT virus, so it is possible that the efficacy of $dPG_{10}SA_{0.15}$ against O1 and O3 was also just reduced, resulting in no detectable reduction of virus titers.

To exclude that the resistance and cross-resistance to other compounds is a MDCK II cell – specific effect, the same experiment was conducted on Calu3 cells (Figure 22B). All viruses used here grew to lower titers on Calu3 cells than on MDCK II cells, but otherwise the results were the same as on MDCK II cells (Figure 22A). Therefore, resistance or susceptibility of the mutant viruses to inhibitors is not thought to depend on the cell line infected.

4.4.4. Mutant viruses display no loss of fitness

During serial passaging, the virus variants were always grown in the presence of compound. To assess whether the mutations are stable without the presence of the compound, serial passaging was conducted with the $LPG_{10}SA_{0.4}$- or Oseltamivir-resistant mutant viruses without adding compounds to the medium. Virus passaged 6 times without compound was tested for $LPG_{10}SA_{0.40}$ susceptibility. The compound was still not able to inhibit L1, L2 or L3 propagation after 6 passages in the absence of $LPG_{10}SA_{0.40}$ (Figure 23), indicating stability of the mutations. The HA segments of passage 6 L1, L2, L3, O1, O2 and O3 viruses were sequenced using Sanger sequencing and all HA sequences were identical to the sequence of the mutant viruses without passaging. There were neither revertants nor additional mutations. This confirms stability of the mutations in cell culture.

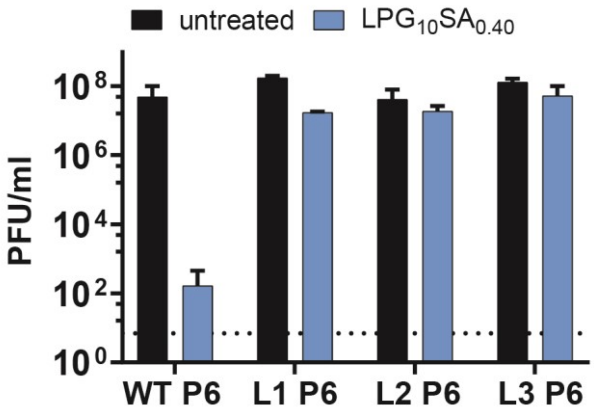

Figure 23: Persistence of the $LPG_{10}SA_{0.40}$-induced mutation.
MDCK II cells were infected with the 6th passage without treatment of X31 WT, L1, L2 or L3 at MOI 0.01 for 24h and treated with 1,67 µM [PG] of $LPG_{10}SA_{0.40}$ or left untreated (Mean ± SD, N=3 in duplicates).

In the two-step inhibition assay, mutant viruses had displayed a tendency to grow to higher titers than WT virus (Figure 22). Therefore, replication of $LPG_{10}SA_{0.40}$-resistant mutant viruses was analyzed further in growth curves (Figure 24A). Untreated, WT virus reached a titer of around 10^7 PFU/ml within 24h and then stayed at this plateau. There was a slight decrease in virus titer at 72 hpi due to the high CPE at this time point. L1, L2 and L3 displayed a steeper increase in virus titer and surpassed 10^7 PFU/ml by 16 hpi. They reached a plateau at around 10^8 PFU/ml by 24 hpi and also displayed the decrease in virus titer at 72 hpi due to the CPE. With $LPG_{10}SA_{0.40}$ treatment, WT virus growth was reduced by around 4 orders of magnitude, whereas L1, L2 and L3 were not affected. The plaque morphology of the mutant viruses also differed from WT virus (Figure 24B). WT virus formed small plaques with a large fuzzy ring around a clear center. L1 and L2 formed

larger plaques with a larger clear center and fuzzy edges. L3 formed plaques that were in size comparable to WT virus, but had no clear center and were generally less distinct. Taken together, these results consolidate the sentiment that virus fitness is not reduced by the mutations in HA. On the contrary, mutant viruses showed the tendency to replicate to higher titers and faster.

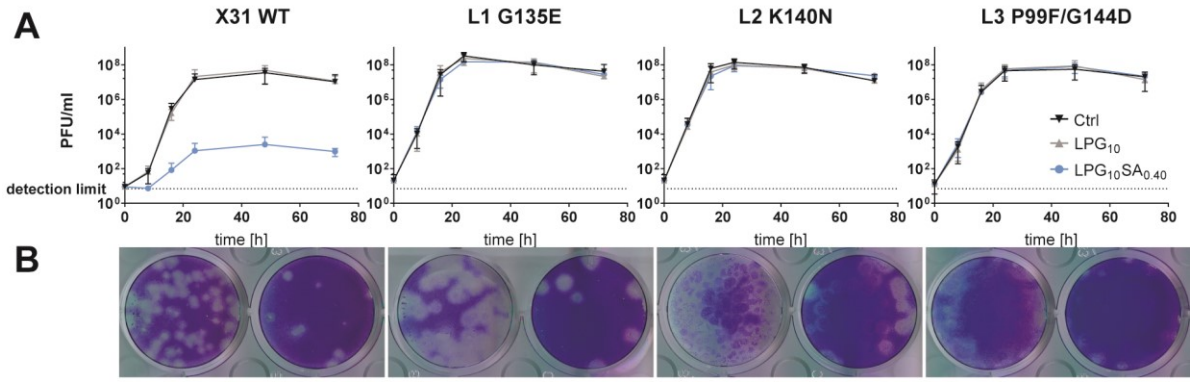

Figure 24: Growth of $LPG_{10}SA_{0.40}$-resistant virus variants.
(A) Growth curves of influenza viruses A/X31 WT, L1, L2 and L3 on MDCK II cells infected with MOI 0.01 and treated with 1.67 µM [PG] of compound or left untreated (Mean ± SD, N=3 in duplicates). (B) Exemplary image of plaques formed by influenza viruses A/X31 WT, L1, L2 and L3.

4.5. Receptor binding of mutant viruses is altered

$LPG_{10}SA_{0.40}$ is a competitive inhibitor of receptor binding and virus escaped by mutations in HA in and around the RBS. The following experiments therefore aimed at gaining a deeper understanding of how receptor binding is affected by the HA mutations.

4.5.1. Receptor binding stability of mutant viruses is reduced

Firstly, the HA elution assay was used for an indirect assessment of HA receptor binding release. Influenza viruses attach to and agglutinate erythrocytes mediated by HA binding to surface glycans and dissociate again mediated by NA cleaving SA off the glycans. The speed of virus elution depends on the HA/NA balance. In case the NA activity is the same, virus elution depends on the HA binding strength only and the HA elution assay thus presents a measure for HA binding strength. Therefore, NA activity of influenza A/X31 WT virus and the mutant viruses was measured and virus amounting to the same NA activity was employed in the HA elution assay (Figure 25A). NA activity of virus grown in chicken eggs differs from NA activity of virus grown on MDCK II cells. To get a measure for differences in NA activity, influenza A/X31 WT virus grown in allantoic fluid of two different chicken eggs was included in the analysis to compare to the MDCK II cell-grown influenza A/X31 WT and mutant viruses.

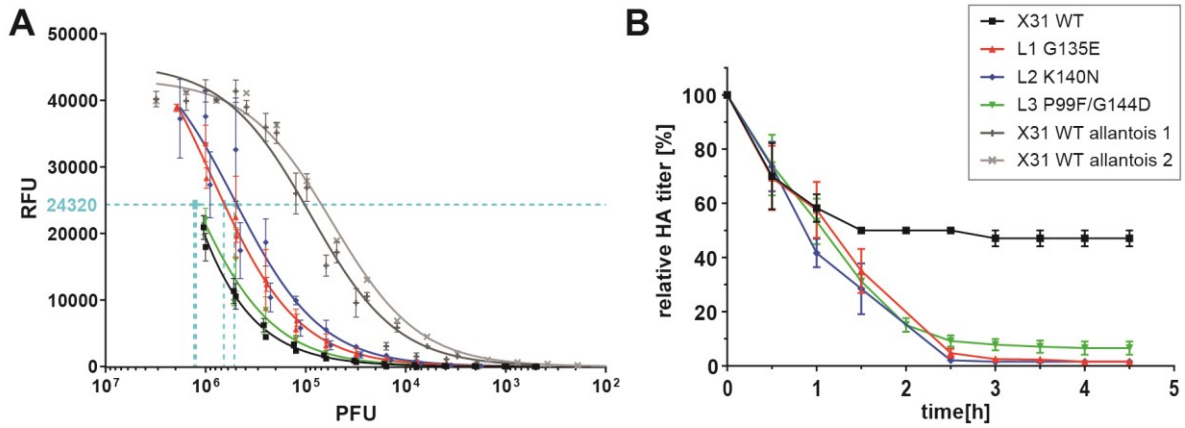

Figure 25: NA activity and receptor binding strength of mutant viruses.
(A) NA activity of A/X31 WT virus (X31 WT) and mutant viruses (L1 G135E, L2 K140N and L3 P99F/G144D) as determined by MUNANA assay. X31 WT and all mutant viruses were grown on MDCK II cells. For comparison, two influenza A/X31 WT virus stocks grown in two different allantoic fluids were included as a measure of differences in NA activity (X31 WT allantois 1 and X31 WT allantois 2). The PFU of each virus resulting in 24320 RFU (dotted cyan line) was input in the HA elution assay. (B) HA elution assay of cell culture-grown influenza A/X31 WT virus and mutant viruses. Viruses were allowed to agglutinate erythrocytes at 4°C for 1h and then eluted at 37°C by NA activity. Values were normalized to the initial HA titer. Mean ± SD, N=3 in duplicates.

NA activity as measured by MUNANA assay revealed that influenza A/X31 WT virus and the mutant viruses differed in their NA activity, but the differences were small compared to the differences observed between egg-grown and MDCK II-grown viruses (Figure 25A). In addition, there was also a small difference in the two egg-grown viruses. The differences between the mutant viruses were therefore deemed not substantial. Since there were no mutations in NA, this conforms to expectations. Small differences may stem from different numbers of NA molecules being incorporated into a virion without a change in activity of the NA itself. MUNANA assay results were used to normalize NA activity for the HA elution assay (Figure 25A, dotted cyan line). Normalized NA activity resulted in the same initial HA titer for influenza A/X31 WT virus and the mutant viruses (not depicted in Figure 25B, because normalized results are shown there). Influenza A/X31 WT virus was eluted from erythrocytes steadily during the first 1.5 h to 50 % of the original HA titer, but was not eluted further afterwards (Figure 25B). In contrast, all mutant viruses were almost completely eluted from erythrocytes after 2.5 h. This indicated that the receptor binding strength of the mutant viruses was reduced compared to influenza A/X31 WT virus.

Single-virus force measurements using atomic force microscopy (AFM) were employed to obtain a direct measurement of the actual interaction of the receptor with WT or mutant viruses. To this end, a PEG-coated glass surface was spotted with 6' sialyllactose (SL) receptors using the streptavidin-biotin interaction. Bifunctional PEG cross-linkers were used to attach virions covalently to the AFM cantilever. The cantilevers were then lowered over the receptor coated glass layer, allowing virions to interact with the spotted SL receptor. Cantilevers were then retracted again. For retraction, a force is required to break the virion-receptor interactions that have formed. These breaking forces are detected and provide an indication for the interaction forces between receptor and virion. Dynamic force spectra for WT virus as well as L1 and L3 were measured and fitted by Malte Hilsch and Valentin Reiter-Scherer (AG Herrmann, Humboldt Universität zu Berlin) (Figure 26). The separation from the energy barrier x_b, kinetic off rate k_{off} and average bond lifetime τ_{off} were calculated by fitting the dynamic force spectra (Table 10). The separation from the free energy barrier x_b was larger for influenza A/X31 WT virus than for the mutant viruses L1 and L2, indicating stronger interaction of the receptor with the parental virus. Furthermore, the kinetic off rate K_{off} of mutant viruses was revealed to be around 30-fold higher for mutant viruses than for WT virus, and as a result, the average bond lifetime τ_{off} was around 30-fold higher for WT virus.

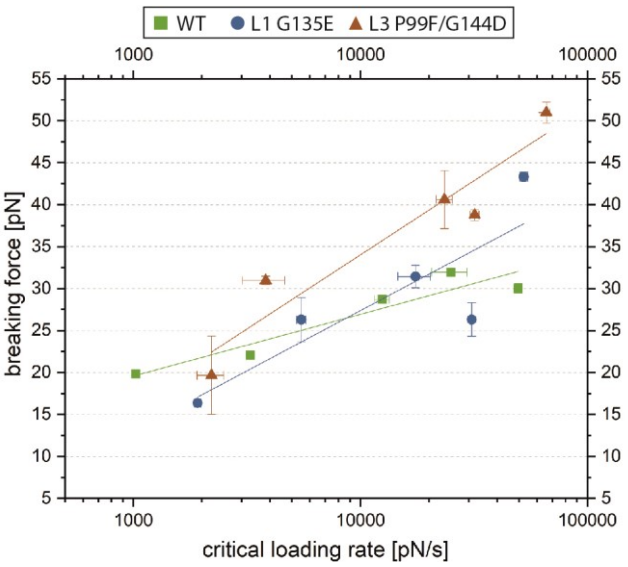

Figure 26: Dynamic force spectrum of a single virus-receptor interaction as determined by AFM.
Influenza virions were covalently attached to AFM cantilevers and lowered onto a PEG-coated glass surface with spotted SL receptor. During retraction of the cantilever from the receptor-coated surface, breaking forces were detected. AFM measurements were conducted and evaluated by Malte Hilsch and Valentin Reiter-Scherer (AG Herrmann, Humboldt Universität zu Berlin). The image was adapted with permission.

Table 10: Separation from the energy barrier x_b, kinetic off rate k_{off} and average bond lifetime τ_{off} calculated from the dynamic force spectra by fitting the data.[1]

	x_b (nm)	k_{off} (s^{-1})	τ_{off} (s)
X31 WT	1.27 ± 0.25	0.68 ± 0.99	1.475
L1 G135E	0.63 ± 0.23	19.93 ± 26.89	0.050
L3 P99F/G144D	0.53 ± 0.10	15.46 ± 11.15	0.065

[1]Results kindly provided by Malte Hilsch and Valentin Reiter-Scherer (AG Herrmann, Humboldt Universität zu Berlin)

4.5.2. Receptor binding profile of mutant viruses is altered

Results from the HA elution assay and AFM measurements suggest that the receptor binding stability of the mutant viruses is weaker compared to influenza A/X31 WT virus. However, virus growth was not negatively affected (Figure 24). Therefore, the mutant viruses probably still enter cells by attaching to their surface via sugar chains. It is unclear if the mutant viruses utilize the same glycan receptors as the WT virus but with lower affinity of if they prefer other glycan receptors altogether. This question of how the receptor binding preference changed due to the HA mutations was explored using glycan array analysis, a tool widely used to investigate influenza virus

binding specificities. Two different arrays were employed: A low-density array produced in the Max Planck Institute of colloids and interfaces that has been used to investigate IAV binding specificity before[112] (Figure 27, Array 1) and a larger commercial array by RayBiotech (Figure 27, Array 2).

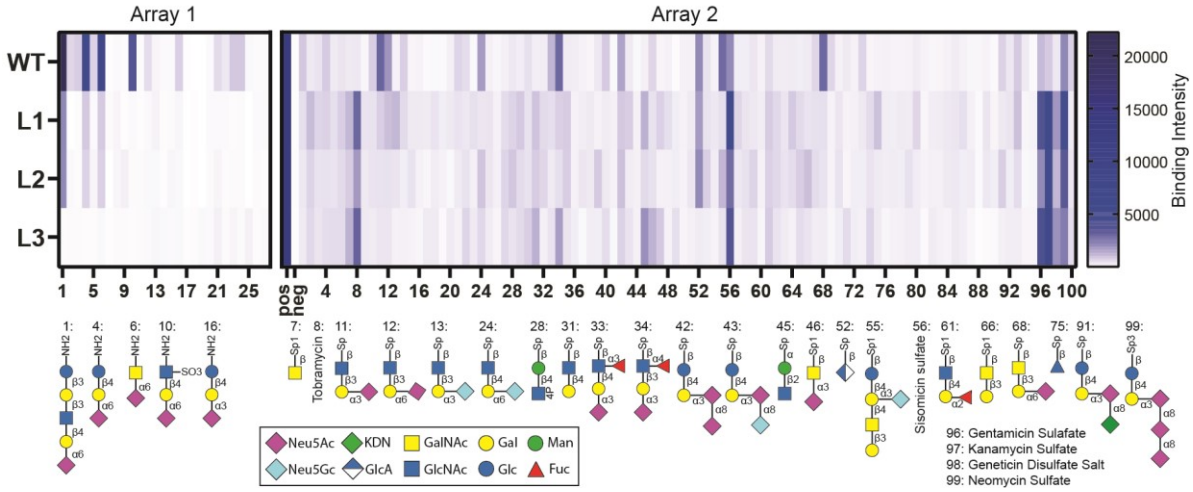

Figure 27: Binding profile of influenza A/X31 WT and mutant viruses on glycan arrays.
A low-density array by the Max Planck institute of colloids and interfaces (Array 1) and a commercial array by RayBiotech (Array 2) were used. Selected glycans which showed virus binding are displayed below the heatmap. Refer to the Appendix for the full list of glycans on the array. Binding intensity was calculated from the median of three independent experiments. Individual slides were normalized to the positive control of the respective array.

On Array 1, 25 glycans were spotted including 14 sialylated glycans, 4 of which have terminal α2,6-linked N-acetylneuraminic acid (Neu5Ac), the canonical human IAV receptor[100]. Array 2 features 100 glycans that display more diversity and also include other sialic acids such as N-glycolylneuraminic acid (Neu5Gc) in addition to the classical Neu5Ac. Influenza A/X31 WT virus bound to human receptor type glycans with terminal α2,6-linked Neu5Ac with high binding intensity (Figure 27). Additionally, WT virus bound some glycans with terminal α2,3-linked Neu5Ac, which is not surprising because influenza A/X31 virus has been passaged in chicken eggs, which express this receptor abundantly[324]. In contrast, the mutant viruses did not bind terminal α2,6-linked Neu5Ac with high binding intensity. L1 and L2 bound to 6´-Sialyllactose, sulfated 6'-sialyl-N-acetyllactosamine and LSTc with around 100-fold reduced binding intensity compared to WT virus and L3 did not bind them at all. Instead, L1 and L2 bound several distinct glycans with terminal α2,8-linked sialic acids or terminal Neu5Gc. L3 on the other hand displayed a preference for fucosylated glycans and α2,3-linked Neu5Ac. All three mutant viruses bound terminal N-acetylglucosamine (GlcNAc) and also terminal galactose. Binding to terminal galactose was especially pronounced for L2. Furthermore, all three mutant viruses bound strongly to all six aminoglycosides presented on array 2. In contrast, WT virus recognized only sisomicin sulfate and neomycin sulfate, and to a lesser extent also gentamicin sulfate and kanamycin sulfate, all with lesser binding intensity than the mutant viruses. However, aminoglycosides are not present on mammalian cells and therefore should not play a role in infection of MDCK II cells. Taken together, the receptor binding preference of each mutant virus was distinct and differed from WT virus. The findings obtained from glycan array analysis indicate that mutant viruses have lost their ability to bind the typical human-type receptors with high affinity. Rather, the mutant viruses acquired or

maintained binding to different glycan receptors, of which MDCK II cells express a vast variety[325-327]. These results suggest that the mutations induced resistance to $LPG_{10}SA_{0.40}$ by altering the receptor binding profile from glycan receptors competing with $LPG_{10}SA_{0.40}$ for binding of HA to receptors that are not affected by the SA-PG.

4.5.3. Cy3-labeled $LPG_{10}SA_{0.40}$ associates with mutant viruses in IF staining

All three mutant viruses were resistant to inhibition by SA-functionalized PGs and displayed altered receptor binding profiles in glycan array analysis. However, they were still inhibited by SA-functionalized phage capsids and showed transient binding to the SL receptor in AFM measurements. This warrants the question of whether Cy3-labeled $LPG_{10}SA_{0.40}$ would still be retained by the mutant virus HA in immunofluorescence analysis.

Although mutant virus propagation was not inhibited by Cy3-$LPG_{10}SA_{10}$, this compound decorated cells infected with mutant viruses as well as influenza A/X31 WT virus (Figure 28A). This pattern of compound binding without inhibition of virus propagation has also been observed for A/Panama/2007/1999 (H3N2) virus (Figure 19). Control compound Cy3-LPG_{10} was washed off during slide preparation as it did not bind anything on the slides (Figure 28B). As observed in AFM measurements, these results confirm that mutant viruses still bind terminal SA on glycans or SA-functionalized PGs, but with a different stability or affinity presumably due to the changed RBS geometry.

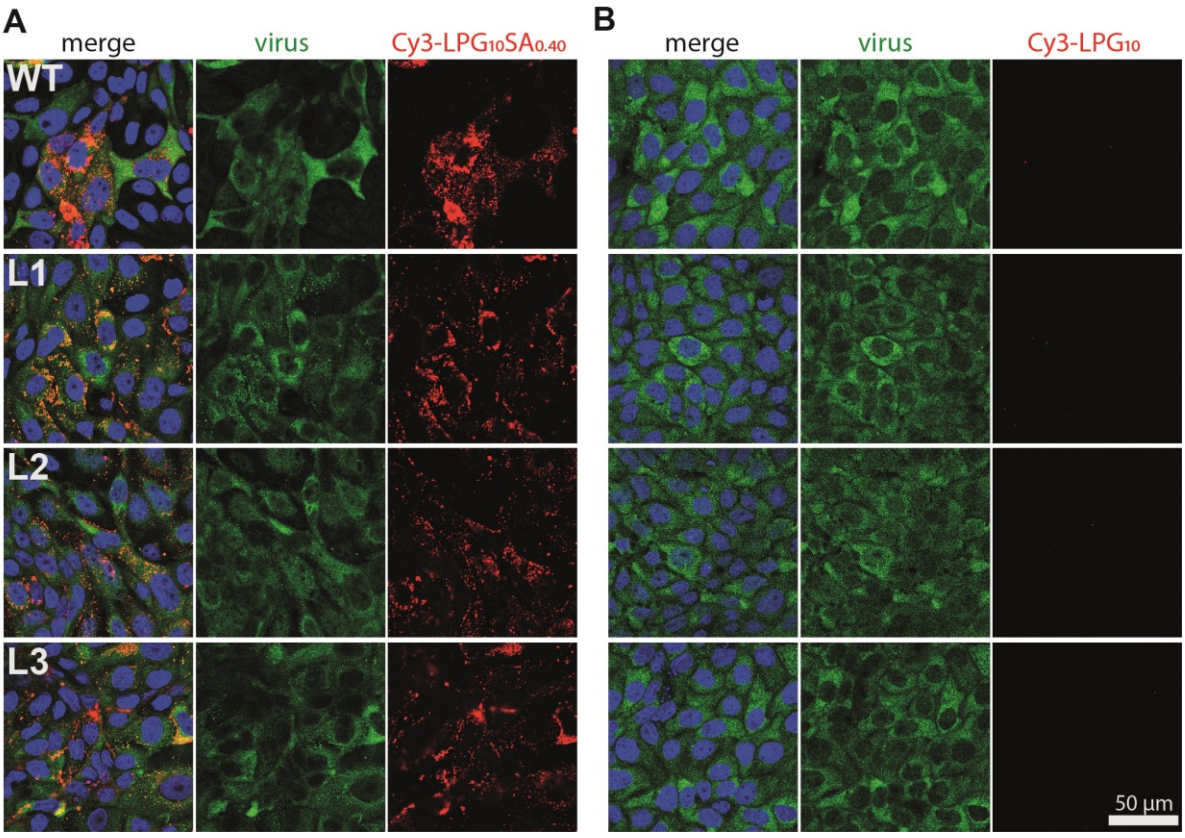

Figure 28: Association of PGs with mutant viruses in immunofluorescence stainings.
MDCK II cells were infected with the indicated virus at MOI 0.01 and treated with 10 µM of Cy3-$LPG_{10}SA_{0.40}$ (A) or Cy3-LPG_{10} (B) for 24 h. Cells were fixed, permeabilized and stained with an antibody against viral NS1 (green). Nuclei were stained with DAPI (blue) and compounds are labeled with Cy3 (red) (scale bar: 50 µM).

4.6. Mutated positions alone do not determine susceptibility

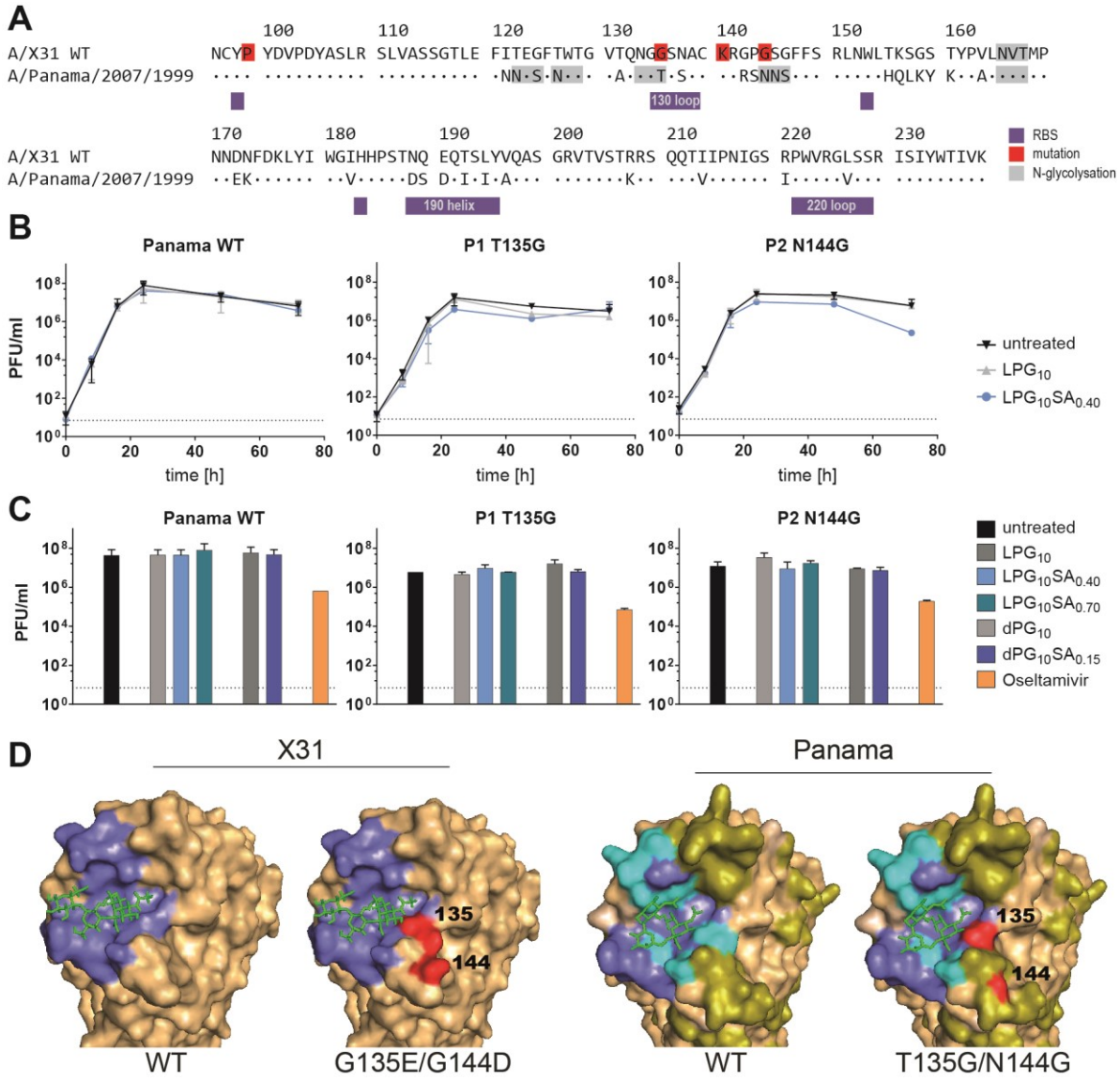

Figure 29: Effect of the reverse $LPG_{10}SA_{0.40}$-resistance mutations in influenza A/Panama/2007/1999 virus.
(A) Partial HA sequence including the RBS (purple). The amino acid identity of influenza A/Panama/2007/1999 virus with influenza A/X31 WT virus is indicated. Positions that are mutated in L1, L2 or L3 are highlighted in red and possible N-glycosylation sites are marked in grey. (B) Growth curves of influenza A/Panama/2007/1999 WT virus and the mutant viruses P1 and P2. MDCK II cells were infected at MOI 0.01 and treated with 1.67 µM [PG] of compound or left untreated for the indicated time (Mean ± SD, N=2 in duplicates). (C) Two-step inhibition assay of influenza A/Panama/2007/1999 WT virus and the mutant viruses P1 and P2. MDCK II cells were infected at MOI 0.01 and treated with 1.67 µM [PG] of compound or left untreated for 24h (Mean ± SD, N=2 in duplicates). (D) HA head monomer surface representation with RBS (purple), SL (green) and mutated amino acids (red). Differences between influenza viruses A/X31 and A/Panama/2007/1999 are visualized in olive and differences in the RBS are colored cyan. Crystal structures of the HA protein of influenza A/X31 virus (PDB, 1HGG)[2] or influenza A/Wyoming/3/2003 virus (PDB, 6BKR)[328] were generated using PyMOL[3]. Amino acids of influenza A/Wyoming/3/2003 virus were changed to match the influenza A/Panama/2007/1999 virus sequence.

One (G135E in L1 and K140N in L2) or two (P99F and G144D in L3) mutations in HA were sufficient to render influenza A/X31 virus resistant against $LPG_{10}SA_{0.40}$. An alignment of influenza viruses A/X31 and A/Panama/2007/1999 HA sequences shows that two of the positions, namely P99 and K140, are the same in the two viruses (Figure 29A). As A/Panama/2007/1999 virus is not susceptible to $LPG_{10}SA_{0.40}$, these positions alone should not determine susceptibility in general but only in influenza A/X31 virus. Positions 135 and 144 are part of the possible N-glycosylation sites

NGT and NNS, respectively, in A/Panama/2007/1999 virus. There is no N-glycosylation motif at these positions in influenza A/X31 virus. HA glycosylation plays an important role in receptor binding, with additional HA glycosylations generally reducing receptor binding affinity [81, 120]. It is therefore conceivable that changing positions 135 and 144 of A/Panama/2007/1999 virus to glycine as in influenza A/X31 virus and thereby destroying the N-glycosylation sites might render the virus susceptible to SA-functionalized PGs. To test this hypothesis, recombinant A/Panama/2007/1999 viruses carrying the HA mutation T135G (P1) or N144G (P2) were generated. For this purpose, mutations were introduced into an HA encoding plasmid using site-directed mutagenesis. Subsequently, the mutated plasmids were each transfected together with plasmids containing the remaining genomic information of A/Panama/2007/1999 virus and the resulting A/Panama/2007/1999 mutant viruses were rescued.

First, growth of the influenza A/Panama/2007/1999 mutant viruses was analyzed in comparison to influenza A/Panama/2007/1999 WT virus (Figure 29B). Untreated, influenza A/Panama/2007/1999 WT virus reached a titer of around 10^8 PFU/ml after 24 hpi and then stayed at this plateau. Afterwards, the virus titer decreased slightly due to the increasing CPE. $LPG_{10}SA_{0.40}$ treatment did not affect influenza A/Panama/2007/1999 WT virus growth, as also observed in the two-step inhibition assay and immunofluorescence analysis (Figure 18 and Figure 19). Virus titers of P1 and P2 rose to 10^7 PFU/ml within 24 hpi and afterwards displayed the same slight decrease in titer. $LPG_{10}SA_{0.40}$ treatment did not affect P1 or P2 virus growth substantially. This indicates that positions 135 and 144 alone do not determine susceptibility to $LPG_{10}SA_{0.40}$ in general but only in influenza A/X31 virus. Interestingly, P1 and P2 virus showed the tendency to grow to lower titers than influenza A/Panama/2007/1999 WT virus. This mirrors growth of L1, L2 and L3 viruses, which grew to higher titers than influenza A/X31 WT virus. P1 and P2 viruses were not susceptible to $LPG_{10}SA_{0.70}$ or $dPG_{10}SA_{0.15}$ either (Figure 29C), indicating that resistance of P1 and P2 virus may not be limited to one compound, just as influenza A/Panama/2007/1999 WT virus or influenza A/X31 mutant viruses L1, L2 and L3. Inhibition by Oseltamivir remained unaffected by the mutations, as expected. The crystal structure of influenza A/Panama/2007/1999 WT-like virus and influenza A/X31 WT virus HA in comparison to the mutated HA is shown in Figure 29D. There is no crystal structure available for influenza A/Panama/2007/1999 virus, therefore the most similar available structure (A/Wyoming/3/2003, 95.94% sequence identity) was modified to match the influenza A/Panama/2007/1999 virus HA sequence used for imaging. Even though the HA of influenza A/X31 virus and A/Panama/2007/1999 virus has an overall sequence identity of 87.63% at the amino acid level and the RBS is structurally similar, there are still many amino acid differences especially on the surface of the HA head (Figure 29D, olive) and also in the RBS (Figure 29D, cyan). Other amino acid differences between the HA of influenza viruses A/X31 and A/Panama/2007/1999 probably compensate the effect of changing position 135 or 144 in P1 and P2. To render influenza A/Panama/2007/1999 virus susceptible to SA-functionalized PGs, more than one amino acid change might be required.

4.7. Strategies to improve compounds

PGs functionalized with SA do inhibit influenza A/X31 virus but do not cover a broad range of other strains (Figure 18). Viral resistance against LPG10SA0.40 develops rapidly (Figure 20) by altering the receptor binding profile (Figure 27). The SA binding strength of mutant HA is reduced but not abolished completely (Figure 25B, Figure 26 and Figure 28). Mutant viruses still bind to glycans with terminal SA but with different binding stability and with a preference for different glycans, probably due to the changed RBS geometry. Inhibition of viral HA by SA-functionalized PGs appears to be very sensitive to variations. One amino acid change was observed to be sufficient to render a SA-functionalized PG inhibitor ineffective. Minor changes in PG configuration such as the degree of functionalization or scaffold flexibility were not sufficient to broaden the spectrum of inhibited virus strains even within the H3N2 subtype. The specific presentation of the SA functionalization, however, did strongly affect the antiviral activity, as seen with phage capsid constructs (Figure 22). In an attempt to extend the spectrum of susceptible strains and subtypes by making PG-based inhibitors less susceptible towards amino acid variations in HA, PG functionalization and the presentation thereof was changed in additional compounds in collaboration with the group of Prof. Haag (Freie Universität Berlin).

Glycan structures are highly diverse[99], and influenza virus binding is known to be impacted by the underlying sugars and not only the terminal SA[112, 113]. A meta-analysis of a variety of influenza viruses on a variety of glycan arrays revealed SL to be a structure commonly bound[116]. Furthermore, even if compared to WT virus binding to SL was reduced in L1 and L2 and nearly abolished in L3, it was one of very few glycans that was at least in part bound both by influenza A/X31 WT virus and the mutant viruses. PGs functionalized with SL were hence synthesized to aim at an increased number of inhibited influenza viruses. To address the importance of SA presentation, two slightly different presentations of the sugar residues on the PGs were investigated by incorporating two different linkers (Figure 30). All compounds were synthesized by the group of Prof. Haag (Freie Universität Berlin). In the following, advances comprising these modifications are introduced.

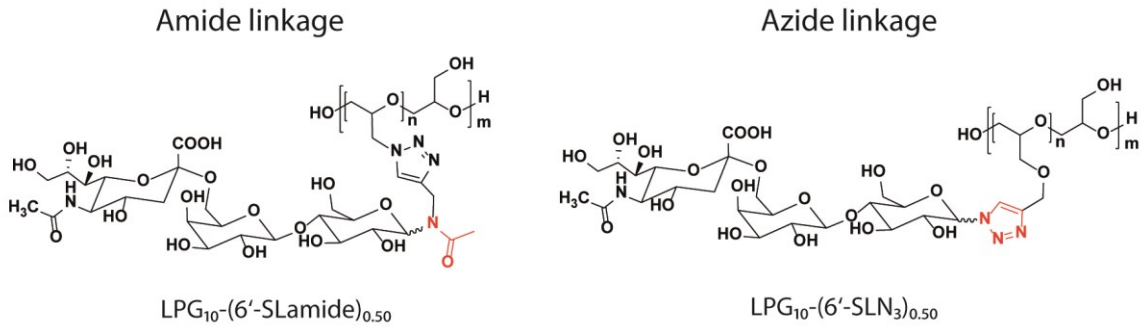

Figure 30: Structure of Amide and Azide linkers.
The sugar functionalization was attached to the PG scaffold using either an amide group (left) or an azide group (right) in the anomeric position. As an example for a PG with an amide linker LPG_{10}-(6'-SLamide)$_{0.50}$ is depicted, and as an example for a PG with an azide linker LPG_{10}-(6'-SLN_3)$_{0.50}$ is depicted. The image was provided by Sumati Bhatia (AG Haag, FU Berlin) and modified with permission.

PGs were modified by changing the functionalization and incorporating different linkers in order to improve the activity range of multivalent compounds. For this analysis, sialyllactose (SL) instead of only SA was attached to PGs via either amide or azide linkers. A variety of PGs was synthesized with SL in α2,6 and α2,3 configuration, different SL densities and linear or dendritic PG configuration. All compounds were synthesized by the AG Haag (Freie Universität Berlin). As with SA-PGs, compound names are made up of their configuration as follows: scaffold$_{MW}$-(sugar linkage-SLlinker)$_{DF}$, where N_3 corresponds to the azide linker and amide corresponds to an amide linker. DF, the degree of functionalization, represents the SL density. Compounds without functionalization of both the linear and the dendritic scaffold were used as control compounds (LPG_{10} and dPG_{10}). These are the same as used before as controls for the SA-functionalized PGs, because the scaffolds remained unchanged. All modified compounds were screened for antiviral activity in the two-step inhibition assay.

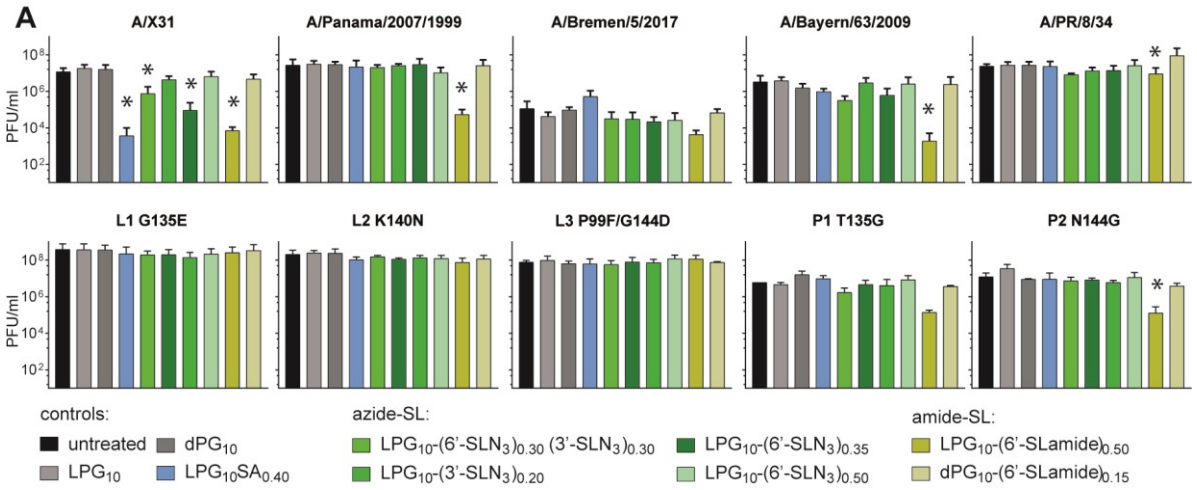

Figure 31: Inhibition of various strains of influenza virus using SL-functionalized PGs.
Two-step inhibition assay of the indicated virus strains (A), $LPG_{10}SA_{0.40}$-resistant influenza A/X31 mutant viruses (B) or recombinant influenza A/Panama/2007/1999 viruses (C). MDCK II cells were infected at MOI 0.01 and treated with 5 µM [PG] of compound or left untreated for 24h. LPG_{10} and dPG_{10} are control compounds with linear or dendritic scaffold, respectively, which were not functionalized (Mean ± SD, N=2-3 in duplicates, *p<0.05 compared to untreated).

Virus titers of influenza A/X31 virus were reduced significantly by several SL-functionalized PGs such as LPG_{10}-(6'-SLN_3)$_{0.35}$, LPG_{10}-(6'-SLN_3)$_{0.30}$(3-SLN_3)$_{0.30}$, and LPG_{10}-(6'-SLamide)$_{0.50}$ (Figure 31A). The α2,3 configuration SL LPG_{10}-(3'-SLN_3)$_{0.20}$ and the dPG dPG_{10}-(6'-SLamide)$_{0.15}$, respectively, were not able to reduce virus propagation. This is in agreement with the binding preference of influenza A/X31 virus for human type receptors and with LPGs outperforming dPGs. Interestingly, LPG_{10}-(6'-SLN_3)$_{0.50}$, which differs from LPG_{10}-(6'-SLamide)$_{0.50}$ only in linker, was not able to reduce virus titers of influenza A/X31 virus. This indicated that the linker between SL and PG is a crucial factor in determining the inhibitory potency of a compound. Reduction of propagation of other strains was only marginal for azide linked SL-PGs, reflecting the results with SA-PGs (Figure 18). However, amide linker compound LPG_{10}-(6'-SLamide)$_{0.50}$ was able to reduce virus titers of not only influenza A/X31 virus but also the more recent influenza viruses A/Panama/2007/1999 (H3N2) and A/Bayern/63/2009 (H1N1pdm) by two to three orders of magnitude (Figure 31A). The titer of influenza A/Bremen/5/2017 (H3N2) virus was reduced by more than one order of magnitude and the titer of non-circulating influenza A/PR/8/34 (H1N1) virus was reduced significantly albeit by less

than one order of magnitude, overall solidifying LPG_{10}-(6'-SLamide)$_{0.50}$' potential of broad activity. As with influenza A/X31 virus, the analog azide linker compound LPG_{10}-(6'-SLN_3)$_{0.50}$ was not able to substantially inhibit virus propagation, indicating that the linkage of SL is indeed essential to the antiviral effectivity of the compounds. Nonetheless, dPG_{10}-(6'-SLamide)$_{0.15}$ was not able to reduce virus titers albeit amide linkage, suggesting that the right linkage alone is not decisive but the specific compound configuration is pivotal for antiviral efficacy.

An effect of the degree of functionalization (DF) was observed for influenza A/X31 virus, were azide compound LPG_{10}-(6'-SLN_3)$_{0.35}$ was able to reduce virus titers and LPG_{10}-(6'-SLN_3)$_{0.50}$ was not able to reduce virus titers despite the higher SL density. It is possible that there is also a DF-dependent effect in amide linker compounds. Further analysis of amide linker compounds differing in DF is required to address this aspect. Presenting a mixture of α2,6- and α2,3-linked SL (LPG_{10}-(6'-SLN_3)$_{0.30}$(3-SLN_3)$_{0.30}$) did not add to the inhibitory potential of the compound. This might be due to the fact that the α2,3-linked SL compound LPG_{10}-(3'-SLN_3)$_{0.20}$ did not inhibit any of the strains tested here, therefor including α2,3-linked SL in the compound did not add to the inhibitory effect. Avian influenza strains are presumably more susceptible to this compound. Unfunctionalized control compounds were not able to reduce virus titers. Strikingly, none of the SL-PGs were able to inhibit propagation of the $LPG_{10}SA_{0.40}$ resistant mutant viruses, not even LPG_{10}-(6'-SLamide)$_{0.50}$ (Figure 31B). The recombinant Panama viruses display the same behavior as the Panama WT virus and are thus only inhibited by LPG_{10}-(6'-SLamide)$_{0.50}$ (Figure 31C). This data suggests that other amino acids in addition to positions 99, 135, 140 and 144 determine resistance or susceptibility of SL-PGs. It is curious, however, that A/X31 variants L1, L2 and L3 are not inhibited by LPG_{10}-(6'-SLamide)$_{0.50}$. So far, the broad resistance of L1, L2 and L3 had been comparable to other virus strains like A/Panama/2007/1999. But in this analysis, they are the only H3N2 viruses tested that are completely resistant to LPG_{10}-(6'-SLamide)$_{0.50}$. In conclusion, LPG_{10}-(6'-SLamide)$_{0.50}$ has a broader activity than PGs tested before and therefore represents valuable progress. However, it's inhibitory efficacy still has some limitations and further optimization is warranted in order to obtain a multivalent sialylated inhibitor that is truly broadly active against an even more expanded spectrum of influenza viruses.

5. Discussion

Influenza virus is the causative agent of the flu in humans and annually leads to around 3 to 5 million cases of severe illness and around 290 000 to 650 000 death worldwide[6]. This disease burden is accompanied by a substantial economic burden resulting from direct medical costs as well as indirect costs caused by absenteeism and a loss of productivity[7, 10]. Several vaccines and several classes of antiviral drugs are available to combat influenza. However, influenza virus evolves rapidly[329], resulting in unsatisfactory protection by the vaccine and resistance against existing antivirals[208, 330]. Therefore, additional antiviral agents are needed urgently.

The viral surface protein hemagglutinin (HA) mediates attachment to cells by binding to glycans with terminal sialic acid (SA) on the host cell surface. As an individual HA-SA interaction is weak and has a dissociation constant in the millimolar range[90], multiple receptor interactions are required to stabilize the attachment[91, 93]. Targeting HA with compounds presenting SA units on their surface multivalently is a promising approach to inhibit influenza virus attachment and consequently infection[252, 253]. To this end, multivalently functionalized polyglycerols have proven advantageous due to their high biocompatibility and easy synthesis[292, 293]. Previous work proved that derivatized linear polyglycerol inhibited influenza A/X31 virus propagation more efficiently than derivatized dendritic polyglycerol and determined 40 % as the optimal degree of functionalization of linear polyglycerol with SA[275]. However, the potential of this optimized compound, $LPG_{10}SA_{0.40}$, to inhibit the propagation of a broad range of influenza viruses had not been investigated fully. Since influenza virus evolution can impact determinants of receptor binding[87], it is crucial that new drug candidates are tested for broad activity.

Here, $LPG_{10}SA_{0.40}$, the previously optimized linear polyglycerol with 40 % SA functionalization[275], was initially evaluated for its capacity to inhibit a broad range of influenza virus strains. Cell culture experiments revealed that the inhibitory capacity of $LPG_{10}SA_{0.40}$ was limited and suggested that the SA-functionalized PGs are sensitive to subtle differences in the HA RBS. This study therefore focused on elucidating the molecular basis for this limitation in PG broad activity with the aim to modify and adjust the compounds in order to broaden the spectrum of susceptible IAV strains. To this end, $LPG_{10}SA_{0.40}$ – resistant virus variants were induced in the susceptible IAV strain A/X31 via serial passaging. The resulting amino acid changes in HA, namely G135E (L1), K140N (L2) and P99F/G144D (L3) were investigated for their impact on receptor binding. Indeed, the mutant viruses differed in their receptor binding profile in glycan array analysis. However, resistance and susceptibility do not hinge on these amino acids alone, as reverse genetically engineered A/Panama/2007/1999 mutant viruses carrying these same amino acid changes were not rendered susceptible to $LPG_{10}SA_{0.40}$. Finally, strategies to improve the multivalent polyglycerol compounds were explored. In the following paragraphs the findings are discussed in more detail.

5.1. PGs as inhibitors of influenza A/X31 virus (H3N2)

Despite the limitations of multivalent sialylated polyglycerols described in this study and discussed in later chapters, the compounds are very effective against influenza A/X31 virus. Therefore, this section focuses on inhibition of influenza A/X31 virus and the insights gained from this work.

In a previous study, polyglycerols were optimized regarding their flexibility and the degree of functionalization[275]. Linear, flexible PGs $LPG_{10}SA_{0.40}$ and $LPG_{10}SA_{0.70}$ with a degree of functionalization with SA of 40 % and 70 %, respectively, and dendritic, rigid PG $dPG_{10}SA_{0.15}$ with 15 % SA functionalization were identified as most effective at inhibiting influenza A/X31 virus propagation. Here, IC_{50} values of these PGs were determined (Table 8). The linear PGs had around 5-fold lower IC_{50} values than the dendritic PG, consistent with the findings of Bhatia et al.[275]. Moreover, $LPG_{10}SA_{0.40}$ was confirmed as being most effective at inhibiting influenza A/X31 virus propagation. Notably, the IC_{50} value of $LPG_{10}SA_{0.40}$ was more than 100-fold lower than that of Oseltamivir. It has to be taken into account that $LPG_{10}SA_{0.40}$ is functionalized with 60 SA units, so it has 60 functional units, whereas Oseltamivir is a small molecule, which is only one functional unit. However, even when calculating the IC_{50} value for a single functional unit, meaning a single SA moiety, the IC_{50} of $LPG_{10}SA_{0.40}$ is around three-fold lower than that of Oseltamivir. Still, Oseltamivir activity was most likely underestimated in this study, as experiments were conducted on MDCK II cells. Because MDCK II cells do not express high levels of α2,6-linked Neu5Ac, influenza A viruses rely less on NA activity and are therefore less sensitive to NA inhibitors like Oseltamivir when propagated in these cells [331]. The IC_{50} of $LPG_{10}SA_{0.40}$ relating to one molecule of $LPG_{10}SA_{0.40}$ with 60 SA units is 15.13 nM, which is comparable to or better than the IC_{50} value achieved with other multivalent constructs. For example, phage capsids and peptide-nanoparticles are active in the low nanomolar particle range[271, 291]. Dendritic polymers functionalized with SL require much more compound and have an IC_{50} in the low to high micromolar range[260, 261]. Di- and Trivalent carbohydrate-based constructs aiming for chelation effects have an IC_{50} in the high nanomolar range.

Because $LPG_{10}SA_{0.40}$ is a competitive inhibitor of influenza virus HA binding, it associates with virus when in proximity. This interaction was investigated using Cy3-labeled PG and influenza A/X31 virus immunofluorescence analysis of infected cells (Figure 15 and Figure 16). Cy3-labeled $LPG_{10}SA_{0.40}$ indeed associated with the fluorescent signal of stained virus proteins in infected cells. When treated, infection was limited to a few isolated cells, demonstrating inhibition of virus propagation by $LPG_{10}SA_{0.40}$. In contrast, the whole cell layer of mock-treated cells was infected. Thus, Cy3-labeled $LPG_{10}SA_{0.40}$ protected these cells from infection albeit not being detectable around cells without virus. This can be explained when considering that virions, which are inactivated by compound binding, may not be able to bind the glycan receptors on the host cell surface and are thus washed off during slide preparation (Figure 32, 1). This explanation is consistent with Cy3-labeled $LPG_{10}SA_{0.40}$ acting as a competitive inhibitor of HA receptor binding. The Cy3-labeled $LPG_{10}SA_{0.40}$ that is detected in immunofluorescence is associated with virus, hence presumable bound to viral HA, and this virus is in turn most likely associated with host cells and not

washed off. Z-stack images revealed that compound is mostly found at the cell membrane and only sporadically taken up into the cytoplasm, probably together with virus or by endocytosis (Figure 16). It is conceivable that PG molecules are bound to HA on the virion surface in a way that enough HA units were left unblocked so that the virus was still able to attach to the cell membrane (Figure 32, 2). No Cy3-labeled $LPG_{10}SA_{0.40}$ was found associated with uninfected cells, but compound was detected inside the cytoplasm sporadically. This indicates that the internalization of virions which attached to the cell membrane despite some PG compound interaction was most likely not prevented, ultimately resulting in infection (Figure 32, 3). Because compound was present in the medium for the entire incubation time, it can also attach to HA of progeny virus about to bud from the cell membrane (Figure 32, 4). This last possibility probably accounts for most of the compound detected in IF, since it conforms well to most compound being detected at the cell membrane of infected cells. $LPG_{10}SA_{0.40}$ probably does not impede virus release, as there was no effect of the compound on NA activity in a MUNANA assay (Chuanxiong Nie, AG Haag, Freie Universität Berlin, personal communication, 2019).

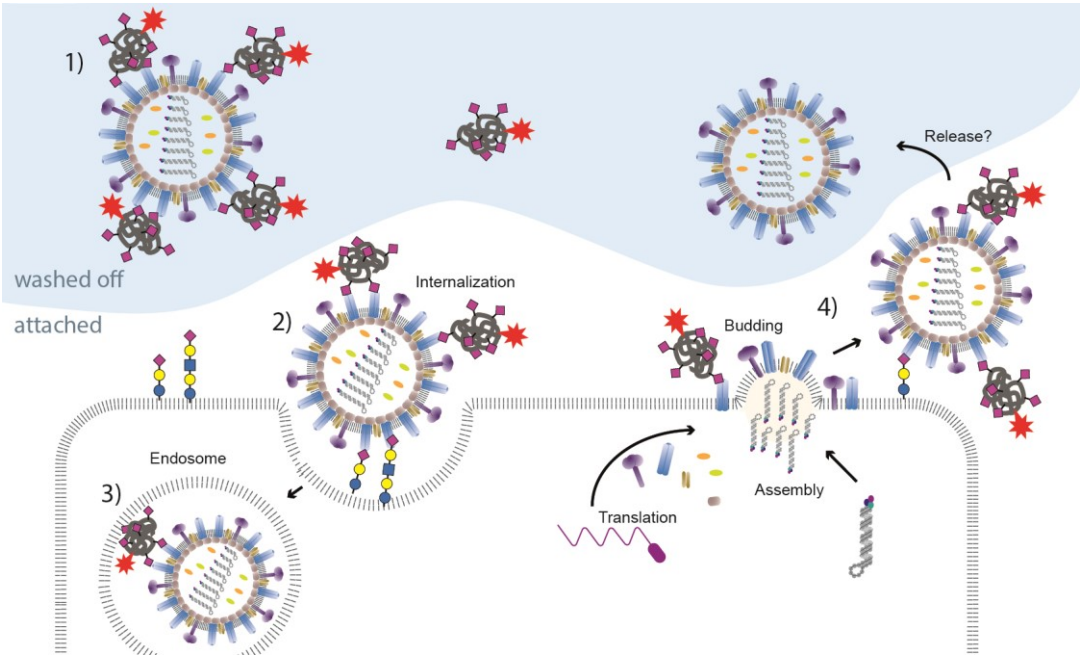

Figure 32: Schematic detailing possible explanations for the detection of Cy3-labeled compound in IF analysis.
Compounds can block attachment of virions to the cell surface (1). Particles that are not bound to the cell surface are washed off during slide preparation. This includes free compound and virions not bound to the cell surface. Compound binding can result in incomplete blocking of virus attachment (2). This can entail the uptake of compound into the cell alongside virus particles (3). Compounds can also bind to progeny virus budding from the cell surface (4). Both binding to HA inserted into the cell membrane and at binding to complete virus particles still attached to the cell surface is possible.

Some drugs act in synergy when applied together, meaning that their actual effect is bigger than the expected additive effect. Synergy results in a therapy being more effective and may allow to reduce dosing. It is a concept widely explored in anti-human immunodeficiency virus (HIV) treatments, to which drug combinations are vital[332-334] and also in cancer therapy[335]. In addition, synergy between host targeting and virus targeting drugs might advance treatment of hepatitis C virus infections[336].

To explore whether the combination of $LPG_{10}SA_{0.40}$ with NA inhibitor Oseltamivir resulted in drug synergy, serial dilutions of both compounds were applied together in the two-step inhibition assay. Synergy can be calculated in different ways and each model makes different assumptions. There is no clear consensus on which model to use for which situation[337, 338], so it is reasonable to apply more than one calculation method to confirm the results. Therefore, several models were applied for the calculation of drug synergy here. All of them yielded the result that there was neither synergy nor antagonism between $LPG_{10}SA_{0.40}$ and Oseltamivir (Figure 17).

Combinations of other anti-influenza drugs, such as the polymerase inhibitors Favipiravir, Pimodivir and Baloxavir, with NA inhibitors have shown synergy when tested in cell culture[199]. An HA-binding lectin[317] and a small molecule inhibitor[339] that both inhibit influenza virus replication at the fusion step have displayed significant synergy with Oseltamivir. For multivalent, sialylated inhibitors of HA attachment synergy was often assumed from data based on one concentration of each compound without calculating the difference between additive and actual effect[275, 280]. Real synergy has been shown in HAI assay[340] and in cell culture using MDCK cells expressing β-Galactoside a2-6-sialyltransferase I and the puromycin *N*-acetyltransferase gene[341]. On these modified MDCK II cells, influenza viruses have been shown to be more sensitive to NA inhibitors than on the parental MDCK II cells[331, 342]. In non-modified MDCK II cells, influenza viruses rely less on NA activity, therefore the lack of synergy between HA inhibitor $LPG_{10}SA_{0.40}$ and NA inhibitor Oseltamivir displayed in this study may be cell type specific. Another explanation is provided by the HA/NA balance, which is essential for viral fitness[123]. Viruses escaping inhibition with Oseltamivir by developing HA mutations decreasing receptor affinity have been observed before[175, 322]. Thus, an HA inhibitor decreasing receptor binding can in theory contribute to compensating NA inhibition, especially in a mucus environment, where HA/NA interplay is particularly important[124]. However, this is likely of little effect in cell culture, where no mucus is present. $LPG_{10}SA_{0.40}$ itself has no effect on NA activity, as demonstrated by MUNANA assay (Chuanxiong Nie, AG Haag, Freie Universität Berlin, personal communication, 2019).

5.2. Broad activity

Influenza A/X31 virus is a reassortant laboratory virus strain with the HA and NA segment of influenza virus A/Aichi/2/1968 (H3N2) in a background of influenza virus A/PR/8/1934. It is very distant from currently circulating seasonal influenza strains, which have evolved since. As such, it is far from ideal for testing antivirals with desired activity against influenza virus strains contributing to the annual epidemics. However, influenza A/X31 virus is a well-established strain used by many laboratories across the world and therefore provides a good measure for comparison to other groups' efforts. Still, it can only serve as a starting point and it is imperative to test any drug candidate against more recent influenza virus strains. This is especially true for antivirals targeting the viral HA, since variation there is particularly high. The sequence identity of the surface of an H3 HA from 1968 and H3 HA from 2012 is only 70% on the amino acid level[87] and intersubtype variations of different HA can be as low as 30%[86]. In addition, the number of HA head glycosylations possibly resulting in shielding effects and impacting receptor binding properties has increased over

time[79]. These differences mandate that the efficacy of new antivirals be tested against a panel of influenza virus strains representative of this diversity. Here, this was accounted for by testing PG activity against nine influenza virus strains including old and more recent H3N2 viruses, prepandemic and pandemic H1N1 viruses as well as an H1N2 and an H7N1 virus (Figure 18A). Given that influenza A/Panama/2007/1999 (H3N2) virus is not a recent strain, compound activity against influenza A/Bremen/5/2017 virus propagation was analyzed in further analyses (Figure 31). The sialylated PGs $LPG_{10}SA_{0.40}$ and $LPG_{10}SA_{0.70}$ inhibited the propagation of some closely related old H3N2 strains such as influenza A/Udorn/1972 virus and the H7N1 virus A/turkey/Italy/472/1999, but not the propagation of H1N1 viruses and the H3N2 virus A/Panama/2007/1999 (Figure 18A). This indicated that subtle differences in the HA RBS impact the effectivity of the sialylated PGs. Larger differences in the amino acid sequence of HA, as between H1N1 and H3N2 viruses, render the sialylated PGs infeffective. H1 belongs to group 1 HAs, whereas H3 belongs to group 2 HAs (Figure 4). As HAs are grouped according to their amino acid sequence, a high divergence is evident. In addition to the amino acid sequence, H1 and H3 HAs also differ in their glycosylation patterns. H3 HAs accumulated more glycosylation sites on the HA head than H1 HAs, which also might impact receptor and inhibitor binding[79]. Depending on whether it is bound to the RBS of H3 or H1, the same sialylated glycan receptor adopts a different conformation[343]. The tested sialylated PGs might not be able to account for the differences required for binding to the HA RBS of H1N1 viruses.

Although influenza A viruses all bind terminal SA on N-linked glycan receptors for attachment to host cells [42, 43], the terminal SA does not determine attachment alone. Sugar structures on the surface of mammalian cells are highly complex and diverse[99] and sugars underlying the terminal SA influence HA binding[112, 113]. Differences in HA can impact the preference of these underlying sugars, resulting in alterations in the receptor binding profile on a glycan array. H3N2 viruses have evolved from binding a great spectrum of diverse glycans in 1968 to a narrower binding profile in recent years[95, 118]. The receptor binding profile of influenza viruses is so diverse, that when testing 45 human H3N2 influenza virus isolates, there was no single glycan that was bound by all of them[121]. Even the avidity to the prototypic α2,6-linked trisaccharide receptor has decreased dramatically from 1986 to 2010[117]. There are no sugars underlying the terminal SA on the sialylated PGs. However, the SA moieties are presented at a certain angle on a certain linker with a certain length and at a certain distance to the next SA moiety. The PG itself provides the context. Based on the findings that SA-functionalized PGs inhibited the propagation of only a limited number of IAV strains, the context provided in this PG configuration appeared to match only the receptor binding preference of those virus strains. The influenza virus strains that were inhibited by $LPG_{10}SA_{0.40}$ and $LPG_{10}SA_{0.70}$ were isolated almost 50 years ago, like influenza A/X31 virus with HA from 1968 or A/Udorn/1972 from 1972, which fits the observation that the binding profile has become more specific over time[87, 95].

Notably, binding of PG compound did not necessarily result in inhibition. Using immunofluorescence analysis (Figure 19), three different cases were observed: 1) virus was bound by sialylated PG and virus propagation subsequently inhibited (A/X31 (H3N2)) (Figure 33A), 2) virus

was bound by sialylated PG but virus propagation was not affected (A/Panama/2007/1999 (H3N2)) (Figure 33B) and 3) virus was not bound by sialylated PG and consequently the propagation was not inhibited (A/PR/8/1934 (H1N1)) (Figure 33C). Binding resulting in inhibition and no binding resulting in no inhibition are straightforward cases, but case 2) requires a more nuanced view. The result suggests that in addition to binding to the virus, a certain affinity of a compound to HA is required for effective inhibition of virus propagation. A compound bound to HA with too low affinity does not pose a good competitive inhibitor and thus might be displaced by cellular glycan receptors easily. This notion implies that not all glycans bound by a virus in glycan array analysis may actually be bound with sufficient affinity to facilitate virus entry in an infection setting, congruent with the fact that glycan array binding profiles cannot predict virus infectivity[99].

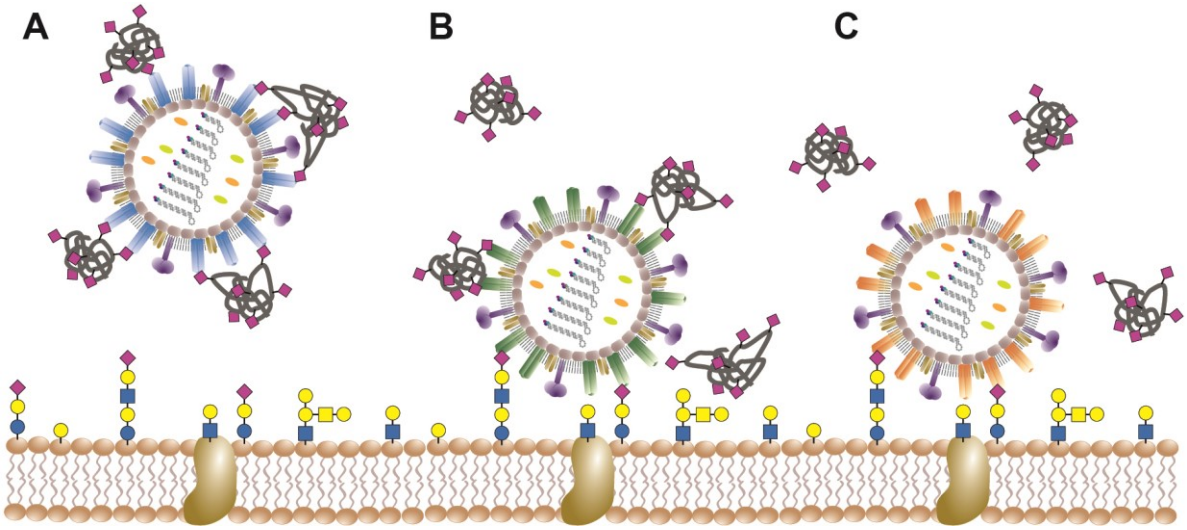

Figure 33: The three different cases of compound and virus binding.
Some viruses, such as influenza A/X31 (H3N2) virus are bound by $LPG_{10}SA_{0.40}$, resulting in inhibition of virus attachment to host cell glycans and consequently infection (A). Other viruses, such as influenza A/Panama/2007/1999 (H3N2) virus or the mutant viruses, display some compound binding but their propagation is not inhibited (B). The third class of viruses, such as influenza A/PR/8/34 virus, is not bound by $LPG_{10}SA_{0.40}$ and therefore the propagation of these viruses is also not inhibited (C). The differences in the HA protein between the viruses is represented by different colors.

The PGs have the advantage that their configuration is flexible and can be modified. In case the context of the presented SA does not match the receptor binding preference of a broad range of influenza viruses, that context can be modified. As influenza A/Panama/2007/1999 (H3N2) virus was an example of case 2), in which the sialylated PG was able to bind to the HA albeit without inhibitory effect, it is conceivable that less modifications to the PG would be sufficient to achieve inhibition than might be required to achieve inhibition of influenza A/PR/8/1934 (H1N1) virus inhibition, as the latter was an example of case 3), in which the sialylated PG was not able to bind to the HA at all. Indeed, the modified, improved compound LPG_{10}-(6'-SLamide)$_{0.50}$ with amide liker and SL-functionalization was able to inhibit influenza A/Panama/2007/1999 (H3N2) virus propagation by around three orders of magnitude. In contrast, influenza A/PR/8/1934 (H1N1) virus titers were reduced by less than one order of magnitude, although still significantly. LPG_{10}-(6'-SLamide)$_{0.50}$ and other modified PGs are further discussed in section 5.4.

Broad activity is generally a challenge for anti-influenza virus measurements targeting HA. Other multivalent sialylated compounds with a variety of scaffolds display very different effectivity

depending on the virus subtype and strain tested. For example, early acrylamide-based constructs functionalized with aminobenzylglycosides of *N*-acetylneuraminic acid (Neu5Ac) were active against human H3N2 viruses but not against avian H3N2 viruses, H1N1 viruses, H2N2 viruses or influenza B viruses[253]. The authors assumed that their configuration of multivalent SA mimicked the NeuSAc-α2,6-Gal receptor determinants and was therefore recognized by human H3N2 viruses. They went on to probe a variety of different influenza viruses with modified synthetic Neu5Ac analogs and identified determinants within the Neu5Ac required for binding by all tested influenza virus strains. Substantial differences in binding between H3N2 and H1N1 viruses were observed in the glycan receptors not being part of the sialic acid itself[344]. Furthermore, dendritic polymers functionalized with SA were only effective against some virus strains[258, 259] and even updated dendritic polymers carrying SL, which include underlying sugars and were effective against more virus strains than the early compounds, vary greatly in their effectivity depending on the virus strain and subtype[261]. Along the same line, liposomes functionalized with sialylneolacto-N-tetraose c (LSTc), while being active against the tested H1N1 and H3N2 viruses, differed in their effectivity depending on virus strain and subtype[268]. This is also true for the sophisticated phage capsid scaffold. Sialylated phage capsids are highly active against a variety of influenza viruses, but the effectiveness against different influenza virus subtypes depends on the linker length between SA and the scaffold[271].

Notably, broad activity remains a challenge for influenza virus vaccination as well. The seasonal vaccine contains antigen from Influenza A virus subtypes H1N1 and H3N2 and from both influenza B lineages. The individual components need to be reviewed and adapted regularly. Nonetheless, there is always the possibility of vaccine mismatch, which can dramatically reduce vaccine effectiveness[137]. The need for broad protection against all influenza viruses is reflected in the effort to create a universal influenza vaccine[345, 346]. This underlines that broad activity of both antivirals and vaccines is difficult to achieve but should be aimed for nonetheless.

Optimization of the PG compounds regarding scaffold flexibility and SA density[275] as well as linker and functionalization (Figure 31) resulted in the PG compound LPG_{10}-(6'-SLamide)$_{0.50}$, which is able to inhibit a broader spectrum of influenza viruses. Nonetheless this PG compound is not able to inhibit the propagation of some virus strains, e.g. A/PR/8/1934 (H1N1), satisfactorily (Figure 31). This mirrors the findings described above for other multivalent sialylated constructs as well as the experience with influenza vaccination. Looking forward, it may be necessary to employ heteromultivalent compounds in order to account for the high variability of influenza viruses. A heteromultivalent PG could contain several different glycans and thus present an optimal binding partner for a variety of influenza viruses. As one option, this heteromultivalent PG could be functionalized with the top six glycan receptors that were identified in a glycan array screen of 45 H3N2 viruses spanning from 1968 until 2012 with one virus representing each year[121]. PGs additionally carrying NA inhibitors and thus targeting both HA and NA are also conceivable.

5.3. Development of resistance mutations

As described in the previous section, influenza virus receptor binding is influenced by many factors on the receptor side, including the sugars underlying the terminal SA on the glycan receptor. However, molecular factors on the HA side are equally important to the receptor binding. In order to elucidate the molecular basis for the limited broad activity, resistance to $LPG_{10}SA_{0.40}$ was induced in influenza virus A/X31 (H3N2) by serial passaging.

Serial passaging of influenza virus A/X31 (H3N2) on MDCK II cells in the presence of escalating concentrations of $LPG_{10}SA_{0.40}$ resulted in the rapid development of adaption and resistance. One independent $LPG_{10}SA_{0.40}$-resistant variant was identified from passage ten of each of three replicates with the HA mutations G135E, K140N and P99F/G144D (H3 numbering), respectively. Most of these mutations appeared at an earlier passage, with the earliest passage containing resistant virus being passage 4 (Table 9). However, passages 1 to 3 were not sequenced, so it is possible that resistant virus variants were present even earlier. The rapid development of resistance here is in agreement with the development of resistance against other influenza inhibitors. Influenza virus developed resistance against amantadines after two to three passages *in vitro*[347]. Resistance against Oseltamivir has been described to appear in passage three[176] and resistance against Zanamivir developed as early as passage one[175]. The way serial passaging is performed differs between the studies and stringency of the passaging can impact the speed with which resistance develops. For example, if a very low amount of compound is applied, the development of resistance may be slower, because the selection pressure is low. In contrast, selection pressure is high in the presence of a high amount of compound, so resistance likely develops faster. Therefore, it is difficult to directly compare the passages from one study with the passages from another. However, all studies mentioned above have in common that resistance appeared early within few passages. Moreover, three independent variants developed rather than the same mutations occurring in all replicates. This may reflect the high evolutionary capacity of influenza viruses[89, 329].

Due to viral evolution, developing resistance poses a threat to all antiviral therapies, especially if virus replication is not entirely abrogated and treatment is required over a prolonged period of time[348]. For example, resistance against nucleoside analogues used to inhibit the reverse transcriptase of hepatitis B virus (HBV) develops especially in chronic infections[349-351]. Combination therapy with two or more antiviral agents can help fight infections with resistant HBV[352, 353]. However, for some resistance mutations, such as the reverse transcriptase amino acid change combinations rtA181V+rtN236T or rtS106C+rtH126Y+rtD134E+rtL269I which confer resistance to tenofovir, no rescue therapy is available[354, 355]. Going forward, combination therapy with host targeting agents may be a new treatment option[336]. As another example, several therapies are available for treatment of HIV, but roughly one fourth of circulating HIV already carries resistance to first-generation drugs[356]. Newer generations of therapies have a higher barrier to the development of resistance, but resistance remains a looming threat. Despite the inevitable development of resistance to all kinds of antivirals, antiviral drugs can provide a substantial

contribution to the alleviation of disease as long as resistance is not widespread. Moreover, there is an advantage to having several therapies available, because combination therapy can raise the barrier to the development of resistance[357]. Additionally, host-directed antiviral therapy may delay the development of resistance, but high toxicity and low tolerability complicate the development[358]. The combination of host-directed and antiviral therapy is a promising strategy to overcome these difficulties.

Resistance mutations against $LPG_{10}SA_{0.40}$ mapped in or close to the influenza virus RBS (Figure 21). This is congruent with expectations, because $LPG_{10}SA_{0.40}$ is a competitive inhibitor of HA receptor binding[91, 275]. Upon receptor binding, amino acid G135 is in direct contact with SA via a hydrogen bond[359], so a change in this position directly impacts the receptor interaction. An effect on receptor binding can also be achieved by mutations in more distal positions, as the HA-SA interaction is stabilized by amino acids in the vicinity without direct contact to SA[43]. The tyrosine at position 98 is in direct contact with the receptor[359], but P99F is more likely to have an effect on the 220 loop, which is located directly opposite and may be affected by the larger side chain of phenylalanine compared to proline. Positions 135, 140 and 144 are on the HA surface and part of antigenic site A (Figure 34). As such, they are subject to selection pressure. The amino acids at position 135 and 144 have changed several times in the course of the evolution of influenza H3N2 viruses[87]. G135E and G144D in particular have occurred naturally as part of transition between antigenic clusters. Although K140N has not contributed to new antigenic clusters, changes at K140 have been detected in circulating strains[360]. Furthermore, positions 135, 140 and 144 displayed no clear amino acid preference in deep mutational scanning, revealing an inherent high mutational tolerance[363]. Taken together, the genetic barrier for developing mutations in these positions is probably low, which explains the rapid adaption in serial passaging. In contrast, position 99 is not on the HA surface (Figure 21) and therefore not subject to the same selection pressure. In addition, there is a clear preference for a proline in this position[363]. When considering amino acid properties, the phenylalanine selected here comes closest to the proline. They are both hydrophobic and polar uncharged, which makes sense given the position rather inside the protein than on the surface. They both possess a ring structure. Tryptophan fulfills these criteria as well, but is much bigger and may be too large to occupy position 99, which is on the inside of the protein behind the RBS. Therefore, P99F may be a mutation with a relatively small structural impact compared to other changes at this position and occurred despite an overall

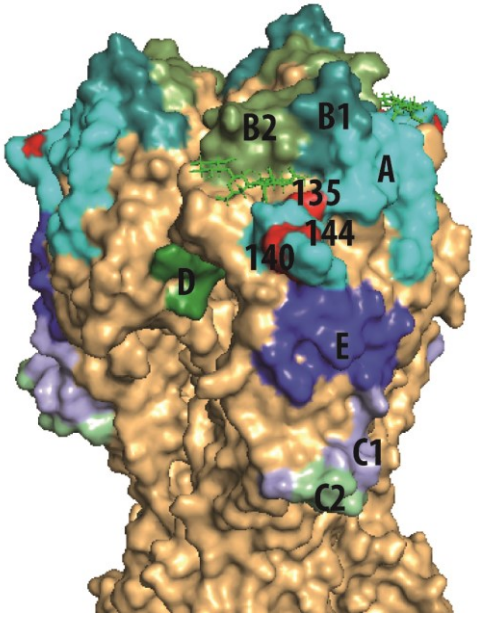

Figure 34: Antigenic sites on the HA of A/X31 virus. The antigenic sites of the HA head are colored in different shades of green and blue and labeled with the name of the respective site. Mutations are colored in red and labeled with their amino acid position. Images of the HA protein of influenza A/X31 virus (PDB, 1HGG)[2] were generated using PyMOL[3]. Antigenic site positions were derived from Ye et al.[5].

preference for a proline in this position. Notably, P99F was not detected in passage 4 or 7, so it must have occurred between passages 8 and 10, indicating a higher genetic barrier for this mutation than for the other mutations.

Resistance mutations against Oseltamivir included HA mutations G135E, N188D, S228G, N296T and A495T but no mutations in NA, despite Oseltamivir being an NA inhibitor. In cell culture, mutations in HA conferring resistance to Oseltamivir have been extensively described before[175, 322]. These HA mutations decrease receptor affinity and thus may compensate the lowered NA activity by restoring the HA/NA balance. However, Oseltamivir mutant viruses O1 and O3 were not completely resistant to Oseltamivir (Figure 22), so the HA mutations do not appear to compensate the lowered NA activity fully. O1 virus has mutations N188D as well as N296T. N188D has been observed in combination with changes in NA and may influence receptor binding by increasing the local negative charge[364]. In the absence of additional mutations, O1 retained some sensitivity to Oseltamivir. In contrast, O2 virus has the same mutations as O1 virus, and in addition also G135E, and O2 virus is fully Oseltamivir resistant. In this virus, G135E appears to be responsible for full resistance to Oseltamivir, as G135E has been described to confer resistance to Oseltamivir without altering NA activity before[176].

Notably, the Oseltamivir mutant viruses were also partly resistant to inhibition by PGs and the LPG mutant viruses had reduced sensitivity to inhibition by Oseltamivir. It is no surprise that HA mutations that decrease receptor affinity impact sensitivity to LPG compounds, which interfere with receptor binding, and at the same time also impact sensitivity to Oseltamivir by restoring the HA/NA balance.

Arbidol resistance was accompanied by mutations K380N, D438V and E443R, which map to the lower HA stem region but not directly to the Arbidol binding site, which is located in the middle part of the stem region (Figure 8). Other mutations described to confer resistance to Arbidol were also not directly located at the Arbidol binding site but in the vicinity [1, 212]. The extensive structural rearrangements of the HA protein during fusion have been speculated to be the reason for this[1].

In addition to mutations in HA, mutations in PB2 were detected in $LPG_{10}SA_{0.40}$-resistant mutant 2 (with HA mutation K140N) and in Oseltamivir-resistant mutants 1 and 3. Increased polymerase activity might compensate for blocking of HA or lower NA activity and thus increase viral fitness. $LPG_{10}SA_{0.40}$-resistant mutant 2 carries the PB2 mutation G76R, which is located in the amino terminal region. This region has been associated with mitochondrial-targeting of PB2 [365] and therefore G76R is probably of little relevance to this study. Oseltamivir-resistant mutant 1 has the PB2 mutation E160G in addition to HA mutations N188D and N296T. E160G of PB2 is also part of the amino terminal region[366]. Oseltamivir-resistant mutant 1 has PB2 mutations P304S and I506V in addition to HA mutation S228G. PB2 positions 204 and 506 are part of the midlink domain, which was shown to be relevant to transcription[367] and thus may have a compensating effect on viral fitness. Notably, PB2 mutations developed more slowly than HA mutations. They were first detected in passage 7 and were present in around 70 % of the sequences in passage 10 (Table 9),

indicating a higher genetic barrier or a low selection pressure. As most HA mutations were present in over 90 % of the sequences at passage 10, there must have been compound-resistant viruses with and without the PB2 mutations. Thus, the compound resistance is most likely determined by the HA mutations rather than the PB2 mutations. A Minigenome assay may help to elucidate the effect of the PB2 mutations selected here on polymerase activity[368].

5.4. Receptor binding properties

The mutations in HA selected in serial passaging mapped to the receptor binding site and rendered the mutant viruses resistant to $LPG_{10}SA_{0.40}$. This implies a difference in receptor interaction of mutant viruses L1 (G135E), L2 (K140N) and L3 (P99F/G144D) compared to influenza A/X31 WT virus. Hence, the effect of these HA mutations on receptor binding was investigated using several assays, which are discussed in this section.

The HA elution assay revealed that receptor binding strength of $LPG_{10}SA_{0.40}$-resistant mutant viruses was reduced compared to influenza A/X31 WT virus (Figure 25). In addition, single-virus force measurements using atomic force microscopy performed by Malte Hilsch (AG Herrmann, Humboldt Universität zu Berlin) specified that indeed the receptor binding stability of the mutant viruses was around 20 to 30-fold reduced compared to WT virus (Figure 26). It is important to note that both assays found receptor binding to be reduced, not abolished. This is in agreement with immunofluorescence analysis results using Cy3-labeled $LPG_{10}SA_{0.40}$, in which the mutant viruses did display compound association albeit a lack of inhibition of virus propagation (Figure 28). Therefore, the mutant viruses fall into the second category of viruses alongside A/Panama/2007/1999 (H3N2) virus which do bind the compound but are not inhibited (refer to section 5.2 and Figure 33). The alteration in the RBS of the mutant viruses is only one or two amino acids and thus likely very subtle, which explains why $LPG_{10}SA_{0.40}$ binding is retained. However, this binding is of reduced stability with a very short bond life-time that is 20 to 30-fold reduced compared to WT virus (Figure 26). As a result, $LPG_{10}SA_{0.40}$ bound to mutant virus HA is likely easily outcompeted and displaced by glycan receptors on the cell surface which renders $LPG_{10}SA_{0.40}$ an ineffective competitive inhibitor of the mutant viruses. The reduced receptor binding stability that facilitates displacement of $LPG_{10}SA_{0.40}$ can be overcome by compounds with higher avidity or affinity. Another SA-based compound, the sialylated phage capsid, is still able to inhibit mutant virus propagation (Figure 22). Phage capsids are designed to spatially match the three RBS on one HA trimer resulting in K_D values (dissociation constant) in the low nanomolar range[271] as compared to the K_D value of 10 µM of $LPG_{10}SA_{0.40}$[275]. The concomitant higher avidity of phage capsids probably enables effective inhibition of the mutant viruses despite their reduced SA-binding stability.

Altered receptor binding stability of the mutant viruses was accompanied by altered receptor binding preferences. In glycan array analysis, influenza A/X31 WT virus bound 6´-sialyllactose, sulfated 6'-sialyl-N-acetyllactosamine, LSTc and sialyl-TN antigen as well as several other glycans with terminal 6´-Neu5Ac or 3´-Neu5Ac with high binding intensity (Figure 27). These glycans bound by influenza A/X31 WT virus are established receptors of influenza A/X31 virus attachment[112], demonstrating the validity of the analysis. Binding to 3'-Neu5Ac, the prototypical receptor of avian

influenza viruses, results from passaging influenza A/X31 virus in chicken eggs, which express glycans with terminal 3´-Neu5Ac abundantly[324]. The mutant viruses L1 and L2, with the HA mutations G135E and K140N, respectively, bound only 6´-sialyllactose, sulfated 6'-sialyl-N-acetyllactosamine and LSTc of the established receptors and with a 100-fold reduced binding intensity compared to influenza A/X31 WT virus. Instead, they bound several distinct glycans with α2,8-linked SA and with N-Glycolylneuraminic acid (Neu5Gc), though with low overlap between receptors of mutant virus L1 and L2. The mutant virus L3 with the HA mutations P99F and G144D bound to none of the typical human-type receptors on the glycan array. Rather, it bound several fucosylated glycans and glycans with α2,3-linked SA. Apart from glycans with terminal SA, all three mutant viruses and in particular L2 bound glycans with terminal N-acetylglucosamine (GlcNAc) and galactose.

The common 6´-Neu5Ac glycan receptor can only be bound by HAs with relatively high affinity. It has one rotatable bond more than 3´-Neu5Ac, which enables multiple conformations, and also more points of contact with HA. Therefore, the conformational restriction of the 6'-Neu5Ac causes a high entropic penalty upon HA binding[115]. A high binding affinity is required to facilitate binding despite the high entropic penalty[369]. A reduced binding affinity of mutant virus HA to 6'-Neu5Ac might not be able to overcome the entropic penalty incurred by the binding and thus result in less binding of mutant viruses to this glycan receptor. This is not the first time glycans besides the typical glycan receptors were identified as receptors for influenza viruses. Influenza viruses of different host species were found to bind Neu5Ac-α2,8-Neu5Acα substructures, Neu5Gc and even terminal galactose or GlcNAc before[116, 370]. An important notion to explain receptor binding to atypical glycan receptors is that receptor binding appears not to rely on the sialic acid itself but rather on the shape of the receptor and topological features[114-116]. The mutant viruses may have adapted these alternative receptors for attachment due to a reduced affinity for their formerly preferred receptor. This changed receptor binding preference did not come at a cost in viral fitness (Figure 24) and did not result in revertants in the absence of compound (Figure 23). In general, changes in receptor affinity or preference are not necessarily expected to result in reduced viral fitness or infectivity[121]. This is due to the vast variety of glycan receptors presenting abundant alternatives available to the virus, as also expressed on MDCK II cells[325-327]. Thus, there is no selection pressure on the virus due to these mutations even in the absence of $LPG_{10}SA_{0.40}$. Because the variety of glycans present in the human lung is even larger[99], the mutant virus fitness is probably not reduced *in vivo* either.

A major limitation of the glycan arrays used here is that they cover only 125 glycans, which is a small fraction of the vast variety of glycans present in respiratory tissue[99]. It is likely that some glycan receptors of the mutant viruses were missed in this analysis. A larger array would be required in order to elucidate the full receptor profile of the mutant viruses. Arrays that may be employed for this purpose are the glycan array of the Consortium for Functional Glycomics, which currently covers 609 glycans[371] or the human lung-shotgun N-glycan microarray[370] containing N-glycans that were directly isolated from human lung tissue. Especially the latter may be able to provide the full spectrum of glycan receptors relevant to influenza virus infections.

It is interesting to note that some alternate glycan receptors, which have terminal galactose or GlcNAc, are not available for cleavage by NA, since NA only cleaves the glycosidic linkage of sialic acids. Still, the mutant viruses are not hampered in their propagation. Therefore, both moving along the cell surface before final attachment[44, 92] and release of progeny virus[66], which are NA-dependent, must be occurring despite binding to receptors that are not cleaved off by NA. HA receptor interactions are highly dynamic and have short half-life of 0.8 to 5.5 s[93]. As such, in the absence of internalization, HA is naturally released from the receptor, often accompanied by statistical rebinding[249] to a different receptor. For the mutant viruses, this process may be aided by a low affinity of mutant HA to some receptors. Hence, movement and release may be possible even if not all receptors can be cleaved by NA.

5.5. Importance of HA positions 135 and 144

The HA mutations G135E in L1, K140N in L2 and P99F/G144D in L3 were sufficient to render influenza A/X31 (H3N2) virus resistant to $LPG_{10}SA_{0.40}$, this warranted the question of how important these single positions were for $LPG_{10}SA_{0.40}$ susceptibility. Given the high variability of the HA protein and the highly diverse glycan binding profiles of different influenza viruses, it seems unlikely that one single amino acid that is not highly conserved may be responsible for such drastic changes. However, positions 135 and 144 are part of the N-glycosylation motives NGT and NNS, respectively, in influenza A/Panama/2007/1999 virus HA, whereas influenza A/X31 virus HA does not have N-glycosylation motives at these positions. Additional HA glycosylations have been shown to decrease receptor binding [81, 120]. Especially the N-glycosylation site at position 144 has proven important for antibody recognition[372]. It appeared conceivable that HA head N-glycosylation may be impacting receptor and inhibitor binding in influenza A/Panama/2007/1999 virus. Therefore, destroying the N-glycosylation sites by changing positions 135 and 144 to an A/X31-like configuration could have an impact on susceptibility to $LPG_{10}SA_{0.40}$. However, $LPG_{10}SA_{0.40}$ was not active against recombinant influenza A/Panama/2007/1999 viruses P1 and P2 (Figure 29). Furthermore, other PGs including modified PGs functionalized with SL (refer to section 5.6) did not discriminate between influenza A/Panama/2007/1999 WT virus and recombinant viruses P1 and P2 (Figure 29C and Figure 31C). Thus, positions 135 and 144 did not prove important to susceptibility to $LPG_{10}SA_{0.40}$ in influenza A/Panama/2007/1999 virus. In contrast, positions 135 and 144 did make the difference between resistance and susceptibility in influenza A/X31 virus. Notably, mutations G135E and G144D did not lead to the acquisition of additional glycosylation sites to the influenza A/X31 virus HA. Thus, the escape mechanism does not seem to rely on HA head glycosylations. However, there are many more differences in the HA of influenza viruses A/X31 and A/Panama/2007/1999, amounting to only around 87% sequence identity on the amino acid level despite a structurally similar RBS (Gene Bank DQ865956.1[373]). Other differences in HA probably mitigate or even abolish any effect T135G and N144G might have on influenza A/Panama/2007/1999 virus susceptibility to $LPG_{10}SA_{0.40}$. Taken together, the high variability of the HA surface and also of the HA RBS may contribute to the molecular determinants of resistance probably also varying depending on the virus strain at hand. The HA positions identified for

influenza A/X31 virus were not transferable to influenza A/Panama/2007/1999 virus and most likely cannot be extended to other influenza A viruses either.

5.6. Strategies to improve PG compounds

In order to overcome the high susceptibility of SA functionalized PGs towards HA amino acid variations and consequently limited antiviral activity, effort was focused on improving the PG compounds and their anti-IAV spectrum. To this extend, PGs can be modified in several ways including the degree of functionalization, scaffold flexibility, functionalization and linkage between scaffold and functionalization.

A higher SA density, as in compound $LPG_{10}SA_{0.70}$, or a lower scaffold flexibility, as in compound $dPG_{10}SA_{0.15}$, where not sufficient to restore susceptibility to sialylated PGs in the mutant viruses (Figure 22). Apparently, these compounds are too similar and resistance to $LPG_{10}SA_{0.40}$ conferred cross-resistance to the other PG-based compounds functionalized with SA. This was also the case for the Oseltamivir-resistant mutants. Oseltamivir-resistance conferred reduced sensitivity to $LPG_{10}SA_{0.40}$, as also discussed in Section 5.3, and this was accompanied by a reduced sensitivity to $LPG_{10}SA_{0.70}$ and $dPG_{10}SA_{0.15}$. This finding is in agreement with the results achieved with different IAV strains (Figure 18). There was no broad activity and small differences in HA even within the same subtype were sufficient for SA-functionalized PGs to be ineffective inhibitors. Small modifications to the PG, like a change in the degree of functionalization, were not able to extend the spectrum of inhibited IAV strains. Refer to section 5.2 for a detailed discussion on broad activity of antiviral compounds against a variety of IAV strains.

Taken together, the inhibition by SA-functionalized PGs is very sensitive to even small alterations, as evident by a single amino acid change in HA leaving SA-PG-inhibitors ineffective. Because changes in the degree of functionalization or scaffold flexibility did not broaden the antiviral activity to different IAV strains or to the mutant viruses, other properties of the PGs needed to be modified.

One of these other factors to modify is the functionalization. In case the virus binding to SA is reduced, a different sugar functionalization might result in stronger binding, possibly leading to more effective inhibition. Including more sugar groups than just SA in the functionalization might provide a more suitable receptor environment that may improve binding, as underlying sugars have been shown to be important to the HA-receptor interaction[112, 113]. The ideal glycan to be used for functionalization should be bound by an extensive variety of influenza viruses. However, glycan preference varies greatly between influenza viruses[121]. Even so closely related viruses as influenza A/X31 WT virus and the mutant viruses showed very different receptor binding patterns in glycan array analysis (Figure 27). One glycan structure, that was at least in part commonly bound by WT and mutant viruses, was α2,6-sialyllactose (α2,6-SL). The binding intensity of WT virus to α2,6-SL was much higher compared to the mutant viruses and L3 virus only showed minor binding to α2,6-SL. However, there was even less overlap in the binding of other glycans. Furthermore, SL has been identified as a receptor of a variety of IAV on a variety of glycan arrays[116]. Other multivalent

compounds have successfully inhibited IAV propagation using SL as functionalization[278, 280, 374], and a broader spectrum of inhibited virus strains was achieved by incorporating SL instead of SA into the PAMAM backbone[259-261]. It was even suggested that SL-functionalization may be able to inhibit all human IAV[288, 299]. Therefore, the functionalization of PGs was changed to SL.

However, the functionalization is not the sole decisive factor. Phage capsids functionalized with SA only were still able to inhibit the mutant viruses (Figure 22). The specific presentation of the sugar group on a multivalent scaffold appears to have a strong impact on antiviral activity. The phage capsid scaffold was designed to match the HA homotrimer[271], and thus phage capsid compounds probably bind with a higher avidity, which renders them more robust to changes in HA. This is evident in the low K_D value of phage capsids against influenza A/X31 virus ranging from 1.6 nM to 90.6 nM depending on linker length[271]. The K_D of phage capsids is six orders of magnitude lower than that of Neu5Ac[90] and almost four orders of magnitude than that of $LPG_{10}SA_{0.40}$[275]. However, the matched geometry was slightly different for H3N2 and H1N1 viruses, requiring a different ethyleneglycol linker length for effective inhibition depending on the IAV subtype[271]. In fact, linkage between sugar group and scaffold has proven important for a variety of multivalent scaffolds including PAMAM[258], PEG and DNA scaffolds[94], glycycopolymers[278] and diverse other scaffolds[280]. Linkers were also identified as crucial factors in molecular modeling[283]. Therefore, different linkage options were explored here and the SL functionalization was attached to the PG scaffold with either an azide or an amide group at the anomeric position. Depending on whether an azide or an amide group is used as a linker, the angle with which SL is attached to the PG is slightly different (Figure 30), accounting for different presentations of the sugar group. Both the α2,3 and the α2,6 configuration of SL was analyzed.

Several of the modified compounds inhibited the propagation of influenza A/X31 (H3N2) virus (Figure 31). Only the dendritic SL-PG and the α2,3 configuration SL-PG had little effect on influenza A/X31 virus propagation. This is in line with results with SA-functionalized PGs, were linear PGs outperformed dendritic PGs in the inhibition of influenza A/X31 (H3N2) virus (refer to section 4.2.1). Since influenza A/X31 virus was grown in chicken eggs and showed some binding to α2,3-linked SA in glycan array analysis (Figure 27), an inhibitory effect by the α2,3 configuration SL-PG appeared plausible. However, since influenza A/X31 virus does bind mainly human type receptors it is also not unexpected that the α2,3 configuration SL-PG did not inhibit influenza A/X31 virus propagation. Consequently, the mixed PG with both α2,3 and α2,6 configuration SL did not show any enhanced inhibitory effect either.

Strikingly, a significant reduction of propagation of several H3N2 viruses and also H1N1 viruses was only achieved by the amide linker compound LPG_{10}-(6'-SLamide)$_{0.50}$ (Figure 31). The analog azide linker compound LPG_{10}-(6'-SLN_3)$_{0.50}$, which differs only in linkage, had no inhibitory effect. This result stresses the importance of the correct presentation of the sugar groups for effective inhibition of virus propagation. Interestingly, azide or amide linkage was not the single determining factor. LPG_{10}-(6'-SLN_3)$_{0.35}$, which differs from LPG_{10}-(6'-SLN_3)$_{0.50}$ in degree of functionalization, inhibited A/X31 virus propagation, although it had little effect on the other tested viruses. The

dendritic compound dPG_{10}-(6'-SLamide)$_{0.15}$ did not have any inhibitory effect at all, despite amide linkage. These data underline that the exact configuration of the compound is pivotal. All properties, including the degree of functionalization, the scaffold flexibility, the linkage and the functionalization are essential for effective and broad inhibition of virus propagation.

Curiously, none of the modified compounds were able to inhibit the influenza A/X31 mutant viruses L1, L2 and L3, not even LPG_{10}-(6'-SLamide)$_{0.50}$ (Figure 31), although so far the mutant viruses had matched influenza A/Panama/2007/1999 (H3N2) virus in their inhibition and PG binding pattern (refer to Figure 18, Figure 19, Figure 22, Figure 28 and section 5.2). The inhibition pattern of the recombinant influenza A/Panama/2007/1999 (H3N2) viruses P1 and P2 was comparable to influenza A/Panama/2007/1999 WT virus. These data indicate that HA positions 135 and 144 are not solely decisive in determining resistance or susceptibility to SL-PGs. Other differences between influenza A/X31 (H3N2) virus HA and influenza A/Panama/2007/1999 (H3N2) virus HA (Figure 29) likely contribute to the contrasting inhibition pattern observed for these viruses and their respective mutant viruses. To elucidate the other molecular determinants responsible for resistance or susceptibility to sialylated PGs in influenza A/Panama/2007/1999 virus, additional recombinant influenza A/Panama/2007/1999 viruses with different amino acid mutations could be constructed and tested. To narrow down on single or several amino acids, in a first approach the region around the 130 loop and the whole 190 helix, which both show many differences between influenza viruses A/X31 and A/Panama/2007/1999 could be mutated to the A/X31 configuration.

Taken together, the modified compound LPG_{10}-(6'-SLamide)$_{0.50}$ provides valuable progress in the effort towards effective, broadly active anti-influenza drugs. This progress reflects that integrating virological data with structural data in cooperation with chemical synthesis is important for developing novel antiviral drugs. However, there are still some limitations in the inhibitory capacity of LPG_{10}-(6'-SLamide)$_{0.50}$, as evidenced by the mutant viruses L1, L2 and L3, and further optimization is required to obtain a multivalent sialylated PG active against an even more extensive spectrum of influenza viruses.

5.7. Conclusion and Perspective

The results presented in thus study revealed that susceptibility to sialylated multivalent PGs originated in receptor binding properties of influenza viruses. Resistance against $LPG_{10}SA_{0.40}$ was accompanied by a lower receptor binding stability and an altered glycan receptor binding profile. The molecular determinants of resistance or susceptibility were different for two different influenza viruses of the same subtype and are thus likely not universal. This can be explained by the high variability and evolutionary capacity of influenza virus HA, which poses a challenge to all efforts trying to develop multivalent antivirals targeting HA receptor attachment[253, 258, 278, 297, 298]. A reason why even refined, highly effective multivalent compounds struggle with inhibiting a spectrum of different influenza strains may be that all approaches try to fit this broad variety with one glycan receptor. However, in the case of influenza virus HA, it may be difficult to find one compound that suits all strains. HA is highly diverse and the receptor binding preference of IAV is highly diverse as well, so targeting this structure diversity with a more diverse compound might be

a more promising approach. A heteromultivalent compound with various functionalizations may be able reflect such diversity.

One heteromultivalent compound that can be envisioned could incorporate several glycans, for example the six most commonly bound glycan structures identified in a glycan array screen of a variety of H3N2 viruses[121]. Such a compound would probably be broadly active and could be updated to match the binding preference of currently circulating seasonal influenza viruses as required. With such a compound, the threshold for developing resistance might be higher, as options for altering the receptor binding profile in order to escape are limited. Another heteromultivalent compound could target not only HA receptor attachment but also incorporate NA inhibitors with the aim to interfere with the viral replication cycle at several steps at once. The recently developed heteromultivalent red blood cell membrane-based compounds are an example of a successful inhibitor comprising both approaches[375]. There, cell membranes served as a source of diverse glycans, and the inhibitory effect was enhanced by the additional incorporation of NA inhibitor Zanamivir.

Fortunately, besides being biocompatible, PGs are versatile structures and can be modified easily. Heteromultivalent PGs incorporating several diverse glycans are thus conceivable. In fact, heteromultivalent PGs functionalized with SL and Zanamivir have been synthesized and successfully inhibited the propagation of a variety of IAV strains, suggesting great potential for broad activity (unpublished data by AG Haag, FU Berlin, and AG Wolff, RKI).

Going forward, it is important to integrate chemical synthesis with structural data and extensive knowledge on the HA receptor interaction in order to attain broad inhibition of HA receptor binding. The data presented here demonstrate how resistance against inhibitors of HA binding develops and provide insights into how a successful broadly active anti-influenza drug can be designed.

Bibliography

1. Kadam, R.U. & Wilson, I.A. Structural basis of influenza virus fusion inhibition by the antiviral drug Arbidol. *Proceedings of the National Academy of Sciences of the United States of America* **114**, 206-214 (2017).
2. Sauter, N.K. et al. Binding of influenza virus hemagglutinin to analogs of its cell-surface receptor, sialic acid: analysis by proton nuclear magnetic resonance spectroscopy and X-ray crystallography. *Biochemistry* **31**, 9609-9621 (1992).
3. Schrodinger, LLC (2015).
4. Wu, W.W. & Panté, N. The directionality of the nuclear transport of the influenza A genome is driven by selective exposure of nuclear localization sequences on nucleoprotein. *Virology journal* **6**, 68 (2009).
5. Ye, J., Shao, H. & Perez, D.R. Passive immune neutralization strategies for prevention and control of influenza A infections. *Immunotherapy* **4**, 175-186 (2012).
6. World Health Organization (World Health Organization, 2018).
7. ECDC, Vol. 2020 (ECDC, 2018).
8. Tokars, J.I., Olsen, S.J. & Reed, C. Seasonal Incidence of Symptomatic Influenza in the United States. *Clinical Infectious Diseases* **66**, 1511-1518 (2017).
9. CDC (CDC, 2019).
10. Putri, W.C.W.S., Muscatello, D.J., Stockwell, M.S. & Newall, A.T. Economic burden of seasonal influenza in the United States. *Vaccine* **36**, 3960-3966 (2018).
11. Belser, J.A. & Tumpey, T.M. The 1918 flu, 100 years later. *Science* **359**, 255-255 (2018).
12. CDC, Vol. 2020 (2018).
13. Krammer, F. et al. Influenza. *Nature Reviews Disease Primers* **4**, 3 (2018).
14. Kilbourne, E.D. Influenza pandemics of the 20th century. *Emerging infectious diseases* **12**, 9-14 (2006).
15. Burrell, C.J., Howard, C.R. & Murphy, F.A. in Fenner and White's Medical Virology (Fifth Edition). (eds. C.J. Burrell, C.R. Howard & F.A. Murphy) 355-365 (Academic Press, London; 2017).
16. Hause, B.M. et al. Characterization of a Novel Influenza Virus in Cattle and Swine: Proposal for a New Genus in the Orthomyxoviridae Family. *mBio* **5**, e00031-00014 (2014).
17. Yoon, S.W., Webby, R.J. & Webster, R.G. Evolution and ecology of influenza A viruses. *Current topics in microbiology and immunology* **385**, 359-375 (2014).
18. Tong, S. et al. New World Bats Harbor Diverse Influenza A Viruses. *PLOS Pathogens* **9**, e1003657 (2013).
19. Tong, S. et al. A distinct lineage of influenza A virus from bats. *Proceedings of the National Academy of Sciences of the United States of America* **109**, 4269-4274 (2012).
20. Fouchier, R.A.M. et al. Characterization of a novel influenza A virus hemagglutinin subtype (H16) obtained from black-headed gulls. *Journal of virology* **79**, 2814-2822 (2005).
21. World Health Organization, Vol. 2020 (World Health Organization, 2018).
22. Tanner, W.D., Toth, D.J.A. & Gundlapalli, A.V. The pandemic potential of avian influenza A(H7N9) virus: a review. *Epidemiology and Infection* **143**, 3359-3374 (2015).
23. CDC (CDC, 2019).
24. Kates, M., Allison, A.C., Tyrell, D.A. & James, A.T. Origin of lipids in influenza virus. *Cold Spring Harbor symposia on quantitative biology* **27**, 293-301 (1962).
25. Vahey, M.D. & Fletcher, D.A. Low-Fidelity Assembly of Influenza A Virus Promotes Escape from Host Cells. *Cell* **176**, 281-294.e219 (2019).
26. Bouvier, N.M. & Palese, P. The biology of influenza viruses. *Vaccine* **26 Suppl 4**, D49-D53 (2008).
27. Harris, A. et al. Influenza virus pleiomorphy characterized by cryoelectron tomography. *Proceedings of the National Academy of Sciences of the United States of America* **103**, 19123–19127 (2006).
28. Wasilewski, S., Calder, L.J., Grant, T. & Rosenthal, P.B. Distribution of surface glycoproteins on influenza A virus determined by electron cryotomography. *Vaccine* **30**, 7368-7373 (2012).
29. Murti, K.G. & Webster, R.G. Distribution of hemagglutinin and neuraminidase on influenza virions as revealed by immunoelectron microscopy. *Virology* **149**, 36-43 (1986).
30. Vahey, M.D. & Fletcher, D.A. Influenza A virus surface proteins are organized to help penetrate host mucus. *eLife* **8**, e43764 (2019).
31. Murti, K.G., Webster, R.G. & Jones, I.M. Localization of RNA polymerases on influenza viral ribonucleoproteins by

immunogold labeling. *Virology* **164**, 562-566 (1988).
32. Noda, T. et al. Architecture of ribonucleoprotein complexes in influenza A virus particles. *Nature* **439**, 490-492 (2006).
33. Brooke, C.B. Biological activities of 'noninfectious' influenza A virus particles. *Future Virology* **9**, 41-51 (2014).
34. Russell, A.B., Trapnell, C. & Bloom, J.D. Extreme heterogeneity of influenza virus infection in single cells. *eLife* **7**, e32303 (2018).
35. Desselberger, U., Racaniello, V.R., Zazra, J.J. & Palese, P. The 3' and 5'-terminal sequences of influenza A, B and C virus RNA segments are highly conserved and show partial inverted complementarity. *Gene* **8**, 315-328 (1980).
36. Flick, R., Neumann, G., Hoffmann, E., Neumeier, E. & Hobom, G. Promoter elements in the influenza vRNA terminal structure. *RNA (New York, N.Y.)* **2**, 1046-1057 (1996).
37. Crescenzo-Chaigne, B., Barbezange, C. & van der Werf, S. Non coding extremities of the seven influenza virus type C vRNA segments: effect on transcription and replication by the type C and type A polymerase complexes. *Virology journal* **5**, 132-132 (2008).
38. Hutchinson, E.C. et al. Conserved and host-specific features of influenza virion architecture. *Nature Communications* **5**, 4816 (2014).
39. Vasin, A.V. et al. Molecular mechanisms enhancing the proteome of influenza A viruses: An overview of recently discovered proteins. *Virus research* **185**, 53-63 (2014).
40. Yamayoshi, S., Watanabe, M., Goto, H. & Kawaoka, Y. Identification of a Novel Viral Protein Expressed from the PB2 Segment of Influenza A Virus. *Journal of virology* **90**, 444-456 (2016).
41. Bogdanow, B. et al. The dynamic proteome of influenza A virus infection identifies M segment splicing as a host range determinant. *Nature Communications* **10**, 5518 (2019).
42. Matlin, K.S., Reggio, H., Helenius, A. & Simons, K. Infectious entry pathway of influenza virus in a canine kidney cell line. *J Cell Biol* **91**, 601-613 (1981).
43. Wiley, D.C. & Skehel, J.J. The structure and function of the hemagglutinin membrane glycoprotein of influenza virus. *Annual review of biochemistry* **56**, 365–394 (1987).
44. Sakai, T., Nishimura, S.I., Naito, T. & Saito, M. Influenza A virus hemagglutinin and neuraminidase act as novel motile machinery. *Scientific reports* **7**, 45043 (2017).
45. Rust, M.J., Lakadamyali, M., Zhang, F. & Zhuang, X. Assembly of endocytic machinery around individual influenza viruses during viral entry. *Nature structural & molecular biology* **11**, 567-573 (2004).
46. Chen, C. & Zhuang, X. Epsin 1 is a cargo-specific adaptor for the clathrin-mediated endocytosis of the influenza virus. *Proceedings of the National Academy of Sciences of the United States of America* **105**, 11790-11795 (2008).
47. de Vries, E. et al. Dissection of the influenza A virus endocytic routes reveals macropinocytosis as an alternative entry pathway. *PLoS Pathog* **7**, e1001329 (2011).
48. Rossman, J.S., Leser, G.P. & Lamb, R.A. Filamentous influenza virus enters cells via macropinocytosis. *Journal of virology* **86**, 10950-10960 (2012).
49. Chu, V.C. & Whittaker, G.R. Influenza virus entry and infection require host cell N-linked glycoprotein. *Proceedings of the National Academy of Sciences of the United States of America* **101**, 18153-18158 (2004).
50. Lakadamyali, M., Rust, M.J., Babcock, H.P. & Zhuang, X. Visualizing infection of individual influenza viruses. *Proceedings of the National Academy of Sciences of the United States of America* **100**, 9280-9285 (2003).
51. Pinto, L.H. & Lamb, R.A. The M2 Proton Channels of Influenza A and B Viruses. *Journal of Biological Chemistry* **281**, 8997-9000 (2006).
52. Li, S. et al. pH-Controlled Two-Step Uncoating of Influenza Virus. *Biophysical journal* **106**, 1447-1456 (2014).
53. Yoshimura, A. & Ohnishi, S. Uncoating of influenza virus in endosomes. *Journal of virology* **51**, 497-504 (1984).
54. Harrison, S.C. Viral membrane fusion. *Nature Structural & Molecular Biology* **15**, 690-698 (2008).
55. Hamilton, B.S., Whittaker, G.R. & Daniel, S. Influenza Virus-Mediated Membrane Fusion: Determinants of Hemagglutinin Fusogenic Activity and Experimental Approaches for Assessing Virus Fusion. *Viruses* **4**, 1144-1168 (2012).
56. Babcock, H.P., Chen, C. & Zhuang, X. Using Single-Particle Tracking to Study Nuclear

Trafficking of Viral Genes. *Biophysical journal* **87**, 2749-2758 (2004).
57. Calder, L.J., Wasilewski, S., Berriman, J.A. & Rosenthal, P.B. Structural organization of a filamentous influenza A virus. *Proceedings of the National Academy of Sciences of the United States of America* **107**, 10685-10690 (2010).
58. Fontana, J., Cardone, G., Heymann, J.B., Winkler, D.C. & Steven, A.C. Structural changes in influenza virus at low ph characterized by cryo-electron tomography. *Journal of virology* **86**, 2919-2929 (2012).
59. Cros, J.F., García-Sastre, A. & Palese, P. An unconventional NLS is critical for the nuclear import of the influenza A virus nucleoprotein and ribonucleoprotein. *Traffic (Copenhagen, Denmark)* **6**, 205-213 (2005).
60. Cros, J.F. & Palese, P. Trafficking of viral genomic RNA into and out of the nucleus: influenza, Thogoto and Borna disease viruses. *Virus research* **95**, 3-12 (2003).
61. Fodor, E. The RNA polymerase of influenza a virus: mechanisms of viral transcription and replication. *Acta virologica* **57**, 113-122 (2013).
62. Krug, R.M. Priming of influenza viral RNA transcription by capped heterologous RNAs. *Current topics in microbiology and immunology* **93**, 125-149 (1981).
63. Reich, S. et al. Structural insight into cap-snatching and RNA synthesis by influenza polymerase. *Nature* **516**, 361-366 (2014).
64. Poon, L.L., Pritlove, D.C., Fodor, E. & Brownlee, G.G. Direct evidence that the poly(A) tail of influenza A virus mRNA is synthesized by reiterative copying of a U track in the virion RNA template. *Journal of virology* **73**, 3473-3476 (1999).
65. Smith, G.L., Levin, J.Z., Palese, P. & Moss, B. Synthesis and cellular location of the ten influenza polypeptides individually expressed by recombinant vaccinia viruses. *Virology* **160**, 336-345 (1987).
66. Dou, D., Revol, R., Östbye, H., Wang, H. & Daniels, R. Influenza A Virus Cell Entry, Replication, Virion Assembly and Movement. *Frontiers in Immunology* **9** (2018).
67. Ayllon, J. & García-Sastre, A. in Influenza Pathogenesis and Control - Volume II. (eds. M.B.A. Oldstone & R.W. Compans) 73-107 (Springer International Publishing, Cham; 2015).
68. Copeland, C.S., Doms, R.W., Bolzau, E.M., Webster, R.G. & Helenius, A. Assembly of influenza hemagglutinin trimers and its role in intracellular transport. *J Cell Biol* **103**, 1179-1191 (1986).
69. Leser, G.P. & Lamb, R.A. Influenza virus assembly and budding in raft-derived microdomains: A quantitative analysis of the surface distribution of HA, NA and M2 proteins. *Virology* **342**, 215-227 (2005).
70. Newcomb, L.L. et al. Interaction of the influenza a virus nucleocapsid protein with the viral RNA polymerase potentiates unprimed viral RNA replication. *Journal of virology* **83**, 29-36 (2009).
71. Goto, H., Muramoto, Y., Noda, T. & Kawaoka, Y. The genome-packaging signal of the influenza A virus genome comprises a genome incorporation signal and a genome-bundling signal. *Journal of virology* **87**, 11316-11322 (2013).
72. Rossman, J.S. & Lamb, R.A. Influenza virus assembly and budding. *Virology* **411**, 229-236 (2011).
73. Skehel, J.J. & Wiley, D.C. Receptor binding and membrane fusion in virus entry: the influenza hemagglutinin. *Annual review of biochemistry* **69**, 531–569 (2000).
74. Böttcher-Friebertshäuser, E., Klenk, H.D. & Garten, W. Activation of influenza viruses by proteases from host cells and bacteria in the human airway epithelium. *Pathogens and disease* **69**, 87-100 (2013).
75. Nakamura, K. & Compans, R.W. Host cell- and virus strain-dependent differences in oligosaccharides of hemagglutinin glycoproteins of influenza A viruses. *Virology* **95**, 8-23 (1979).
76. Schwarzer, J. et al. Glycan analysis in cell culture-based influenza vaccine production: influence of host cell line and virus strain on the glycosylation pattern of viral hemagglutinin. *Vaccine* **27**, 4325-4336 (2009).
77. Hiono, T. et al. Lectin microarray analyses reveal host cell-specific glycan profiles of the hemagglutinins of influenza A viruses. *Virology* **527**, 132-140 (2019).
78. Roberts, P.C., Garten, W. & Klenk, H.D. Role of conserved glycosylation sites in maturation and transport of influenza A virus hemagglutinin. *Journal of virology* **67**, 3048-3060 (1993).
79. Tate, M.D. et al. Playing hide and seek: how glycosylation of the influenza virus hemagglutinin can modulate the immune response to infection. *Viruses* **6**, 1294-1316 (2014).

80. Abe, Y. et al. Effect of the addition of oligosaccharides on the biological activities and antigenicity of influenza A/H3N2 virus hemagglutinin. *Journal of virology* **78**, 9605-9611 (2004).
81. Wang, C.-C. et al. Glycans on influenza hemagglutinin affect receptor binding and immune response. *Proceedings of the National Academy of Sciences of the United States of America* **106**, 18137–18142 (2009).
82. Sun, X. et al. N-linked glycosylation of the hemagglutinin protein influences virulence and antigenicity of the 1918 pandemic and seasonal H1N1 influenza A viruses. *Journal of virology* **87**, 8756-8766 (2013).
83. Das, S.R. et al. Glycosylation Focuses Sequence Variation in the Influenza A Virus H1 Hemagglutinin Globular Domain. *PLOS Pathogens* **6**, e1001211 (2010).
84. Kobayashi, Y. & Suzuki, Y. Evidence for N-Glycan Shielding of Antigenic Sites during Evolution of Human Influenza A Virus Hemagglutinin. *Journal of virology* **86**, 3446-3451 (2012).
85. Medina, R.A. et al. Glycosylations in the Globular Head of the Hemagglutinin Protein Modulate the Virulence and Antigenic Properties of the H1N1 Influenza Viruses. *Science translational medicine* **5**, 187ra170-187ra170 (2013).
86. Röhm, C., Zhou, N., Süss, J., Mackenzie, J. & Webster, R.G. Characterization of a novel influenza hemagglutinin, H15: criteria for determination of influenza A subtypes. *Virology* **217**, 508-516 (1996).
87. Yang, H. et al. Structure and receptor binding preferences of recombinant human A(H3N2) virus hemagglutinins. *Virology* **477**, 18–31 (2015).
88. Koel, B.F. et al. Substitutions near the receptor binding site determine major antigenic change during influenza virus evolution. *Science* **342**, 976-979 (2013).
89. Wedde, M., Biere, B., Wolff, T. & Schweiger, B. Evolution of the hemagglutinin expressed by human influenza A(H1N1)pdm09 and A(H3N2) viruses circulating between 2008-2009 and 2013-2014 in Germany. *International journal of medical microbiology : IJMM* **305**, 762-775 (2015).
90. Sauter, N.K. et al. Hemagglutinins from two influenza virus variants bind to sialic acid derivatives with millimolar dissociation constants: a 500-MHz proton nuclear magnetic resonance study. *Biochemistry* **28**, 8388–8396 (1989).
91. Mammen, M., Choi, S.-K. & Whitesides, G.M. Polyvalent Interactions in Biological Systems: Implications for Design and Use of Multivalent Ligands and Inhibitors. *Angewandte Chemie International Edition* **37**, 2754-2794 (1998).
92. Muller, M., Lauster, D., Wildenauer, H.H.K., Herrmann, A. & Block, S. Mobility-Based Quantification of Multivalent Virus-Receptor Interactions: New Insights Into Influenza A Virus Binding Mode. *Nano letters* (2019).
93. Sieben, C. et al. Influenza virus binds its host cell using multiple dynamic interactions. *Proceedings of the National Academy of Sciences of the United States of America* **109**, 13626–13631 (2012).
94. Bandlow, V. et al. Spatial screening of hemagglutinin on Influenza A virus particles: Sialyl-LacNAc displays on DNA and PEG scaffolds reveal the requirements for bivalency enhanced interactions with weak monovalent binders. *J Am Chem Soc* (2017).
95. Peng, W. et al. Recent H3N2 Viruses Have Evolved Specificity for Extended, Branched Human-type Receptors, Conferring Potential for Increased Avidity. *Cell Host Microbe* **21**, 23-34 (2017).
96. Sauter, N.K. et al. Crystallographic detection of a second ligand binding site in influenza virus hemagglutinin. *Proceedings of the National Academy of Sciences of the United States of America* **89**, 324-328 (1992).
97. Reiter-Scherer, V. et al. Force Spectroscopy Shows Dynamic Binding of Influenza Hemagglutinin and Neuraminidase to Sialic Acid. *Biophysical journal* (2019).
98. García-Sastre, A. Influenza Virus Receptor Specificity: Disease and Transmission. *The American Journal of Pathology* **176**, 1584-1585 (2010).
99. Walther, T. et al. Glycomic Analysis of Human Respiratory Tract Tissues and Correlation with Influenza Virus Infection. *PLoS Pathogens* **9**, e1003223 (2013).
100. de Graaf, M. & Fouchier, R.A.M. Role of receptor binding specificity in influenza A virus transmission and pathogenesis. *EMBO J* **33**, 823-841 (2014).
101. Varki, A. & Kornfeld, S. in Essentials of Glycobiology, Edn. 2nd (Cold Spring Harbor Laboratory Press, Cold Spring Harbor (NY), 2009).

102. Stanley, P., Taniguchi, N. & Aebi, M. in Essentials of Glycobiology, Edn. 2nd (Cold Spring Harbor Laboratory Press, Cold Spring Harbor (NY), 2009).
103. Taylor, M.E. & Drickamer, K. Introduction to glycobiology. (Oxford university press, 2011).
104. Varki, N.M. & Varki, A. Diversity in cell surface sialic acid presentations: implications for biology and disease. *Laboratory Investigation* **87**, 851-857 (2007).
105. Schauer, R. Achievements and challenges of sialic acid research. *Glycoconjugate journal* **17**, 485-499 (2000).
106. Gambaryan, A.S. et al. Specification of receptor-binding phenotypes of influenza virus isolates from different hosts using synthetic sialylglycopolymers: non-egg-adapted human H1 and H3 influenza A and influenza B viruses share a common high binding affinity for 6'-sialyl(N-acetyllactosamine). *Virology* **232**, 345-350 (1997).
107. Rogers, G.N. & Paulson, J.C. Receptor determinants of human and animal influenza virus isolates: Differences in receptor specificity of the H3 hemagglutinin based on species of origin. *Virology* **127**, 361-373 (1983).
108. Connor, R.J., Kawaoka, Y., Webster, R.G. & Paulson, J.C. Receptor specificity in human, avian, and equine H2 and H3 influenza virus isolates. *Virology* **205**, 17-23 (1994).
109. Matrosovich, M. et al. Early alterations of the receptor-binding properties of H1, H2, and H3 avian influenza virus hemagglutinins after their introduction into mammals. *Journal of virology* **74**, 8502-8512 (2000).
110. Nicholls, J.M., Chan, R.W., Russell, R.J., Air, G.M. & Peiris, J.S. Evolving complexities of influenza virus and its receptors. *Trends in microbiology* **16**, 149-157 (2008).
111. França, M., Stallknecht, D.E. & Howerth, E.W. Expression and distribution of sialic acid influenza virus receptors in wild birds. *Avian Pathol* **42**, 60-71 (2013).
112. Kastner, M. et al. Relevance of host cell surface glycan structure for cell specificity of influenza A virus. *bioRxiv* (2017).
113. Stevens, J. et al. Glycan microarray analysis of the hemagglutinins from modern and pandemic influenza viruses reveals different receptor specificities. *Journal of molecular biology* **355**, 1143–1155 (2006).
114. Chandrasekaran, A. et al. Glycan topology determines human adaptation of avian H5N1 virus hemagglutinin. *Nature biotechnology* **26**, 107–113 (2008).
115. Xu, D. et al. Distinct glycan topology for avian and human sialopentasaccharide receptor analogues upon binding different hemagglutinins: a molecular dynamics perspective. *Journal of molecular biology* **387**, 465–491 (2009).
116. Zhao, N., Martin, B.E., Yang, C.-K., Luo, F. & Wan, X.-F. Association analyses of large-scale glycan microarray data reveal novel host-specific substructures in influenza A virus binding glycans. *Scientific reports* **5**, 15778 (2015).
117. Lin, Y.P. et al. Evolution of the receptor binding properties of the influenza A(H3N2) hemagglutinin. *Proceedings of the National Academy of Sciences of the United States of America* **109**, 21474–21479 (2012).
118. Byrd-Leotis, L. et al. Antigenic Pressure on H3N2 Influenza Virus Drift Strains Imposes Constraints on Binding to Sialylated Receptors but Not Phosphorylated Glycans. *Journal of virology* **93**, e01178-01119 (2019).
119. Ji, Y., White, Y.J., Hadden, J.A., Grant, O.C. & Woods, R.J. New insights into influenza A specificity: an evolution of paradigms. *Current opinion in structural biology* **44**, 219–231 (2017).
120. Ohuchi, M., Ohuchi, R., Feldmann, A. & Klenk, H.D. Regulation of receptor binding affinity of influenza virus hemagglutinin by its carbohydrate moiety. *Journal of virology* **71**, 8377–8384 (1997).
121. Gulati, S. et al. Human H3N2 Influenza Viruses Isolated from 1968 To 2012 Show Varying Preference for Receptor Substructures with No Apparent Consequences for Disease or Spread. *PloS one* **8**, e66325 (2013).
122. Varghese, J.N. & Colman, P.M. Three-dimensional structure of the neuraminidase of influenza virus A/Tokyo/3/67 at 2·2 Å resolution. *Journal of Molecular Biology* **221**, 473-486 (1991).
123. Gaymard, A., Le Briand, N., Frobert, E., Lina, B. & Escuret, V. Functional balance between neuraminidase and haemagglutinin in influenza viruses. *Clinical microbiology and infection : the official publication of the European*

Society of Clinical Microbiology and Infectious Diseases **22**, 975-983 (2016).
124. de Vries, E., Du, W., Guo, H. & de Haan, C.A.M. Influenza A Virus Hemagglutinin–Neuraminidase –Receptor Balance: Preserving Virus Motility. *Trends in microbiology* **28**, 57-67 (2020).
125. Varghese, J.N., McKimm-Breschkin, J.L., Caldwell, J.B., Kortt, A.A. & Colman, P.M. The structure of the complex between influenza virus neuraminidase and sialic acid, the viral receptor. *Proteins: Structure, Function, and Bioinformatics* **14**, 327-332 (1992).
126. Shtyrya, Y.A., Mochalova, L.V. & Bovin, N.V. Influenza virus neuraminidase: structure and function. *Acta Naturae* **1**, 26-32 (2009).
127. McAuley, J.L., Gilbertson, B.P., Trifkovic, S., Brown, L.E. & McKimm-Breschkin, J.L. Influenza Virus Neuraminidase Structure and Functions. *Frontiers in microbiology* **10**, 39-39 (2019).
128. Mohr, P.G., Deng, Y.-M. & McKimm-Breschkin, J.L. The neuraminidases of MDCK grown human influenza A(H3N2) viruses isolated since 1994 can demonstrate receptor binding. *Virology journal* **12**, 67-67 (2015).
129. Zhu, X. et al. Influenza virus neuraminidases with reduced enzymatic activity that avidly bind sialic Acid receptors. *Journal of virology* **86**, 13371-13383 (2012).
130. Barberis, I., Myles, P., Ault, S.K., Bragazzi, N.L. & Martini, M. History and evolution of influenza control through vaccination: from the first monovalent vaccine to universal vaccines. *Journal of preventive medicine and hygiene* **57**, E115-E120 (2016).
131. ECDC (2019).
132. CDC (CDC, 2019).
133. Robert Koch Institute Wissenschaftliche Begründung für die Empfehlung des quadrivalenten saisonalen Influenzaimpfstoffs. *Epidemiologisches Bulletin* **02** (2018).
134. Robert Koch Institute Stellungnahme der Ständigen Impfkommission (STIKO) beim Robert Koch-Institut (RKI). *Epidemiologisches Bulletin* **32/33** (2020).
135. Wu, N.C. & Wilson, I.A. A Perspective on the Structural and Functional Constraints for Immune Evasion: Insights from Influenza Virus. *J Mol Biol* **429**, 2694-2709 (2017).
136. Wiley, D.C., Wilson, I.A. & Skehel, J.J. Structural identification of the antibody-binding sites of Hong Kong influenza haemagglutinin and their involvement in antigenic variation. *Nature* **289**, 373-378 (1981).
137. Belongia, E.A. et al. Variable influenza vaccine effectiveness by subtype: a systematic review and meta-analysis of test-negative design studies. *Lancet Infect Dis* **16**, 942-951 (2016).
138. Kissling, E., Rondy, M. & team, I.-M.I.-M.s. Early 2016/17 vaccine effectiveness estimates against influenza A(H3N2): I-MOVE multicentre case control studies at primary care and hospital levels in Europe. *Eurosurveillance* **22**, 30464 (2017).
139. World Health Organization, Vol. 2020 (2009).
140. Kelso, J.K., Halder, N. & Milne, G.J. Vaccination strategies for future influenza pandemics: a severity-based cost effectiveness analysis. *BMC infectious diseases* **13**, 81-81 (2013).
141. van de Wakker, S.I., Fischer, M.J.E. & Oosting, R.S. New drug-strategies to tackle viral-host interactions for the treatment of influenza virus infections. *European Journal of Pharmacology* **809**, 178-190 (2017).
142. Lampejo, T. Influenza and antiviral resistance: an overview. *European Journal of Clinical Microbiology & Infectious Diseases* **39**, 1201-1208 (2020).
143. Hussain, M., Galvin, H.D., Haw, T.Y., Nutsford, A.N. & Husain, M. Drug resistance in influenza A virus: the epidemiology and management. *Infection and drug resistance* **10**, 121-134 (2017).
144. Malakhov, M.P. et al. Sialidase fusion protein as a novel broad-spectrum inhibitor of influenza virus infection. *Antimicrob Agents Chemother* **50**, 1470-1479 (2006).
145. Triana-Baltzer, G.B. et al. Novel pandemic influenza A(H1N1) viruses are potently inhibited by DAS181, a sialidase fusion protein. *PloS one* **4**, e7788 (2009).
146. Belser, J.A. et al. DAS181, a novel sialidase fusion protein, protects mice from lethal avian influenza H5N1 virus infection. *J Infect Dis* **196**, 1493-1499 (2007).
147. Zenilman, J.M. et al. Phase 1 clinical trials of DAS181, an inhaled sialidase, in healthy adults. *Antiviral research* **123**, 114-119 (2015).
148. Triana-Baltzer, G.B. et al. Phenotypic and genotypic characterization of influenza virus mutants selected with the sialidase

fusion protein DAS181. *The Journal of antimicrobial chemotherapy* **66**, 15-28 (2011).
149. Rossignol, J.F., La Frazia, S., Chiappa, L., Ciucci, A. & Santoro, M.G. Thiazolides, a new class of anti-influenza molecules targeting viral hemagglutinin at the post-translational level. *The Journal of biological chemistry* **284**, 29798-29808 (2009).
150. Haffizulla, J. et al. Effect of nitazoxanide in adults and adolescents with acute uncomplicated influenza: a double-blind, randomised, placebo-controlled, phase 2b/3 trial. *The Lancet. Infectious diseases* **14**, 609-618 (2014).
151. Gamiño-Arroyo, A.E. et al. Efficacy and Safety of Nitazoxanide in Addition to Standard of Care for the Treatment of Severe Acute Respiratory Illness. *Clinical infectious diseases : an official publication of the Infectious Diseases Society of America* **69**, 1903-1911 (2019).
152. Cady, S.D. et al. Structure of the amantadine binding site of influenza M2 proton channels in lipid bilayers. *Nature* **463**, 689-692 (2010).
153. Wang, C., Takeuchi, K., Pinto, L.H. & Lamb, R.A. Ion channel activity of influenza A virus M2 protein: characterization of the amantadine block. *Journal of virology* **67**, 5585 (1993).
154. Jefferson, T., Demicheli, V., Di Pietrantonj, C. & Rivetti, D. Amantadine and rimantadine for influenza A in adults. *Cochrane Database Syst Rev* **2006**, CD001169-CD001169 (2006).
155. Hubsher, G., Haider, M. & Okun, M.S. Amantadine: the journey from fighting flu to treating Parkinson disease. *Neurology* **78**, 1096-1099 (2012).
156. Belshe, R.B., Smith, M.H., Hall, C.B., Betts, R. & Hay, A.J. Genetic basis of resistance to rimantadine emerging during treatment of influenza virus infection. *Journal of virology* **62**, 1508 (1988).
157. Hay, A.J., Zambon, M.C., Wolstenholme, A.J., Skehel, J.J. & Smith, M.H. Molecular basis of resistance of influenza A viruses to amantadine. *Journal of Antimicrobial Chemotherapy* **18**, 19-29 (1986).
158. Bright, R.A., Shay, D.K., Shu, B., Cox, N.J. & Klimov, A.I. Adamantane Resistance Among Influenza A Viruses Isolated Early During the 2005-2006 Influenza Season in the United States. *JAMA* **295**, 891-894 (2006).
159. Koch-Institut, R. (Robert Koch-Institut, 2019).
160. Colman, P.M., Varghese, J.N. & Laver, W.G. Structure of the catalytic and antigenic sites in influenza virus neuraminidase. *Nature* **303**, 41-44 (1983).
161. McKimm-Breschkin, J.L. Resistance of influenza viruses to neuraminidase inhibitors--a review. *Antiviral research* **47**, 1-17 (2000).
162. von Itzstein, M. et al. A study of the active site of influenza virus sialidase: an approach to the rational design of novel anti-influenza drugs. *J Med Chem* **39**, 388-391 (1996).
163. Colman, P.M. Influenza virus neuraminidase: structure, antibodies, and inhibitors. *Protein science : a publication of the Protein Society* **3**, 1687-1696 (1994).
164. von Itzstein, M. et al. Rational design of potent sialidase-based inhibitors of influenza virus replication. *Nature* **363**, 418-423 (1993).
165. Kim, C.U. et al. Influenza neuraminidase inhibitors possessing a novel hydrophobic interaction in the enzyme active site: design, synthesis, and structural analysis of carbocyclic sialic acid analogues with potent anti-influenza activity. *J Am Chem Soc* **119**, 681-690 (1997).
166. Hurt, A.C. & Kelly, H. Debate Regarding Oseltamivir Use for Seasonal and Pandemic Influenza. *Emerging infectious diseases* **22**, 949-955 (2016).
167. Jefferson, T. et al. Neuraminidase inhibitors for preventing and treating influenza in healthy adults and children. *Cochrane Database Syst Rev* **2014**, CD008965-CD008965 (2014).
168. Adisasmito, W. et al. Effectiveness of antiviral treatment in human influenza A(H5N1) infections: analysis of a Global Patient Registry. *J Infect Dis* **202**, 1154-1160 (2010).
169. Muthuri, S.G. et al. Effectiveness of neuraminidase inhibitors in reducing mortality in patients admitted to hospital with influenza A H1N1pdm09 virus infection: a meta-analysis of individual participant data. *Lancet Respir Med* **2**, 395-404 (2014).
170. Louie, J.K., Yang, S., Samuel, M.C., Uyeki, T.M. & Schechter, R. Neuraminidase inhibitors for critically ill children with influenza. *Pediatrics* **132**, e1539-1545 (2013).
171. Burnham, A.J., Baranovich, T. & Govorkova, E.A. Neuraminidase inhibitors for influenza B virus infection:

Efficacy and resistance. *Antiviral research* **100**, 520-534 (2013).
172. Ison, M.G. et al. Early treatment with baloxavir marboxil in high-risk adolescent and adult outpatients with uncomplicated influenza (CAPSTONE-2): a randomised, placebo-controlled, phase 3 trial. *Lancet Infect Dis* **20**, 1204-1214 (2020).
173. Moscona, A. Oseltamivir Resistance — Disabling Our Influenza Defenses. *New England Journal of Medicine* **353**, 2633-2636 (2005).
174. Gamblin, S.J. & Skehel, J.J. Influenza hemagglutinin and neuraminidase membrane glycoproteins. *The Journal of biological chemistry* **285**, 28403–28409 (2010).
175. Blick, T.J. et al. The interaction of neuraminidase and hemagglutinin mutations in influenza virus in resistance to 4-guanidino-Neu5Ac2en. *Virology* **246**, 95-103 (1998).
176. Chin, A.W.H., Yen, H.L., Krauss, S., Webby, R.J. & Poon, L.L.M. Recombinant influenza virus with a pandemic H2N2 polymerase complex has a higher adaptive potential than one with seasonal H2N2 polymerase complex. *J Gen Virol* **97**, 611-619 (2016).
177. Bloom, J.D., Gong, L.I. & Baltimore, D. Permissive secondary mutations enable the evolution of influenza oseltamivir resistance. *Science (New York, N.Y.)* **328**, 1272-1275 (2010).
178. Lina, B. et al. Five years of monitoring for the emergence of oseltamivir resistance in patients with influenza A infections in the Influenza Resistance Information Study. *Influenza and other respiratory viruses* **12**, 267-278 (2018).
179. Kramarz, P., Monnet, D., Nicoll, A., Yilmaz, C. & Ciancio, B. Use of oseltamivir in 12 European countries between 2002 and 2007--lack of association with the appearance of oseltamivir-resistant influenza A(H1N1) viruses. *Euro Surveill* **14** (2009).
180. CDC Update: influenza activity--United States, September 28-November 29, 2008. *MMWR Morb Mortal Wkly Rep* **57**, 1329-1332 (2008).
181. Lackenby, A. et al. Emergence of resistance to oseltamivir among influenza A(H1N1) viruses in Europe. *Eurosurveillance* **13**, 3-4%P 8026 (2008).
182. Hurt, A.C. et al. Antiviral resistance during the 2009 influenza A H1N1 pandemic: public health, laboratory, and clinical perspectives. *Lancet Infect Dis* **12**, 240-248 (2012).
183. Lackenby, A. et al. Continued emergence and changing epidemiology of oseltamivir-resistant influenza A(H1N1)2009 virus, United Kingdom, winter 2010/11. *Eurosurveillance* **16**, 19784 (2011).
184. Food and Drug Administration, Vol. 2020 (2015).
185. European Medicinces Agency, Vol. 2020 (2018).
186. McKimm-Breschkin, J.L. Influenza neuraminidase inhibitors: antiviral action and mechanisms of resistance. *Influenza and other respiratory viruses* **7 Suppl 1**, 25-36 (2013).
187. Kashiwagi, S. et al. Long-acting Neuraminidase Inhibitor Laninamivir Octanoate as Post-exposure Prophylaxis for Influenza. *Clinical infectious diseases : an official publication of the Infectious Diseases Society of America* **63**, 330-337 (2016).
188. Schade, D. et al. Development of novel potent orally bioavailable oseltamivir derivatives active against resistant influenza A. *J Med Chem* **57**, 759-769 (2014).
189. Cheng, T.-J.R. et al. Development of oseltamivir phosphonate congeners as anti-influenza agents. *Journal of medicinal chemistry* **55**, 8657-8670 (2012).
190. Kim, J.H. et al. Mechanism-based covalent neuraminidase inhibitors with broad-spectrum influenza antiviral activity. *Science* **340**, 71-75 (2013).
191. Tarbet, E.B. et al. A zanamivir dimer with prophylactic and enhanced therapeutic activity against influenza viruses. *The Journal of antimicrobial chemotherapy* **69**, 2164-2174 (2014).
192. Watson, K.G. et al. Highly potent and long-acting trimeric and tetrameric inhibitors of influenza virus neuraminidase. *Bioorg Med Chem Lett* **14**, 1589-1592 (2004).
193. Furuta, Y. et al. Favipiravir (T-705), a novel viral RNA polymerase inhibitor. *Antiviral research* **100**, 446-454 (2013).
194. Mifsud, E.J., Hayden, F.G. & Hurt, A.C. Antivirals targeting the polymerase complex of influenza viruses. *Antiviral research* **169**, 104545 (2019).
195. Shiraki, K. & Daikoku, T. Favipiravir, an anti-influenza drug against life-threatening RNA virus infections. *Pharmacol Ther* **209**, 107512-107512 (2020).

196. Daikoku, T., Yoshida, Y., Okuda, T. & Shiraki, K. Characterization of susceptibility variants of influenza virus grown in the presence of T-705. *J Pharmacol Sci* **126**, 281-284 (2014).
197. Baranovich, T. et al. T-705 (favipiravir) induces lethal mutagenesis in influenza A H1N1 viruses in vitro. *Journal of virology* **87**, 3741-3751 (2013).
198. Goldhill, D.H. et al. The mechanism of resistance to favipiravir in influenza. *Proceedings of the National Academy of Sciences of the United States of America* **115**, 11613-11618 (2018).
199. Hayden, F.G. & Shindo, N. Influenza virus polymerase inhibitors in clinical development. *Curr Opin Infect Dis* **32**, 176-186 (2019).
200. Fu, Y. et al. JNJ872 inhibits influenza A virus replication without altering cellular antiviral responses. *Antiviral research* **133**, 23-31 (2016).
201. Finberg, R.W. et al. Phase 2b Study of Pimodivir (JNJ-63623872) as Monotherapy or in Combination With Oseltamivir for Treatment of Acute Uncomplicated Seasonal Influenza A: TOPAZ Trial. *J Infect Dis* **219**, 1026-1034 (2019).
202. Johnson, J.P.C.o.J., Vol. 2020 (Janssen Pharmaceutical Companies of Johnson & Johnson, prnewswire; 2020).
203. Heo, Y.A. Baloxavir: First Global Approval. *Drugs* **78**, 693-697 (2018).
204. Food and Drug Administration, Vol. 2020 (2018).
205. Hayden, F.G. et al. Baloxavir Marboxil for Uncomplicated Influenza in Adults and Adolescents. *New England Journal of Medicine* **379**, 913-923 (2018).
206. Jones, J.C. et al. Identification of the I38T PA Substitution as a Resistance Marker for Next-Generation Influenza Virus Endonuclease Inhibitors. *mBio* **9**, e00430-00418 (2018).
207. Omoto, S. et al. Characterization of influenza virus variants induced by treatment with the endonuclease inhibitor baloxavir marboxil. *Scientific reports* **8**, 9633 (2018).
208. Imai, M. et al. Influenza A variants with reduced susceptibility to baloxavir isolated from Japanese patients are fit and transmit through respiratory droplets. *Nature microbiology* **5**, 27–33 (2020).
209. Reshef, R. et al. Blockade of Lymphocyte Chemotaxis in Visceral Graft-versus-Host Disease. *New England Journal of Medicine* **367**, 135-145 (2012).
210. Lataillade, M. et al. Safety and efficacy of the HIV-1 attachment inhibitor prodrug fostemsavir in heavily treatment-experienced individuals: week 96 results of the phase 3 BRIGHTE study. *The Lancet HIV* **7**, e740-e751 (2020).
211. Blaising, J., Polyak, S.J. & Pecheur, E.I. Arbidol as a broad-spectrum antiviral: an update. *Antiviral research* **107**, 84-94 (2014).
212. Leneva, I.A., Russell, R.J., Boriskin, Y.S. & Hay, A.J. Characteristics of arbidol-resistant mutants of influenza virus: Implications for the mechanism of anti-influenza action of arbidol. *Antiviral research* **81**, 132-140 (2009).
213. Wang, Y. et al. Inhibition of the infectivity and inflammatory response of influenza virus by Arbidol hydrochloride in vitro and in vivo (mice and ferret). *Biomedicine & pharmacotherapy = Biomedecine & pharmacotherapie* **91**, 393-401 (2017).
214. Lian, N. et al. Umifenovir treatment is not associated with improved outcomes in patients with coronavirus disease 2019: a retrospective study. *Clinical microbiology and infection : the official publication of the European Society of Clinical Microbiology and Infectious Diseases* **26**, 917-921 (2020).
215. Koszalka, P., Tilmanis, D. & Hurt, A.C. Influenza antivirals currently in late-phase clinical trial. *Influenza and other respiratory viruses* **11**, 240-246 (2017).
216. Lim, J.J. et al. A Phase 2 Randomized, Double-Blind, Placebo-Controlled Trial of MHAA4549A, a Monoclonal Antibody, plus Oseltamivir in Patients Hospitalized with Severe Influenza A Virus Infection. *Antimicrobial Agents and Chemotherapy* **64**, e00352-00320 (2020).
217. Yi, K.S. et al. Broader neutralization of CT-P27 against influenza A subtypes by combining two human monoclonal antibodies. *PloS one* **15**, e0236172-e0236172 (2020).
218. Sparrow, E., Friede, M., Sheikh, M., Torvaldsen, S. & Newall, A.T. Passive immunization for influenza through antibody therapies, a review of the pipeline, challenges and potential applications. *Vaccine* **34**, 5442-5448 (2016).
219. Hershberger, E. et al. Safety and efficacy of monoclonal antibody VIS410 in adults with uncomplicated influenza A infection: Results from a randomized, double-blind, phase-2, placebo-

controlled study. *EBioMedicine* **40**, 574-582 (2019).
220. Lin, Q. et al. Structural Basis for the Broad, Antibody-Mediated Neutralization of H5N1 Influenza Virus. *Journal of virology* **92** (2018).
221. Paules, C.I. et al. The Hemagglutinin A Stem Antibody MEDI8852 Prevents and Controls Disease and Limits Transmission of Pandemic Influenza Viruses. *The Journal of Infectious Diseases* **216**, 356-365 (2017).
222. Robert Koch Institute (2016).
223. Group., T.I.-R.S. Palivizumab, a Humanized Respiratory Syncytial Virus Monoclonal Antibody, Reduces Hospitalization From Respiratory Syncytial Virus Infection in High-risk Infants. *Pediatrics* **102**, 531-537 (1998).
224. Elawar, F. et al. Pharmacological targets and emerging treatments for respiratory syncytial virus bronchiolitis. *Pharmacol Ther* **220**, 107712 (2021).
225. Mulangu, S. et al. A Randomized, Controlled Trial of Ebola Virus Disease Therapeutics. *N Engl J Med* **381**, 2293-2303 (2019).
226. Food and Drug Administration. (ed. C. Tantibanchachai) (2020).
227. Wec, A.Z. et al. Development of a Human Antibody Cocktail that Deploys Multiple Functions to Confer Pan-Ebolavirus Protection. *Cell Host Microbe* **25**, 39-48.e35 (2019).
228. Food and Drug Administration. (ed. C. Tantibanchachai) (2020).
229. Food and Drug Administration. (ed. C. Tantibanchachai) (2020).
230. Wang, P. et al. Antibody resistance of SARS-CoV-2 variants B.1.351 and B.1.1.7. *Nature* **593**, 130-135 (2021).
231. Taylor, P.C. et al. Neutralizing monoclonal antibodies for treatment of COVID-19. *Nature Reviews Immunology* **21**, 382-393 (2021).
232. Cherian, S. et al. Convergent evolution of SARS-CoV-2 spike mutations, L452R, E484Q and P681R, in the second wave of COVID-19 in Maharashtra, India. *bioRxiv*, 2021.2004.2022.440932 (2021).
233. Al-Azzam, S. et al. Peptides to combat viral infectious diseases. *Peptides* **134**, 170402-170402 (2020).
234. Lin, D. et al. Potent influenza A virus entry inhibitors targeting a conserved region of hemagglutinin. *Biochemical pharmacology* **144**, 35-51 (2017).
235. Wu, W. et al. Super short membrane-active lipopeptides inhibiting the entry of influenza A virus. *Biochimica et Biophysica Acta (BBA) - Biomembranes* **1848**, 2344-2350 (2015).
236. Kingsley, C.N. et al. Probing the metastable state of influenza hemagglutinin. *The Journal of biological chemistry* **292**, 21590-21597 (2017).
237. EU Clinica Trials Register, Vol. 2020 (2017).
238. Memczak, H. et al. Anti-Hemagglutinin Antibody Derived Lead Peptides for Inhibitors of Influenza Virus Binding. *PloS one* **11**, e0159074 (2016).
239. Sevy, A.M. et al. Computationally Designed Cyclic Peptides Derived from an Antibody Loop Increase Breadth of Binding for Influenza Variants. *Structure* **28**, 1114-1123.e1114 (2020).
240. Kadam, R.U. et al. Potent peptidic fusion inhibitors of influenza virus. *Science (New York, N.Y.)* **358**, 496-502 (2017).
241. van Dongen, M.J.P. et al. A small-molecule fusion inhibitor of influenza virus is orally active in mice. *Science (New York, N.Y.)* **363**, eaar6221 (2019).
242. Nicol, M.Q., Ligertwood, Y., Bacon, M.N., Dutia, B.M. & Nash, A.A. A novel family of peptides with potent activity against influenza A viruses. *J Gen Virol* **93**, 980-986 (2012).
243. Matsubara, T. Potential of peptides as inhibitors and mimotopes: selection of carbohydrate-mimetic peptides from phage display libraries. *J Nucleic Acids* **2012**, 740982-740982 (2012).
244. Kadam, R.U. & Wilson, I.A. A small-molecule fragment that emulates binding of receptor and broadly neutralizing antibodies to influenza A hemagglutinin. *Proceedings of the National Academy of Sciences* (2018).
245. Chen, X. et al. Neoechinulin B and its analogues as potential entry inhibitors of influenza viruses, targeting viral hemagglutinin. *European journal of medicinal chemistry* **93**, 182-195 (2015).
246. Toogood, P.L., Galliker, P.K., Glick, G.D. & Knowles, J.R. Monovalent sialosides that bind tightly to influenza A virus. *Journal of Medicinal Chemistry* **34**, 3138-3140 (1991).
247. Jencks, W.P. On the attribution and additivity of binding energies. *Proceedings of the National Academy of Sciences of the United States of America* **78**, 4046-4050 (1981).
248. Olsson, T.S.G., Ladbury, J.E., Pitt, W.R. & Williams, M.A. Extent of enthalpy-entropy compensation in protein-ligand interactions. *Protein science : a*

publication of the Protein Society **20**, 1607-1618 (2011).
249. Alghrair, Z.K., Fernig, D.G. & Ebrahimi, B. Enhanced inhibition of influenza virus infection by peptide-noble-metal nanoparticle conjugates. *Beilstein J Nanotechnol* **10**, 1038-1047 (2019).
250. Choi, S.K., Mammen, M. & Whitesides, G.M. Generation and in situ evaluation of libraries of poly(acrylic acid) presenting sialosides as side chains as polyvalent inhibitors of influenza- mediated hemagglutination. *Journal of the American Chemical Society* **119**, 4103-4111 (1997).
251. Sigal, G.B., Mammen, M., Dahmann, G. & Whitesides, G.M. Polyacrylamides bearing pendant α-sialoside groups strongly inhibit agglutination of erythrocytes by influenza virus: The strong inhibition reflects enhanced binding through cooperative polyvalent interactions. *Journal of the American Chemical Society* **118**, 3789-3800 (1996).
252. Lees, W.J., Spaltenstein, A., Kingery-Wood, J.E. & Whitesides, G.M. Polyacrylamides Bearing Pendant .alpha.-Sialoside Groups Strongly Inhibit Agglutination of Erythrocytes by Influenza A Virus: Multivalency and Steric Stabilization of Particulate Biological Systems. *Journal of Medicinal Chemistry* **37**, 3419-3433 (1994).
253. Matrosovich, M.N., Mochalova, L.V., Marinina, V.P., Byramova, N.E. & Bovin, N.V. Synthetic polymeric sialoside inhibitors of influenza virus receptor-binding activity. *FEBS Letters* **272**, 209-212 (1990).
254. Choi, S.K., Mammen, M. & Whitesides, G.M. Monomeric inhibitors of influenza neuraminidase enhance the hemagglutination inhibition activities of polyacrylamides presenting multiple C-sialoside groups. *Chem Biol* **3**, 97-104 (1996).
255. Mangan, D. & Snyder, I.S. The effect of acrylamide on human polymorphonuclear neutrophils in vitro. *Br J Ind Med* **35**, 305-311 (1978).
256. Spencer, P.S. & Schaumburg, H.H. Nervous system degeneration produced by acrylamide monomer. *Environ Health Perspect* **11**, 129-133 (1975).
257. Gambaryan, A.S. et al. Polymeric inhibitor of influenza virus attachment protects mice from experimental influenza infection. *Antiviral research* **55**, 201-205 (2002).
258. Reuter, J.D. et al. Inhibition of viral adhesion and infection by sialic-acid-conjugated dendritic polymers. *Bioconjug Chem* **10**, 271-278 (1999).
259. Landers, J.J. et al. Prevention of influenza pneumonitis by sialic acid-conjugated dendritic polymers. *Journal of Infectious Diseases* **186**, 1222-1230 (2002).
260. Kwon, S.J. et al. Nanostructured glycan architecture is important in the inhibition of influenza A virus infection. *Nature nanotechnology* (2016).
261. Günther, S.C. et al. Antiviral potential of 3'-sialyllactose- and 6'-sialyllactose-conjugated dendritic polymers against human and avian influenza viruses. *Scientific reports* **10**, 768 (2020).
262. Labieniec-Watala, M. & Watala, C. PAMAM Dendrimers: Destined for Success or Doomed to Fail? Plain and Modified PAMAM Dendrimers in the Context of Biomedical Applications. *Journal of Pharmaceutical Sciences* **104**, 2-14 (2015).
263. Li, X., Wu, P., Gao, G.F. & Cheng, S. Carbohydrate-functionalized chitosan fiber for influenza virus capture. *Biomacromolecules* **12**, 3962–3969 (2011).
264. Makimura, Y. et al. Chemoenzymatic synthesis and application of a sialoglycopolymer with a chitosan backbone as a potent inhibitor of human influenza virus hemagglutination. *Carbohydrate research* **341**, 1803-1808 (2006).
265. Kingery-Wood, J.E., Williams, K.W., Sigal, G.B. & Whitesides, G.M. The agglutination of erythrocytes by influenza virus is strongly inhibited by liposomes incorporating an analog of sialyl gangliosides. *Journal of the American Chemical Society* **114**, 7303-7305 (1992).
266. Reichert, A., Nagy, J.O., Spevak, W. & Charych, D. Polydiacetylene Liposomes Functionalized with Sialic Acid Bind and Colorimetrically Detect Influenza Virus. *Journal of the American Chemical Society* **117**, 829-830 (1995).
267. Spevak, W. et al. Polymerized liposomes containing C-glycosides of sialic acid: potent inhibitors of influenza virus in vitro infectivity. *Journal of the American Chemical Society* **115**, 1146-1147 (1993).
268. Hendricks, G.L. et al. Sialylneolacto-N-tetraose c (LSTc)-bearing liposomal decoys capture influenza A virus. *The Journal of biological chemistry* **288**, 8061-8073 (2013).

269. Papp, I. et al. Inhibition of influenza virus infection by multivalent sialic-acid-functionalized gold nanoparticles. *Small* **6**, 2900-2906 (2010).
270. Vonnemann, J. et al. Virus inhibition induced by polyvalent nanoparticles of different sizes. *Nanoscale* **6**, 2353-2360 (2014).
271. Lauster, D. et al. Phage capsid nanoparticles with defined ligand arrangement block influenza virus entry. *Nature nanotechnology* (2020).
272. Nie, C. et al. Topology-Matching Design of an Influenza-Neutralizing Spiky Nanoparticle-Based Inhibitor with a Dual Mode of Action. *Angewandte Chemie (International ed. in English)* **59**, 15532-15536 (2020).
273. Nie, C. et al. Spiky Nanostructures with Geometry-matching Topography for Virus Inhibition. *Nano letters* **20**, 5367-5375 (2020).
274. Papp, I. et al. Inhibition of influenza virus activity by multivalent glycoarchitectures with matched sizes. *Chembiochem* **12**, 887-895 (2011).
275. Bhatia, S. et al. Linear polysialoside outperforms dendritic analogs for inhibition of influenza virus infection in vitro and in vivo. *Biomaterials* **138**, 22-34 (2017).
276. Vonnemann, J. et al. Size dependence of steric shielding and multivalency effects for globular binding inhibitors. *J Am Chem Soc* **137**, 2572-2579 (2015).
277. Bhatia, S., Camacho, L.C. & Haag, R. Pathogen Inhibition by Multivalent Ligand Architectures. *J Am Chem Soc* **138**, 8654-8666 (2016).
278. Nagao, M., Matsubara, T., Hoshino, Y., Sato, T. & Miura, Y. Synthesis of Various Glycopolymers Bearing Sialyllactose and the Effect of Their Molecular Mobility on Interaction with the Influenza Virus. *Biomacromolecules* (2019).
279. Richards, S.-J., Baker, A.N., Walker, M. & Gibson, M.I. Polymer-Stabilized Sialylated Nanoparticles: Synthesis, Optimization and Differential Binding to Influenza Hemagglutinins. *Biomacromolecules* (2020).
280. Lu, W. et al. Enhanced Inhibition of Influenza A Virus Adhesion by Di- and Trivalent Hemagglutinin Inhibitors. *Journal of Medicinal Chemistry* **62**, 6398-6404 (2019).
281. Tang, S. et al. Antiviral Agents from Multivalent Presentation of Sialyl Oligosaccharides on Brush Polymers. *ACS Macro Letters* **5**, 413-418 (2016).
282. Kane, R.S. Thermodynamics of Multivalent Interactions: Influence of the Linker. *Langmuir : the ACS journal of surfaces and colloids* **26**, 8636-8640 (2010).
283. Liese, S. & Netz, R.R. Quantitative Prediction of Multivalent Ligand-Receptor Binding Affinities for Influenza, Cholera and Anthrax Inhibition. *ACS Nano* (2018).
284. Ribeiro-Viana, R. et al. Virus-like glycodendrinanoparticles displaying quasi-equivalent nested polyvalency upon glycoprotein platforms potently block viral infection. *Nature Communications* **3**, 1303 (2012).
285. Kiran, P. et al. Exploring Rigid and Flexible Core Trivalent Sialosides for Influenza Virus Inhibition. *Chemistry* **24**, 19373-19385 (2018).
286. Nagao, M., Matsubara, T., Hoshino, Y., Sato, T. & Miura, Y. Topological Design of Star Glycopolymers for Controlling the Interaction with the Influenza Virus. *Bioconjugate chemistry* **30**, 1192-1198 (2019).
287. Waldmann, M. et al. A nanomolar multivalent ligand as entry inhibitor of the hemagglutinin of avian influenza. *J Am Chem Soc* **136**, 783-788 (2014).
288. Gambaryan, A.S. et al. Polymer-bound 6' sialyl-N-acetyllactosamine protects mice infected by influenza virus. *Antiviral research* **68**, 116-123 (2005).
289. Yeh, H.-W. et al. S-Linked sialyloligosaccharides bearing liposomes and micelles as influenza virus inhibitors. *Organic & biomolecular chemistry* **13**, 11518–11528 (2015).
290. Hidari, K.I.P.J. et al. Chemoenzymatic synthesis, characterization, and application of glycopolymers carrying lactosamine repeats as entry inhibitors against influenza virus infection. *Glycobiology* **18**, 779-788 (2008).
291. Lauster, D. et al. Multivalent Peptide-Nanoparticle Conjugates for Influenza-Virus Inhibition. *Angewandte Chemie (International ed. in English)* (2017).
292. Calderón, M., Quadir, M.A., Sharma, S.K. & Haag, R. Dendritic polyglycerols for biomedical applications. *Advanced Materials* **22**, 190-218 (2010).
293. Thomas, A., Müller, S.S. & Frey, H. Beyond poly(ethylene glycol): linear polyglycerol as a multifunctional polyether for biomedical and pharmaceutical applications. *Biomacromolecules* **15**, 1935-1954 (2014).

294. Imran ul-haq, M., Lai, B.F.L., Chapanian, R. & Kizhakkedathu, J.N. Influence of architecture of high molecular weight linear and branched polyglycerols on their biocompatibility and biodistribution. *Biomaterials* **33**, 9135-9147 (2012).
295. O'Brien, R.D. Fats and Oils: Formulating and Processing for Applications, Third Edition. (CRC Press, 2008).
296. Bhatia, S., Dimde, M. & Haag, R. Multivalent glycoconjugates as vaccines and potential drug candidates. *Medchemcomm* **5**, 862-878 (2014).
297. Mochalova, L.V. et al. Synthetic polymeric inhibitors of influenza virus receptor-binding activity suppress virus replication. *Antiviral research* **23**, 179-190 (1994).
298. Landers, J.J. et al. Prevention of Influenza Pneumonitis by Sialic Acid–Conjugated Dendritic Polymers. *The Journal of Infectious Diseases* **186**, 1222–1230 (2002).
299. Bovin, N.V., Tuzikov, A.B., Chinarev, A.A. & Gambaryan, A.S. Multimeric glycotherapeutics: New paradigm. *Glycoconjugate journal* **21**, 471-478 (2004).
300. Ogata, M. et al. Synthesis of multivalent sialyllactosamine-carrying glyco-nanoparticles with high affinity to the human influenza virus hemagglutinin. *Carbohydrate Polymers* **153**, 96-104 (2016).
301. Terabayashi, T., Morita, M., Ueno, M., Nakamura, T. & Urashima, T. Inhibition of influenza-virus-induced cytopathy by sialylglycoconjugates. *Carbohydrate research* **341**, 2246–2253 (2006).
302. Farabi, K. et al. Concise and Reliable Syntheses of Glycodendrimers via Self-Activating Click Chemistry: A Robust Strategy for Mimicking Multivalent Glycan–Pathogen Interactions. *The Journal of Organic Chemistry* (2020).
303. Johansson, S.M.C. et al. Multivalent sialic acid conjugates inhibit adenovirus type 37 from binding to and infecting human corneal epithelial cells. *Antiviral research* **73**, 92-100 (2007).
304. Johansson, S.M.C., Arnberg, N., Elofsson, M., Wadell, G. & Kihlberg, J. Multivalent HSA Conjugates of 3′-Sialyllactose are Potent Inhibitors of Adenoviral Cell Attachment and Infection. *ChemBioChem* **6**, 358-364 (2005).
305. Clausen, T.M. et al. SARS-CoV-2 Infection Depends on Cellular Heparan Sulfate and ACE2. *Cell* **183**, 1043-1057.e1015 (2020).
306. Kwon, P.S. et al. Sulfated polysaccharides effectively inhibit SARS-CoV-2 in vitro. *Cell Discov* **6**, 50-50 (2020).
307. Baker, A.N. et al. The SARS-COV-2 Spike Protein Binds Sialic Acids and Enables Rapid Detection in a Lateral Flow Point of Care Diagnostic Device. *ACS central science* **6**, 2046-2052 (2020).
308. Sriwilaijaroen, N. & Suzuki, Y. Hemagglutinin Inhibitors are Potential Future Anti-Influenza Drugs for Mono- and Combination Therapies. *Methods in molecular biology (Clifton, N.J.)* **2132**, 547-565 (2020).
309. Fasting, C. et al. Multivalency as a chemical organization and action principle. *Angewandte Chemie (International ed. in English)* **51**, 10472-10498 (2012).
310. Hoffmann, E., Neumann, G., Kawaoka, Y., Hobom, G. & Webster, R.G. A DNA transfection system for generation of influenza A virus from eight plasmids. *Proceedings of the National Academy of Sciences of the United States of America* **97**, 6108-6113 (2000).
311. Zhou, B. et al. Single-reaction genomic amplification accelerates sequencing and vaccine production for classical and Swine origin human influenza a viruses. *Journal of virology* **83**, 10309-10313 (2009).
312. Aich, U. et al. Glycomics-based analysis of chicken red blood cells provides insight into the selectivity of the viral agglutination assay. *FEBS J* **278**, 1699–1712 (2011).
313. Prichard, M.N. & Shipman, C., Jr. A three-dimensional model to analyze drug-drug interactions. *Antiviral research* **14**, 181-205 (1990).
314. Ianevski, A., He, L., Aittokallio, T. & Tang, J. SynergyFinder: a web application for analyzing drug combination dose–response matrix data. *Bioinformatics* **33**, 2413-2415 (2017).
315. BLISS, C.I. THE TOXICITY OF POISONS APPLIED JOINTLY1. *Annals of Applied Biology* **26**, 585-615 (1939).
316. Basu, A. et al. New small molecule entry inhibitors targeting hemagglutinin-mediated influenza a virus fusion. *Journal of virology* **88**, 1447-1460 (2014).
317. Covés-Datson, E.M. et al. A molecularly engineered antiviral banana lectin inhibits fusion and is efficacious against influenza virus infection in vivo.

Proceedings of the National Academy of Sciences **117**, 2122-2132 (2020).
318. Fukao, K. et al. Combination treatment with the cap-dependent endonuclease inhibitor baloxavir marboxil and a neuraminidase inhibitor in a mouse model of influenza A virus infection. *Journal of Antimicrobial Chemotherapy* **74**, 654-662 (2018).
319. Smee, D.F., Hurst, B.L., Wong, M.-H., Bailey, K.W. & Morrey, J.D. Effects of double combinations of amantadine, oseltamivir, and ribavirin on influenza A (H5N1) virus infections in cell culture and in mice. *Antimicrobial agents and chemotherapy* **53**, 2120-2128 (2009).
320. Bedford, T. et al. Integrating influenza antigenic dynamics with molecular evolution. *eLife* **3**, e01914 (2014).
321. Kearse, M. et al. Geneious Basic: an integrated and extendable desktop software platform for the organization and analysis of sequence data. *Bioinformatics* **28**, 1647-1649 (2012).
322. McKimm-Breschkin, J.L. et al. Mutations in a Conserved Residue in the Influenza Virus Neuraminidase Active Site Decreases Sensitivity to Neu5Ac2en-Derived Inhibitors. *Journal of virology* **72**, 2456-2462 (1998).
323. Fediakina, I.T. et al. Sensitivity of influenza A/H5 viruses isolated from wild birds on the territory of Russia to arbidol in the cultured MDCK cells. *Vopr Virusol* **50**, 32-35 (2005).
324. Ito, T. et al. Differences in sialic acid-galactose linkages in the chicken egg amnion and allantois influence human influenza virus receptor specificity and variant selection. *Journal of virology* **71**, 3357-3362 (1997).
325. Barnard, K.N. et al. Expression of 9-O- and 7,9-O-Acetyl Modified Sialic Acid in Cells and Their Effects on Influenza Viruses. *mBio* **10**, e02490-02419 (2019).
326. Moen, A., Hafte, T.T., Tveit, H., Egge-Jacobsen, W. & Prydz, K. N-Glycan synthesis in the apical and basolateral secretory pathway of epithelial MDCK cells and the influence of a glycosaminoglycan domain. *Glycobiology* **21**, 1416-1425 (2011).
327. Tveit, H., Dick, G., Skibeli, V. & Prydz, K. A proteoglycan undergoes different modifications en route to the apical and basolateral surfaces of Madin-Darby canine kidney cells. *The Journal of biological chemistry* **280**, 29596-29603 (2005).
328. Wu, N.C. et al. A complex epistatic network limits the mutational reversibility in the influenza hemagglutinin receptor-binding site. *Nature communications* **9**, 1264 (2018).
329. Smith, D.J. et al. Mapping the antigenic and genetic evolution of influenza virus. *Science* **305**, 371-376 (2004).
330. Takashita, E. et al. Global update on the susceptibility of human influenza viruses to neuraminidase inhibitors, 2013-2014. *Antiviral research* **117**, 27-38 (2015).
331. Hatakeyama, S. et al. Enhanced expression of an alpha2,6-linked sialic acid on MDCK cells improves isolation of human influenza viruses and evaluation of their sensitivity to a neuraminidase inhibitor. *Journal of clinical microbiology* **43**, 4139-4146 (2005).
332. Baum, M.M. et al. Highly synergistic drug combination prevents vaginal HIV infection in humanized mice. *Scientific reports* **10**, 12995 (2020).
333. Feng, J.Y. et al. The triple combination of tenofovir, emtricitabine and efavirenz shows synergistic anti-HIV-1 activity in vitro: a mechanism of action study. *Retrovirology* **6**, 44 (2009).
334. Richman, D. et al. BI-RG-587 is active against zidovudine-resistant human immunodeficiency virus type 1 and synergistic with zidovudine. *Antimicrob Agents Chemother* **35**, 305-308 (1991).
335. Azmi, A.S., Wang, Z., Philip, P.A., Mohammad, R.M. & Sarkar, F.H. Proof of concept: network and systems biology approaches aid in the discovery of potent anticancer drug combinations. *Mol Cancer Ther* **9**, 3137-3144 (2010).
336. Xiao, F. et al. Synergy of entry inhibitors with direct-acting antivirals uncovers novel combinations for prevention and treatment of hepatitis C. *Gut* **64**, 483-494 (2015).
337. Lee, S.-i. Drug interaction: focusing on response surface models. *Korean J Anesthesiol* **58**, 421-434 (2010).
338. Yadav, B., Wennerberg, K., Aittokallio, T. & Tang, J. Searching for Drug Synergy in Complex Dose–Response Landscapes Using an Interaction Potency Model. *Computational and Structural Biotechnology Journal* **13**, 504-513 (2015).
339. Basu, A. et al. New small molecule entry inhibitors targeting hemagglutinin-mediated influenza a virus fusion. *Journal of virology* **88**, 1447-1460 (2014).
340. Choi, S.-K., Mammen, M. & Whitesides, G.M. Monomeric inhibitors of influenza

neuraminidase enhance the hemagglutination inhibition activities of polyacrylamides presenting multiple C-sialoside groups. *Chemistry & Biology* **3**, 97-104 (1996).
341. Sriwilaijaroen, N. et al. 6SLN-lipo PGA specifically catches (coats) human influenza virus and synergizes neuraminidase-targeting drugs for human influenza therapeutic potential. *Journal of Antimicrobial Chemotherapy* **70**, 2797-2809 (2015).
342. Matrosovich, M., Matrosovich, T., Carr, J., Roberts, N.A. & Klenk, H.-D. Overexpression of the alpha-2,6-sialyltransferase in MDCK cells increases influenza virus sensitivity to neuraminidase inhibitors. *Journal of virology* **77**, 8418-8425 (2003).
343. Lazniewski, M., Dawson, W.K., Szczepinska, T. & Plewczynski, D. The structural variability of the influenza A hemagglutinin receptor-binding site. *Briefings in functional genomics* **17**, 415–427 (2018).
344. Matrosovich, M.N. et al. Probing of the Receptor-Binding Sites of the H1 and H3 Influenza A and Influenza B Virus Hemagglutinins by Synthetic and Natural Sialosides. *Virology* **196**, 111-121 (1993).
345. Erbelding, E.J. et al. A Universal Influenza Vaccine: The Strategic Plan for the National Institute of Allergy and Infectious Diseases. *J Infect Dis* **218**, 347-354 (2018).
346. Zhong, M. et al. Amide-sialoside protein conjugates as neomucin bioshields prevent influenza virus infection. *Carbohydrate research* **495**, 108088 (2020).
347. Hay, A.J. in Concepts in Viral Pathogenesis III. (eds. A.L. Notkins & M.B.A. Oldstone) 361-367 (Springer New York, New York, NY; 1989).
348. Pillay, D. & Zambon, M. Antiviral drug resistance. *BMJ* **317**, 660-662 (1998).
349. Zhang, X. et al. Potential resistant mutations within HBV reverse transcriptase sequences in nucleos(t)ide analogues-experienced patients with hepatitis B virus infection. *Scientific reports* **9**, 8078 (2019).
350. Lim, Y.S. Management of Antiviral Resistance in Chronic Hepatitis B. *Gut Liver* **11**, 189-195 (2017).
351. Zoulim, F. Hepatitis B virus resistance to antiviral drugs: where are we going? *Liver Int* **31 Suppl 1**, 111-116 (2011).
352. Park, J.G. & Park, S.Y. Entecavir plus tenofovir versus entecavir plus adefovir in chronic hepatitis B patients with a suboptimal response to lamivudine and adefovir combination therapy. *Clin Mol Hepatol* **21**, 242-248 (2015).
353. Lok, A.S. How to diagnose and treat hepatitis B virus antiviral drug resistance in the liver transplant setting. *Liver Transpl* **14 Suppl 2**, S8-s14 (2008).
354. Hepatology., E.T.H.o. in Journal of Hepatology, Vol. 04/03/19 - Journal of Hepatology (2019).
355. Park, E.-S. et al. Identification of a quadruple mutation that confers tenofovir resistance in chronic hepatitis B patients. *Journal of Hepatology* **70**, 1093-1102 (2019).
356. Organization., W.H., Vol. 2021 (2020).
357. Perelson, A.S., Rong, L. & Hayden, F.G. Combination Antiviral Therapy for Influenza: Predictions From Modeling of Human Infections. *The Journal of Infectious Diseases* **205**, 1642-1645 (2012).
358. Kumar, N. et al. Host-Directed Antiviral Therapy. *Clinical Microbiology Reviews* **33**, e00168-00119 (2020).
359. Weis, W. et al. Structure of the influenza virus haemagglutinin complexed with its receptor, sialic acid. *Nature* **333**, 426 (1988).
360. Sun, H. et al. Using Sequence Data To Infer the Antigenicity of Influenza Virus. *mBio* **4**, e00230-00213 (2013).
361. Steinbrück, L. & McHardy, A.C. Inference of genotype-phenotype relationships in the antigenic evolution of human influenza A (H3N2) viruses. *PLoS Comput Biol* **8**, e1002492-e1002492 (2012).
362. Yao, Y. et al. Predicting influenza antigenicity from Hemagglutintin sequence data based on a joint random forest method. *Scientific reports* **7**, 1545-1545 (2017).
363. Thyagarajan, B. & Bloom, J.D. The inherent mutational tolerance and antigenic evolvability of influenza hemagglutinin. *Elife* **3** (2014).
364. Yamada, S. et al. Adaptation of a Duck Influenza A Virus in Quail. *Journal of virology* **86**, 1411-1420 (2012).
365. Carr, S.M., Carnero, E., García-Sastre, A., Brownlee, G.G. & Fodor, E. Characterization of a mitochondrial-targeting signal in the PB2 protein of influenza viruses. *Virology* **344**, 492-508 (2006).
366. Wandzik, J.M., Kouba, T. & Cusack, S. Structure and Function of Influenza Polymerase. *Cold Spring Harbor Perspectives in Medicine* (2020).

367. Pflug, A. et al. Capped RNA primer binding to influenza polymerase and implications for the mechanism of cap-binding inhibitors. *Nucleic Acids Res* **46**, 956-971 (2018).
368. Gabriel, G. et al. The viral polymerase mediates adaptation of an avian influenza virus to a mammalian host. *Proceedings of the National Academy of Sciences of the United States of America* **102**, 18590-18595 (2005).
369. Ji, Y., White, Y.J.B., Hadden, J.A., Grant, O.C. & Woods, R.J. New insights into influenza A specificity: an evolution of paradigms. *Current Opinion in Structural Biology* **44**, 219-231 (2017).
370. Byrd-Leotis, L. et al. Influenza binds phosphorylated glycans from human lung. *Science advances* **5**, eaav2554-eaav2554 (2019).
371. CFG, Vol. 2021 (2012).
372. Ushirogawa, H. et al. Re-emergence of H3N2 strains carrying potential neutralizing mutations at the N-linked glycosylation site at the hemagglutinin head, post the 2009 H1N1 pandemic. *BMC infectious diseases* **16**, 380 (2016).
373. Barr, I.G. et al. Increased adamantane resistance in influenza A(H3) viruses in Australia and neighbouring countries in 2005. *Antiviral research* **73**, 112-117 (2007).
374. Chung, J. et al. Filamentous anti-influenza agents wrapping around viruses. *J Colloid Interface Sci* **583**, 267-278 (2020).
375. Nie, C. et al. Heteromultivalent topology-matched nanostructures as potent and broad-spectrum influenza A virus inhibitors. *Sci Adv* **7** (2021).

Abbreviations

CPE	cytopatic effect
CPE	cytopathic effect
DF	degree of functionalization
DMSO	dimethyl sulfoxide
dPG	dendritic polyglycerol
EG	ethylene glycol
GA	glycan array
GlcNAc	N-acetylglucosamine
HA	Hemagglutinin
HAI	hemagglutination inhibition assay
HBV	hepatitis B virus
HE	hemagglutinin-esterase
hpi	hours post infection
HPIV	human parainfluenza virus
HSA	highest single agent
IAV	Influenza A Virus
IBV	infectious bronchitis virus
ICV	Influenza C Virus
IF	immunofluorescence
L1	$LPG_{10}SA_{0.40}$ 1b-treated replicate 1 (G135E)
L2	$LPG_{10}SA_{0.40}$ 1b-treated replicate 2 (K140N)
L3	$LPG_{10}SA_{0.40}$ 1b-treated replicate 3 (P99F/G144D)
LPG	linear polyglacerol
M1	matrix protein 1
M2	matrix protein 2
MW	molecular weight
NA	neuramindase
NDV	Newcastle disease virus
NEP/NS2	nuclear export protein/nonstructural protein 2
Neu5Ac	N-acetylneuraminic acid
Neu5Gc	N-glycolylneuraminic acid
NGS	next generation sequencing
NP	nucleoprotein
NS1	nonstructural protein 1
nt	nucleotides
PA	polymerase acid
PA	plaque assay
PB1	polymerase basic1
PB2	polymerase basic2
PBS	phosphate buffered saline
PCR	polymerase chain reaction
PG	Polyglycerol
PRA	plaque reduction assay
RBS	receptor binding site
RFU	relative fluorescence unit
RNP	ribonucleoprotein
RT	room temperature
SA	Sialic Acid
TGEV	transmissible gastroenteritis virus
vRNP	viral RNP

List of Figures

List of Tables

Appendix

Supplementary Table 1: Glycans spotted on the noncommercial glycan array by the MPI.

number	Systematic
1	Neu5Ac(a2-6)Gal(b1-4)GlcNAc(b1-3)Gal(b1-4)Glc(b1-1)aminohexanol
2	Neu5Ac(a2-3)Gal(b1-3)GlcNAc(b1-3)Gal(b1-4)Glc(b1-1)aminohexanol
3	Fuc(a1-3)[Neu5Ac(a2-3)Gal(b1-4)]GlcNAc(b1-3)Gal(b1-4)Glc(b1-1)aminohexanol
4	Neu5Ac(a2-6)Gal(b1-4)Glc(b1-1)aminohexanol
5	Neu5Ac(a2-3)Gal(b1-4)Glc(b1-1)aminohexanol
6	Neu5Ac(a2-6)Gal(b1-4)GlcNAc-6-sulfate(b1-1)aminohexanol
7	Gal(b1-4)Glc(b1-1)aminohexanol
8	Gal(b1-4)GlcNAc-6-sulfate(b1-1)aminohexanol
9	Fuc(a1-3)[Gal(b1-4)]GlcNAc(b1-1)aminopentanol
10	Neu5Ac(a2-6)GalNAc(a1-1)aminopentanol
11	Gal(b1-3)[Fuc(a1-4)]GlcNAc(b1-1)aminopentanol
12	Neu5Ac(a2-8)Neu5Ac(a2-3)[GalNAc(b1-4)]Gal(b1-4)Glc(b1-1)aminopentanol
13	GalNAc(a1-1)AminoLinker2
14	Gal(b1-4)Glc(b1-1)aminopentanol
15	GalNAc(b1-4)Gal(b1-4)Glc(b1-1)aminopentanol
16	Neu5Ac(a2-3)Gal(b1-4)Glc(b1-1)aminopentanol
17	Gal(b1-3)GalNAc(b1-4)Gal(b1-4)Glc(b1-1)aminopentanol
18	Gal(b1-3)GlcNAc(b1-3)Gal(b1-4)Glc(b1-1)aminopentanol
19	Gal(b1-4)GlcNAc(b1-3)Gal(b1-4)Glc(b1-1)aminopentanol
20	Gal(b1-4)GlcNAc(b1-3)Gal(b1-4)GlcNAc(b1-3)Gal(b1-4)Glc(b1-1)
21	Neu5Ac(a2-3)Gal(b1-3)GalNAc(b1-4)Gal(b1-4)Glc(b1-1)aminopentanol
22	Neu5Ac(a2-3)Gal(b1-3)GlcNAc(b1-3)Gal(b1-4)Glc(b1-1)aminopentanol
23	Neu5Ac(a2-3)Gal(b1-4)GlcNAc(b1-3)Gal(b1-4)Glc(b1-1)aminopentanol
24	Neu5Ac(a2-3)Gal(b1-4)GlcNAc(b1-3)Gal(b1-4)GlcNAc(b1-3)Gal(b1-4)Glc(b1-1)
25	Neu5Ac(a2-3)Gal(b1-3)[Fuc(a1-4)]GlcNAc(b1-1)aminopentanol

Supplementary Table 2: Glycans spotted on the commercial glycan array by Raybiotech.

Number	Systematic	Number	Systematic
	Positive control	50	Neu5Ac-α-2,3-Gal-β-1,4-(Fuc-α-1,3)-Glc-β- [3-Sialyl-3-fucosyllactose/ F-SL]-Sp1
	Buffer	51	GlcNAc-β-1,4-GlcNAc-β-Sp1
1	β-Glc-Sp	52	β-D-GlcA-Sp
2	β-Gal-Sp	53	Gal-β-1,4-(6S)GlcNAc-β-Sp
3	α-Man-Sp	54	GlcNAc-α-1,3-(Glc-α-1,2-Glc-α-1,2)-Gal-α-1,3-Glc-α-Sp
4	α-Fuc-Sp	55	Gal-β-1,3-GalNAc-β-1,4-(Neu5Gc-α-2,3)-Gal-β-1,4-Glc-β-Sp1
5	α-Rha-Sp	56	Sisomicin Sulfate
6	β-GlcNAc-Sp	57	GalNAc-α-1,3-(Fuc-α-1,2)-Gal-β-[Blood A antigen trisaccharide]-Sp1
7	β-GalNAc-Sp	58	Fuc-α-1,2-Gal-β-1,4-GlcNAc-β- [Blood H antigen trisaccharide]-Sp1
8	Tobramycin	59	Gal-α-1,3-(Fuc-α-1,2)-Gal-β- [Blood B antigen trisaccharide]-Sp1
9	Gal-β-1,3-GlcNAc-β-Sp	60	Fuc-α-1,2-Gal-β-1,3-GlcNAc-β-1,3-Gal-β-1,4-Glc-β- [LNFP I]-Sp1
10	Gal-α-1,3-Gal-β-1,3-GlcNAc-β-Sp	61	Fuc-α-1,2-Gal-β-1,4-Glc-β- [Blood H antigen trisaccharide]-Sp1
11	Neu5Ac-α-2,3-Gal-β-1,3-GlcNAc-β-Sp	62	Gal-α-1,3-(Fuc-α-1,2)-Gal-β-1,4-Glc-β-[Blood B antigen tetrasaccharide]-Sp1
12	Neu5Ac-α-2,6-Gal-β-1,3-GlcNAc-β-Sp	63	(Fuc-α-1,2)-Gal-β-1,4-(Fuc-α-1,3)-GlcNAc-β- [Lewis Y]-Sp1
13	Neu5Gc-α-2,3-Gal-β-1,3-GlcNAc-β-Sp	64	(Fuc-α-1,2)-Gal-β-1,3-(Fuc-α-1,4)-GlcNAc-β- [Lewis B]-Sp1
14	Neu5Gc-α-2,6-Gal-β-1,3-GlcNAc-β-Sp	65	Gal-β-1,3-(Fuc-α-1,4)-GlcNAc-β-1,3-Gal-β-1,4-(Fuc-α-1,4)-Glc-β- [Lewis A]-Sp1
15	Gal-β-1,3-(Fuc-α-1,4)-GlcNAc-β- [Lewis A] –Sp	66	Gal-β-1,3-GalNAc-β-Sp1
16	Gal-β-1,4-Glc-β-Sp	67	Gal-β-1,3-(Neu5Ac-α-2,6)-GalNAc-β-Sp
17	Gal-α-1,3-Gal-β-1,4-Glc-β-Sp	68	Neu5Ac-α-2,6-Gal-β-1,3-GalNAc-β-Sp
18	Gal-α-1,4-Gal-β-1,4-Glc-β-Sp	69	Neu5Ac-α-2,6-Gal-β-1,3-(Neu5Ac-α-2,6)-GalNAc-β-Sp
19	GlcNAc-β-1,3-Gal-β-1,4-Glc-β-Sp	70	Neu5Ac-α-2,3-Gal-β-1,3-(Neu5Ac-α-2,6)-GalNAc-β-Sp

20	GalNAc-β-1,3-Gal-β-1,4-Glc-β-Sp	71	Neu5Ac-α-2,6-(Neu5Ac-α-2,3)-Gal-β-1,3-GalNAc-β-Sp
21	Neu5Ac-α-2,3-Gal-β-1,4-Glc-β-Sp	72	GalNAc-β-1,4-(Neu5Ac-α-2,3)-Gal-β-1,4-Glc-β- [GM2]-Sp
22	Neu5Ac-α-2,6-Gal-β-1,4-Glc-β-Sp	73	GalNAc-β-1,4-(Neu5Ac-α-2,8-Neu5Ac-α-2,3)-Gal-β-1,4-Glc-β- [GD2]-Sp
23	Neu5Gc-α-2,3-Gal-β-1,4-Glc-β-Sp	74	Gal-α-1,4-Gal-β-1,4-GlcNAc-β-Sp1
24	Neu5Ac-α-2,6-Gal-β-1,4-Glc-β-Sp	75	β-D-Rha-Sp
25	Gal-β-1,4-(Fuc-α-1,3)-Glc-β-Sp	76	Glc-α-1,4-Glc-β-Sp1
26	GalNAc-β-1,3-Gal-α-1,4-Gal-β-1,4-Glc-β-Sp	77	Glc-α-1,6-Glc-α-1,4-Glc-β-Sp1
27	GlcNAc-β-1,6-GlcNAc-β-Sp	78	Maltotriose-β-Sp1
28	4-P-GlcNAc-□-1,4-Man-□-Sp	79	Glc-α-1,6-Glc-α-1,6-Glc-β-Sp1
29	Glc-α-1,2-Gal-α-1,3-Glc-α-Sp	80	Maltotetraose-β-Sp1
30	Gal-β-1,3-GalNAc-α-Sp	81	GlcNAc-α-1,4-GlcA-β-1,4-GlcNAc-α1,4-GlcA-β-Sp
31	Gal-β-1,4-GlcNAc-β-Sp	82	Maltohexaose-β-Sp1
32	Gal-β-1,4 -(Fuc-α-1,3)-GlcNAc-β- [Lewis X] –Sp	83	Maltoheptaose-β-Sp1
33	Neu5Ac-α-2,3-Gal-β-1,4-(Fuc-α-1,3)-GlcNAc-β- [Sialyl Lewis X]-Sp	84	Acarbose-β-Sp1
34	Neu5Ac-α-2,3-Gal-β-1,3 -(Fuc-α-1,4)-GlcNAc-β- [Sialyl Lewis A]-Sp	85	D-pentamannuronic acid-β-Sp1
35	Neu5Gc-α-2,3-Gal-β-1,3-(Fuc-α-1,4)-GlcNAc-β- [Sialyl Lewis A]-Sp	86	L-pentaguluronic acid-β-Sp1
36	Gal-α-1,4-Gal-β-1,3-GlcNAc-β-Sp	87	D-cellose-β-Sp1
37	Gal-β-1,4-GlcNAc-β-1,3-Gal-β-1,4-Glc-β-[LNnT]-Sp	88	Gal-α-1,3-Gal-β-Sp1
38	GlcA-β-1,4-GlcNAc-α-1,4-GlcA-β-Sp	89	β-1,4-Xylotetrose-Sp1
39	GlcNAc-β-1,6-(Gal-β-1,3)-GalNAc-α-O-Ser- Sp4	90	Chitin-trisaccharide-Sp1
40	Neu5Ac-α-2,3Gal-β-1,4-(6S)GlcNAc-β-Sp	91	KDN-α-2,8-Neu5Ac-α-2,3-Gal-β-1,4-Glc-β-Sp
41	GalNAc-β-1,4-GlcNAc-β-Sp2	92	Neu5Ac-α-2,8-Neu5Gc-α-2,3-Gal-β-1,4-Glc-β-Sp
42	Neu5Ac-α-2,8-Neu5Ac-α-2,3-Gal β-1,4-Glc-β-Sp	93	Neu5Ac-α-2,8-Neu5Ac-α-2,8-Neu5Ac-α-2,3-Gal-β-1,4-Glc-β-Sp3
43	Neu5Gc-α-2,8-Neu5Ac-α-2,3-Gal-β-1,4-Glc-β-Sp	94	Neu5Ac-□-2,8-Neu5Ac-□-2,6-Gal-□-1,4-Glc-Sp5
44	GalNAc-α-1,3-(Fuc-α-1,2)-Gal-β-1,4-Glc-	95	Gal-β-1,3-GalNAc-β-1,4-(Neu5Ac-α-

	β- [Blood A antigen tetrose]-Sp1		2,3)-Gal-β-1,4-Glc-β-Sp1
45	GlcNAc-β-1,2-Man-α-Sp	96	Gentamicin Sulfate
46	Neu5Ac-α-2,3-Gal-β-Sp1	97	Kanamycin sulfate
47	Gal-β-1,3 -GalNAc-β-1,3-Gal-β-Sp1	98	Geneticin Disulfate Salt (G418)
48	Glc-α-1,2-Gal-α-Sp	99	Neomycin trisulfate
49	Gal-β-1,4-(Fuc-α-1,3)-GlcNAc-β-1,3-Gal-β-Sp1	100	SGP

Eidesstattliche Erklärung

Hiermit erkläre ich, Marlena Nastassja Stadtmüller, die vorliegende Dissertation selbstständig und nur unter Verwendung der angegebenen Hilfsmittel und Hilfen angefertigt zu haben. Daten, die von anderen Wissenschaftler*innen in einer Kooperation zur Verfügung gestellt wurden, sind als solche gekennzeichnet und mit einem namentlichen Verweis auf den/die Kooperationspartner*in versehen. Alle chemischen Synthesen und Analysen der hier untersuchten Wirkstoffe sind von Kooperationspartner*innen durchgeführt worden, auf die an entsprechender Stelle verwiesen wird.

Ich versichere, dass ich die Dissertation oder Teile davon nur in diesem und in keinem anderen Promotionsverfahren eingereicht habe und, dass diesem Promotionsverfahren kein gescheitertes Promotionsverfahren vorausgegangen ist.

Ort, Datum Marlena Nastassja Stadtmüller